Alfred-Wegener-Institut; Helmholtz-Zentrum für Polar- und Meeresforschung
Universität Potsdam, Institut für Erd- und Umweltwissenschaften

---

Effect of mass wasting on soil organic carbon storage and coastal erosion in permafrost environments

Dissertation
zur Erlangung des akademischen Grades
"doctor rerum naturalium"
(Dr. rer. nat.)
in der Wissenschaftsdisziplin Geologie

in Form einer kumulativen Arbeit
eingereicht an der
Mathematisch-Naturwissenschaftlichen Fakultät
der Universität Potsdam

von
Jaroslav Obu

Potsdam, den 17. 11. 2015

Published online at the
Institutional Repository of the University of Potsdam:
URN urn:nbn:de:kobv:517-opus4-90599
http://nbn-resolving.de/urn:nbn:de:kobv:517-opus4-90599

Table of contents

Abstract

Accelerated permafrost thaw under the warming Arctic climate can have a significant impact on Arctic landscapes. Areas underlain by permafrost store high amounts of soil organic carbon (SOC). Permafrost disturbances may contribute to increased release of carbon dioxide and methane to the atmosphere. Coastal erosion, amplified through a decrease in Arctic sea-ice extent, may also mobilise SOC from permafrost. Large expanses of permafrost affected land are characterised by intense mass-wasting processes such as solifluction, active-layer detachments and retrogressive thaw slumping. Our aim is to assess the influence of mass wasting on SOC storage and coastal erosion.

We studied SOC storage on Herschel Island by analysing active-layer and permafrost samples, and compared non-disturbed sites to those characterised by mass wasting. Mass-wasting sites showed decreased SOC storage and material compaction, whereas sites characterised by material accumulation showed increased storage. The SOC storage on Herschel Island is also significantly correlated to catenary position and other slope characteristics. We estimated SOC storage on Herschel Island to be 34.8 kg C m^{-2}. This is comparable to similar environments in northwest Canada and Alaska.

Coastal erosion was analysed using high resolution digital elevation models (DEMs). Two LIDAR scanning of the Yukon Coast were done in 2012 and 2013. Two DEMs with 1 m horizontal resolution were generated and used to analyse elevation changes along the coast. The results indicate considerable spatial variability in short-term coastline erosion and progradation. The high variability was related to the presence of mass-wasting processes. Erosion and deposition extremes were recorded where the retrogressive thaw slump (RTS) activity was most pronounced. Released sediment can be transported by longshore drift and affects not only the coastal processes in situ but also along adjacent coasts.

We also calculated volumetric coastal erosion for Herschel Island by comparing a stereo-photogrammetrically derived DEM from 2004 with LIDAR DEMs. We compared this volumetric erosion to planimetric erosion, which was based on coastlines digitised from satellite imagery. We found a complex relationship between planimetric and volumetric coastal erosion, which we attribute to frequent occurrence of mass-wasting processes along the coasts. Our results suggest that volumetric erosion corresponds better with environmental forcing and is more suitable for the estimation of organic carbon fluxes than planimetric erosion.

Mass wasting can decrease SOC storage by several mechanisms. Increased aeration following disturbance may increase microbial activity, which accelerates organic matter decomposition. New hydrological conditions that follow the mass wasting event can cause leaching of freshly

exposed material. Organic rich material can also be directly removed into the sea or into a lake. On the other hand the accumulation of mobilised material can result in increased SOC storage. Mass-wasting related accumulations of mobilised material can significantly impact coastal erosion in situ or along the adjacent coast by longshore drift. Therefore, the coastline movement observations cannot completely resolve the actual sediment loss due to these temporary accumulations. The predicted increase of mass-wasting activity in the course of Arctic warming may increase SOC mobilisation and coastal erosion induced carbon fluxes.

Zusammenfassung

Die Erwärmung des arktischen Klimas beschleunigt das Tauen des Permafrosts. Das kann einen erheblichen Einfluss auf arktische Landschaften haben. Permafrostböden speichern große Mengen Kohlenstoff, der aufgrund von Umlagerungsprozessen wie beispielsweise Massenversatz mobilisiert und als Kohlendioxid oder Methan freigesetzt werden kann. Der Kohlenstoff im Boden kann auch durch Küstenerosion mobilisiert werden, die durch den Rückgang des arktischen Meereises und höhere Meerwassertemperaturen künftig stark zunehmen wird. Große Teile der arktischen Permafrostgebiete werden durch intensive Massenversatzprozesse wie Solifluktion, Rutschungen in der saisonalen Auftauschicht (active layer detachments) und rückschreitende Taurutschungen (retrogressive thaw slumps) gekennzeichnet. Unser Ziel ist es, den Einfluss dieser Massenbewegungen auf Kohlenstoffspeicher und Küstenerosion zu bewerten.

Wir haben Auftauschicht- und Permafrostproben untersucht, um den Kohlenstoffspeicher für Herschel Island zu ermitteln. Wir verglichen ungestörtes Terrain mit durch Massenversatz gekennzeichnetem Terrain. Letzteres zeigte verringerte Bodenkohlenstoffspeicher und Materialverdichtung. Durch Akkumulation organischen Materials gekennzeichnete Lagen zeigten eine Zunahme des Kohlenstoffpeichers. Der Bodenkohlenstoffspeicher auf Herschel Insel korreliert außerdem deutlich mit der Lage in Senken und der Hangneigung. Der Kohlenstoffspeicher im Boden von Herschel Island ist etwa so hoch wie in vergleichbaren Landschaften im Nordwesten Kanadas und Alaskas. Wir schätzen ihn auf 34,8 kg C m^{-2}.

Wir ermittelten Küstenerosionsraten mit hochauflösenden Digitalen Geländemodellen (DGM). Dazu benutzten wir zwei LIDAR Aufnahmen der Yukon Küste aus den Jahren 2012 und 2013. Zwei DGMs mit 1 m horizontaler Auflösung wurden erzeugt und verwendet, um die Höhenunterschiede entlang der Küste zu analysieren. Wir fanden eine erhebliche räumliche Variabilität in kurzfristigen Küstenerosionsraten. Wir erklärten die hohe Variabilität mit der räumlichen Heterogenität des Vorkommens von Massenversatzprozessen. Besonders die sogenannten retrogressive thaw slumps bewirkten extrem hohe Erosionsraten an einigen Küstenabschnitten. Durch Strandversetzung wird erodiertes Sediment die Küste entlang transportiert und beeinflusst so nicht nur lokale Küstenprozesse, sondern auch benachbarte Küstenabschnitte.

Um die längerfristige Entwicklung der Küste einschätzen zu können, haben wir volumetrische Erosionsraten aus dem Vergleich eines stereophotogrammetrisch abgeleiteten DGM aus dem Jahr 2004 mit unseren LIDAR DGMs errechnet. Planimetrische Erosionsraten wurden anhand von digitalisierten Küstenlinien aus Satellitenbildern berechnet. So konnte auch der Einfluss von volumetrischer und planimetrischer Erosion eingeschätzt werden. Wir fanden komplexe

Zusammenhänge zwischen planimetrischer und volumetrischer Küstenerosion, die wir auf das gehäufte Auftreten von Massenversatzprozessen entlang einiger Küstenabschnitte zurückführen. Die Ergebnisse legen nahe, dass volumetrische Erosionsraten den beobachteten Umweltbedingungen besser entsprechen als planimetrische Erosionsraten und somit besser geeignet sind zur Einschätzung organischer Kohlenstoffflüsse in Permafrostgebieten entlang der arktischen Küsten.

Massenversatz kann den Kohlenstoffspeicher im Boden mit verschiedenen Mechanismen verringern. Erhöhte Belüftung kann die mikrobielle Aktivität erhöhen, die den Abbau organischer Materie beschleunigt. Durch veränderte hydrologische Bedingungen nach Massenversatz können Stoffe aus der Auftauschicht ausgewaschen werden. Organikreiche Stoffe können auch direkt ins einem Meer in einen See erodiert werden. Andererseits kann die Akkumulation von umgelagertem Material zu einer Erhöhung des Bodenkohlenstoffspeichers an anderer Stelle führen. Die Akkumulation von Material aus Massenversatz kann erhebliche Auswirkungen auf die lokale Küstenerosion, durch Strandversetzung aber auch auf angrenzende Küstenabschnitte haben. Allein durch Beobachtung der Veränderung von Küstenlinien kann aufgrund solcher temporärer Ansammlungen die Einschätzung des tatsächlichen Sedimentverlustes pro Küstenabschnitt nicht präzise wiedergegeben werden. Im Zuge der prognostizierten Erwärmung der Arktis und der damit verbundene Zunahme von Massenversatzprozessen und Küstenerosion wird sich die Mobilisierung von Bodenkohlenstoff aus Permafrost zukünftig beschleunigen.

1 Introduction

1.1 Scientific background

1.1.1 Permafrost and Arctic warming

Permafrost is ground that remains below 0°C for two consecutive years (van Everdingen, 2005). It is a thermal condition of the ground and occurs in bedrocks and sediments and does not necessarily occur as ground ice. The surface layer above permafrost that thaws and refreezes each year is called the active layer. Occurrence of permafrost is controlled by many local factors such as snow thickness and duration, solar radiation, vegetation, soil moisture, etc… (Williams and Smith, 1989), but is ultimately a climatic phenomenon mainly related to air temperature (Smith and Riseborough, 2002).

Any change in in Arctic climate patterns and especially air temperature can therefore have a significant influence on permafrost. Landscapes underlain by permafrost represent 20 % of world's land area and 23 million km2 of the Arctic/northern hemisphere (Figure 1.1) (French, 2013; Zhang et al., 2008). Current air temperature increase in the Arctic is twice as fast as global average (Pachauri et al., 2014) and consequently an increase of permafrost temperatures and active-layer thickness have been observed during last 30 years (Burn and Zhang, 2009; Romanovsky et al. 2010). For this reason, permafrost landscapes are already undergoing drastic changes, which have widespread consequences for the Arctic environment and Arctic societies.

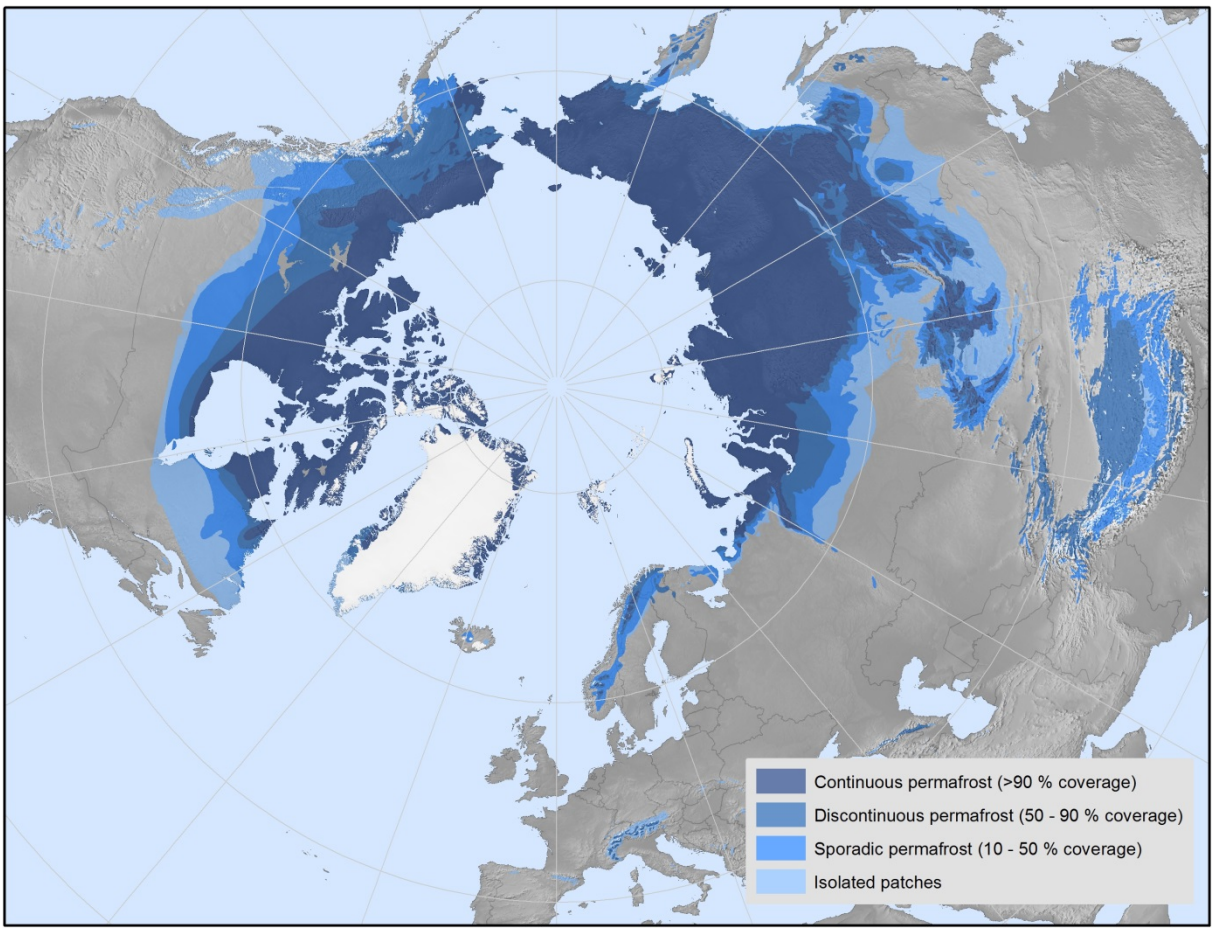

Figure 1.1: Map of the permafrost extent in the Northern Hemisphere showing different permafrost zones according to coverage. Modified after Brown et al. (1997).

1.1.2 Organic matter in Permafrost environments

Permafrost areas were favourable for organic matter (OM) accumulation and acted as a carbon sink during recent geological times (Hobbie et al., 2000). Low temperatures and anoxic conditions due to limited drainage preserved OM that was transported into lower soil horizons by cryoturbation (Bockheim et al., 2007). OM accumulation and incorporation in permafrost was particularly efficient in peatlands and sedimentation environments (Botch et al., 1995; Strauss et al., 2013). Circumpolar estimates of soil organic carbon (SOC) stored in this OM range from 1100 to 1500 Pg for the 0-3 m depth (Hugelius et al. 2014), meaning more than twice the amount that is currently present in the atmosphere (Zimov et al., 2006).

The observed thawing of permafrost and future projections of air temperature increase are leading to OM mobilisation and exposure to microbial activity. Degradation of OM will result in release of greenhouse gases such as carbon dioxide and methane (Schuur et al., 2008). Studies have already demonstrated that old organic carbon that was stored in permafrost is released upon permafrost thaw (Schuur et al., 2009). An increase of greenhouse gases due to permafrost thaw may in turn lead to a further increase of global air temperatures and

permafrost thaw, which is a process, termed the permafrost carbon feedback (Schaefer et al., 2014). This feedback will probably cause climate change to occur faster than is currently predicted by Earth System Models; however, the magnitude and timing remain uncertain (Schuur et al., 2015).

1.1.3 Erosion of permafrost coasts

Arctic permafrost coasts represent between 30 and 34 % of the world's coastlines (Lantuit et al., 2012a). These coasts are characterised by sea-ice cover for as much as 10 months per year, causing high seasonality in erosional, weathering and mass-wasting processes. Despite the fact that erosional processes are limited to few months of the year, erosion rates similar to or higher than those of temperate regions are recorded (Overduin et al., 2014). Erosional rates are particularly high in ice-rich permafrost coasts composed of unconsolidated sediments, where thermal abrasion, a process of combined kinetic wave action and permafrost thawing, is very efficient (Aré, 1988).

The erosion of a permafrost coast at a specific site is controlled by a combination of a variety of regional and local factors. Regional factors are storminess, waves and storm surges, ice-free season duration, sea level, and summertime sea and ground surface temperature. Local factors are parent material properties, ground-ice conditions, backshore-cliff properties and underwater topography (Héquette and Barnes, 1990; Solomon, 2005; Jones et al., 2009). Several studies indicate the importance of different factors, but overall understanding of environmental forcing on permafrost coastal erosion is insufficient (Lantuit et al., 2013). The projected increase of Arctic air temperatures increase will likely increase sea-water temperatures and open-water duration, which can amplify coastal erosion (Overeem, 2011; Stocker et al., 2014; Günther et al., 2015). A recent increase in erosion rates was observed at several sites along the Beaufort Sea coast (Jones et al., 2009; Overduin et al., 2014).

Permafrost coastal erosion can mobilise considerable amounts of sediment and OM (Rachold, 2004). Carbon and nutrient release has a significant impact on Arctic coastal ecosystems and can eventually be released as greenhouse gasses (Ping et al., 2011). Reconstructions from shelf sediment show that half of the mobilised carbon is released as carbon dioxide (Vonk et al., 2012). Estimates of organic carbon released by permafrost coastal erosion range between 4.9-14.0 Tg C a^{-1} (Wegner et al., in press) and are thus in the order of magnitude of vertical carbon emissions from terrestrial permafrost (40.0 to 84.0 Tg C a^{-1}; McGuire et al., 2009) and riverine input (~39 Tg C a^{-1}; McGuire et al., 2009). The main source of uncertainty is the scarcity of in-situ measurements and the information on exact volumes being eroded (Lantuit et al., 2013).

1.1.4 Mass wasting

Mass wasting (also mass movement) is the term that describes downslope movement of debris under the influence of gravity. Although present also in other environments, it is especially effective in cold climates because of the following reasons (French, 2013): (1) Abundance of loose material due to intensive frost action, (2) diurnal and short-term freezing accelerates sediment movements, (3) high moisture contents in thawed active layer due to limited downward water infiltration and (4) permafrost table acts as a water-lubricated slip plane for movement of thawed material. Mass wasting in permafrost areas occurs in several forms that are differentiated by the speed of movement and the amount of released sediment. Here we describe mass-wasting processes that are the most common in terrain developed in unconsolidated and ice-rich sediments, which are characteristic for our study area.

One of the most widespread and slow mass-wasting processes is solifluction. It is a continuous and slow mass movement due to freeze-thaw action and movements of saturated soil related to ground thawing (Matsuoka, 2001). Another very typical form of mass wasting that is common for environments with unconsolidated sediments is active-layer detachment (ALD). This is a translational landslide with a shallow failure plane that occurs on very gentle to moderate slopes in summer-thawed material overlying permafrost (Lewkowicz and Harris, 2005b). Another form of mass wasting occurring in permafrost environments is a retrogressive thaw slump (RTS). RTSs can be initiated by ALDs or coastal erosion (de Krom, 1990) that expose massive ice on sloping terrain, which leads to the formation of C-shaped depressions (Burn and Lewkowicz, 1990; Lantuit and Pollard, 2008). RTSs are polycyclic phenomena and one of the most active permafrost surficial features, where considerable amounts of sediments are moved downslope in form of earth falls and mudflows (Lantuit and Pollard, 2005; French, 2013). This moved material can significantly influence permafrost landscapes. RTSs are most common along coastlines, river banks and lakeshores, where ice-rich ground is being exposed (Lantz and Kokelj, 2008). A very rapid form of mass movement along permafrost coasts is block failure. Block failure involves the collapse of large blocks that detach from cliffs under the influence of gravity. Block failures can occur due to undercutting of a frozen cliff by the formation of a thermo-erosional niche or by failure along ice wedges (Hoque and Pollard, 2009).

Geomorphic work of these mass-wasting processes can be compared to the geomorphic work of their counterparts in mountainous terrain. Lewkowicz (1990) indicated that geomorphic work of solifluction and ALDs on Fosheim Peninsula (Elsmere Island, Canada) is in the same order of magnitude as debris flows and slushflows occurring in nearby mountainous terrain (Lewkowicz and Harris, 2005a). The studied mass wasting can therefore significantly change lowland permafrost landscapes. Increased permafrost thaw will likely result in enhanced

mass-wasting activity (Lantz and Kokelj, 2008; Lewkowicz and Harris, 2005a) and consequently increase its impact on Arctic landscapes. However, their effect on SOC storage and coastal erosion has been studied fractionally (e.g. Lantuit and Pollard, 2008; Pizano et al., 2014).

1.2 Study area

The Yukon Coast is approximately 280 km long and is stretching from the Mackenzie Delta to the Alaskan border. The area was partly glaciated during the Quaternary by a lobe of the Laurentide Ice Sheet (Mackay, 1959; Rampton 1982) and the area is for this reason predominantly covered with glacial sediments. Other sediments are of lacustrine, fluvial and glaciofluvial origin. Sediments are mainly composed of a fine-grained mixture of clay and silt, with pebbles and cobbles occurring in moraines (Bouchard, 1974; Rampton, 1982). Permanently frozen deposits are unconsolidated and contain considerable amounts of ground ice (Pollard, 1990).

Mean annual air temperature in the study area is −11.0°C with an average July maximum of 7.8°C. Mean annual precipitation ranges between 150 and 250 mm (Environment Canada, 2000) and is roughly equally shared between rain and snow. The coastal waters are ice-covered for 8 to 9 months of the year, with a complete sea-ice cover from mid-October through June (Solomon, 2005). Permafrost is continuous with a mean annual ground temperature of -8 °C at zero amplitude depth and active-layer depths range between 40 and 60 cm (Burn and Zhang, 2009).

Herschel Island is located in the western part of the Yukon Coastal Plain and was formed as ice-thrust moraine (Mackay, 1959). It is for this reason characterised by abundant massive ground ice that is predominantly of glacial origin (Fritz et al., 2011). Backshore elevations range from a few metres to 30 m and exceed 50 m only on Herschel Island and Kay Point. The coastline is characterised by numerous ALDs and RTSs (Lantuit and Pollard, 2008). Solifluction and smaller ALDs are also common in the interior of Herschel Island. The abundance of this mass wasting phenomena in unconsolidated and ice-rich sediments makes the Herschel Island and Yukon Coastal Plain ideal locations to study the effect of mass wasting on permafrost landscapes.

1.3 Aim and objectives

The amount and fate of mobilised organic carbon by permafrost thaw and coastal erosion are uncertain due to: (1) amounts and pathways of stored organic carbon remain unresolved partly due to uncertainties in carbon-storage estimates (Hugelius, 2014). (2) The erosion of permafrost coasts can be very rapid, but the factors controlling the behaviour of erosion are poorly understood and the consequent sediment release of carbon and nutrients is highly uncertain (Lantuit et al., 2013).

In order to address these two knowledge gaps, the aim of this thesis is to assess the influence of mass wasting on carbon storage and permafrost coastal erosion in a ground ice-rich permafrost landscape. The specific objectives are:

- to assess the effect of terrain and mass wasting on SOC and total nitrogen storage on Herschel Island,
- to identify short-term geomorphic events along the Yukon Coast and on Herschel Island and to assess their influence on coastline movement, and
- to compare planimetric and volumetric coastal erosion characteristics on Herschel Island and to identify the role of mass wasting for the difference between both erosion types.

1.4 Thesis organisation

This dissertation is organized as a cumulative thesis in accordance with the "Guidelines for cumulative PhD thesis on the Institute of Earth and Environmental Science" (Richtlinien für die Anfertigung einer publikationsbasierten Dissertation in den Lehreinheiten Geoökologie und Geowissenschaften) that were published in September 2014. It consists of three manuscripts that were accepted for publication or are accepted for review in international peer-reviewed ISI journals.

Manuscript No. 1 deals with SOC and nitrogen on Herschel Island and their dependence on terrain and mass movement. It was accepted for publication in the journal "Permafrost and Periglacial Processes". Manuscript No. 2 is a study about short-term geomorphic processes along the Yukon Coast and on Herschel Island. It was submitted to the journal "Geomorphology" and is currently under review. Manuscript No. 3 examines the differences between planimetric and volumetric coastal erosion on Herschel Island. It is under review in the journal "Polar Research". All three manuscripts are dealing with the aspect of mass wasting in permafrost landscapes of the Canadian Arctic, which is bound together in this thesis.

1.5 Contributions of authors

Manuscript No. 1 authors: Jaroslav Obu, Hugues Lantuit, Isla Myers-Smith, Birgit Heim, Juliane Wolter and Michael Fritz.

H. Lantuit, M. Fritz and I. Myers-Smith provided guidelines and help with the framework of the paper. Selection of representative sites, coring coordination and vegetation survey was carried out by M. Fritz, I. Myers-Smith and J. Wolter. B. Heim provided useful advices regarding processing satellite imagery. J. Obu carried out laboratory analyses, satellite imagery processing, spatial analyses and wrote the manuscript with the input from all co-authors.

Manuscript No. 2 authors: Jaroslav Obu, Hugues Lantuit, Guido Grosse, Frank Günther, Torsten Sachs, Veit Helm and Michael Fritz.

H. Lantuit, G. Grosse, F. Günther and M. Fritz provided guidelines and help with the framework of the manuscript. T. Sachs and V. Helm carried out the acquisition and processing of the LIDAR dataset and digital elevation model. J. Obu carried out all GIS and statistical analyses and wrote the manuscript with the input from all co-authors.

Manuscript No. 3 authors: Jaroslav Obu, Hugues Lantuit, Michael Fritz, Wayne H. Pollard, Torsten Sachs and Frank Günther.

H. Lantuit, F. Günther, W.H. Pollard and M. Fritz provided guidelines and help with the framework of the manuscript. T. Sachs carried out the acquisition and processing of LIDAR dataset and digital elevation model. J. Obu carried out all satellite imagery processing, coastline digitalisation, GIS analyses and wrote the manuscript with the input from all co-authors.

2 Manuscript #1 – Effect of terrain characteristics on soil organic carbon and total nitrogen stocks in soils of Herschel Island, western Canadian Arctic

Jaroslav Obu[1,2], Hugues Lantuit[1,2], Isla Myers-Smith[3], Birgit Heim[1], Juliane Wolter[1,2] and Michael Fritz[1]

[1]Department of Periglacial Research, Alfred Wegener Institute Helmholtz Centre for Polar and Marine Research, Telegrafenberg A43, 14473 Potsdam, Germany

[2]Institute of Earth and Environmental Science, University of Potsdam, Am Neuen Palais 10, 14469 Potsdam, Germany

[3]School of GeoSciences, University of Edinburgh, West Mains Road, Edinburgh EH9 3JN, United Kingdom

Accepted for publication: 30 September 2015 in Permafrost and Periglacial Processes journal.

Abstract

Permafrost landscapes experience different disturbances and store large amounts of organic matter, which may become a source of greenhouse gases upon permafrost degradation. We analysed the influence of terrain and geomorphic disturbances (e.g. soil creep, active-layer detachment, gullying, thaw slumping, accumulation of fluvial deposits) on soil organic carbon (SOC) and total nitrogen (TN) storage using 11 permafrost cores from Herschel Island, western Canadian Arctic. Our results indicate a strong correlation between SOC storage and topographic wetness index. Undisturbed sites stored the majority of SOC and TN in the upper 70 cm of soil. Sites characterised by mass wasting showed significant SOC depletion and soil compaction, whereas sites characterised by accumulation of peat and fluvial deposits store SOC and TN along the whole core. We upscaled SOC and TN to estimate total stocks using ecological units determined from vegetation composition, slope angle, and geomorphic disturbance regime. The ecological units were delineated with supervised classification based on RapidEye multispectral satellite imagery and slope angle. Mean SOC and TN storage for the uppermost 1 m of soil on Herschel Island are 34.8 kg C m^{-2} and 3.4 kg N m^{-2}, respectively.

2.1 Introduction

Landscapes underlain by permafrost are favourable environments for organic matter accumulation (Hobbie et al., 2000). Annual ground temperatures below 0ºC coupled with impeded drainage result in low organic matter degradation rates and long-term carbon storage (Bockheim, 2007; Hugelius et al., 2014). Increased Arctic air and ground temperatures enhance permafrost thaw and deepen the active layer (Romanovsky et al., 2010). This warming could transform carbon sinks into sources (Schuur et al., 2009) and release old soil carbon into the atmosphere as carbon dioxide or methane (Zimov et al., 2006). Another important greenhouse gas is nitrous oxide, which can be produced by nitrification and denitrification of activated organic compounds (Ciais et al., 2014). Increased atmospheric concentrations of these greenhouse gases and further increases of air temperatures could lead to "permafrost carbon feedback" (Schaefer et al., 2014). Nitrogen is also considered as a limiting nutrient in northern ecosystems (Shaver and Chapin, 1980) and plays an important role and carbon cycling (Harden et al., 2012). Organic carbon and nitrogen can also be released through coastal erosion and river discharge (Lantuit et al., 2012a; Vonk et al., 2012), impacting aquatic and marine ecosystems (Jones et al., 2005; Frey et al., 2007).

Greenhouse gas and lateral organic carbon and nitrogen fluxes originating from thawed permafrost soil organic matter have not yet been incorporated into global climate projections (Kuhry et al., 2010; Schaefer et al., 2014). Their incorporation is hindered by uncertainties in the amount of soil carbon and nitrogen in a soil profile (Koven, 2013; Burke et al., 2013). Recent global estimates of soil organic carbon (SOC) stocks in permafrost areas range between 1100 and 1500 Pg, and around 472 Pg for the 0-1 m depth only (Tarnocai et al., 2009; Hugelius et al., 2013b, 2014). There is no comparable circum-Arctic estimate for nitrogen stocks. Studies of SOC stocks in permafrost regions use a simple upscaling strategy, averaging values from individual pedons to landscape units (Hugelius and Kuhry, 2009; Hugelius et al., 2010, 2011), geomorphic units (Ping et al., 2011; Zubrzycki et al., 2013), or units derived from the Normalised Difference Vegetation Index (NDVI) (Horwath Burnham and Sletten, 2010). In contrast to estimations of SOC stocks, regional studies of total nitrogen TN stocks in permafrost regions are scarce (Ping et al., 2011; Harden et al., 2012; Zubrzycki et al., 2013).

Disturbances such as fires, permafrost thaw, and anthropogenic activities influence SOC and TN storage in permafrost landscapes (Harden et al., 2000; Turetsky et al., 2002; Myers-Smith et al., 2007; O'Donnell et al., 2011). Geomorphic disturbances can also influence SOC and TN storage. Mass wasting can result in material removal and exposure of lower soil horizons to subaerial processes, which causes altered soil moisture regime and permafrost degradation (Kokelj and Lewkowicz, 1999). Grosse et al. (2011) discussed the possible effect of active-

layer detachments, thermal erosion gullies, and retrogressive thaw slumps (RTSs) on permafrost degradation. Studies of the effect of slow mass wasting (e.g. solifluction) on SOC and TN are lacking. Geomorphic disturbance can, however, also lead to material accumulation, thereby increasing storage through riverine sedimentation (Zubrzycki et al., 2013) or peat accumulation (Botch et al., 1995). In our study, mass wasting is considered to encompass a wide range of processes, from slow solifluction and stream gullying to rapid active-layer detachments and retrogressive thaw slumping. In order to better estimate changes in carbon and nitrogen fluxes caused by permafrost disturbance and thaw, more accurate storage assessments and a better understanding of the role of geomorphic disturbances are required.

The present study addresses the knowledge gaps identified above by testing the hypotheses that: 1) terrain significantly influences SOC and TN storage on Herschel Island; and 2) mass wasting here significantly reduces SOC and TN storage. Our aim is to improve knowledge about processes affecting SOC and TN storage in permafrost environments. Our objectives are: 1) to compile a high-resolution estimate of SOC and TN storage for Herschel Island (Yukon Territory, Canada), a location known for a diverse terrain and large number of mass movements (Lantuit and Pollard, 2008); and 2) to assess the influence of terrain and geomorphic disturbance on SOC and TN storage.

2.2 Study Area

Herschel Island is located at 69°34'N and 138°55'W in the Beaufort Sea off the northwestern mainland Yukon Coast (Canada), 60 km east of the Alaskan border. The island measures 13 x 15 km and covers an area of 110 km^2 (Figure 2.1). The mean annual air temperature is -9°C and daily averages rise above 5°C in July and August (Burn, 2012). Yearly precipitation is between 150 and 200 mm. Due to strong winds, snow is blown from higher ground and accumulates in snow beds in low-lying parts of the landscape (Burn, 2012). Herschel Island is a push moraine formed by the Laurentide Ice Sheet (Bouchard, 1974; Fritz et al., 2012). The island is made of unconsolidated and mostly fine-grained marine sediment and is characterised by abundant massive ice of glacial origin (Bouchard, 1974; Pollard, 1990; Fritz et al., 2011). Permafrost is continuous, with a mean annual ground temperature of -8 °C at the depth of zero amplitude depth at Collinson Head. Active-layer depths normally range between 40 and 60 cm depending on topography (Burn and Zhang, 2009).

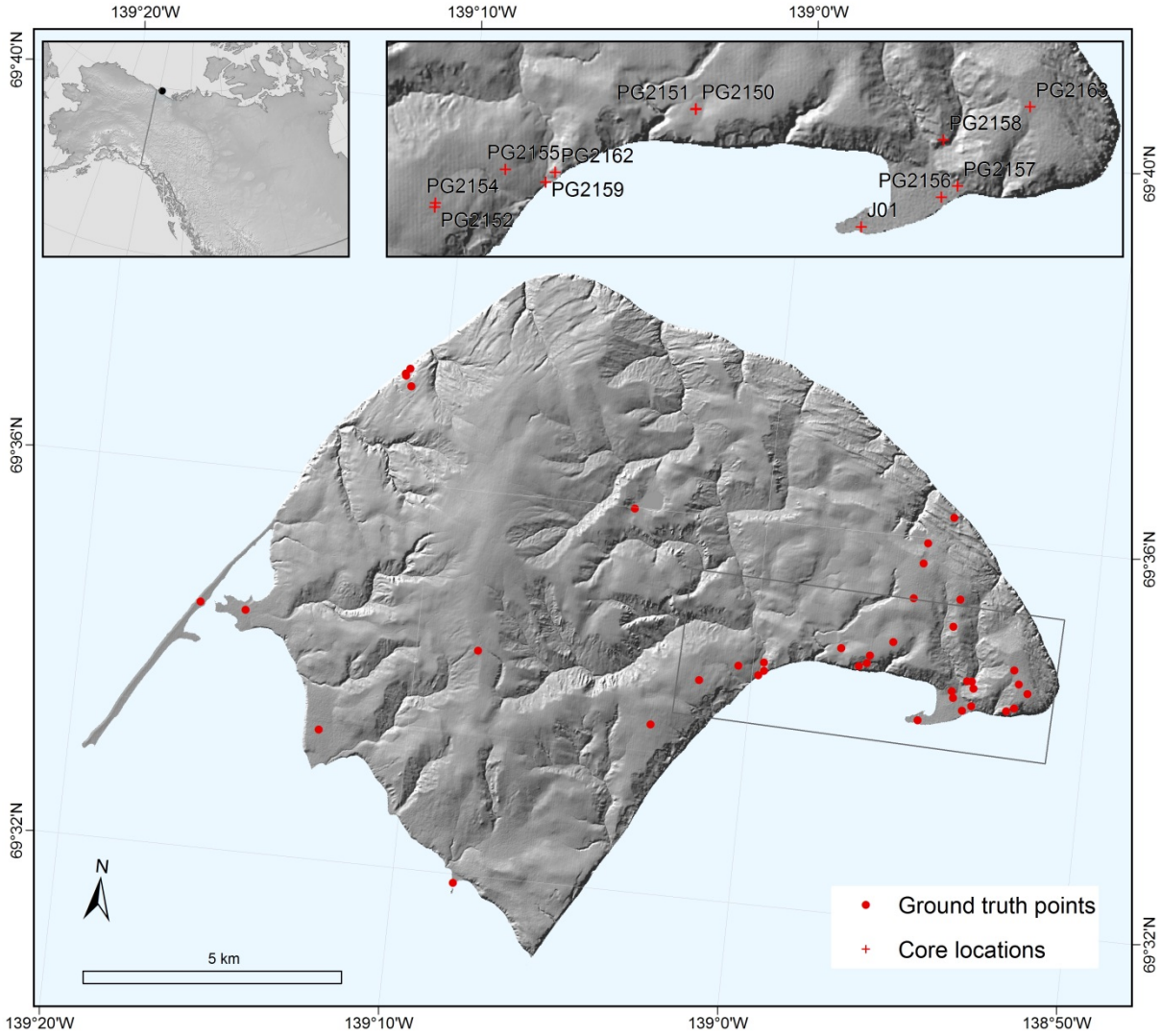

Figure 2.1: Overview map of Herschel Island with ground truth points used for supervised classification. The upper left panel shows the location of Herschel Island. The upper right panel, whose area is delineated by the rectangle in the lower main figure, shows the coring sites.

Herschel Island rises to a maximum height of 180 m above sea level (a.s.l.). Its undulating topography is cut by numerous valleys and gullies. Gully walls often lack vegetation and are undergoing strong geomorphic disturbance. A number of gullies end in alluvial fans. Wet polygonal terrain is present on flatter ground and in enclosed depressions. Slopes are characterised by mass movements ranging from slow solifluction to rapid active-layer detachments (Figure 2.2). Beaches are characterised by high bluffs or spits. The coastline is often disturbed by RTSs that form because ground-ice-rich headwalls wear back laterally (Lantuit et al., 2012b). Coasts experience high rates of erosion (Lantuit and Pollard, 2008).

Soils on Herschel Island were classified according to the Canadian system of soil classification (Canada Soil Survey Committee, 1978). Organic Cryosols predominate and other soil types are present only on beaches and spits which are not underlain by near-surface permafrost (Smith et al., 1989). The most typical subtypes are Turbic Cryosols, characterised by cryoturbation, and Static Cryosols, characterised by recent disturbance. Soils that are not underlain by permafrost are either Regosols or Brunisols (Smith et al., 1989). The general vegetation type on Herschel Island is lowland tundra (Myers-Smith et al., 2011). Smith et al. (1989) defined eight ecological units on Herschel Island (Table 2.1), based on the vegetation, soil characteristics and geomorphic disturbance.

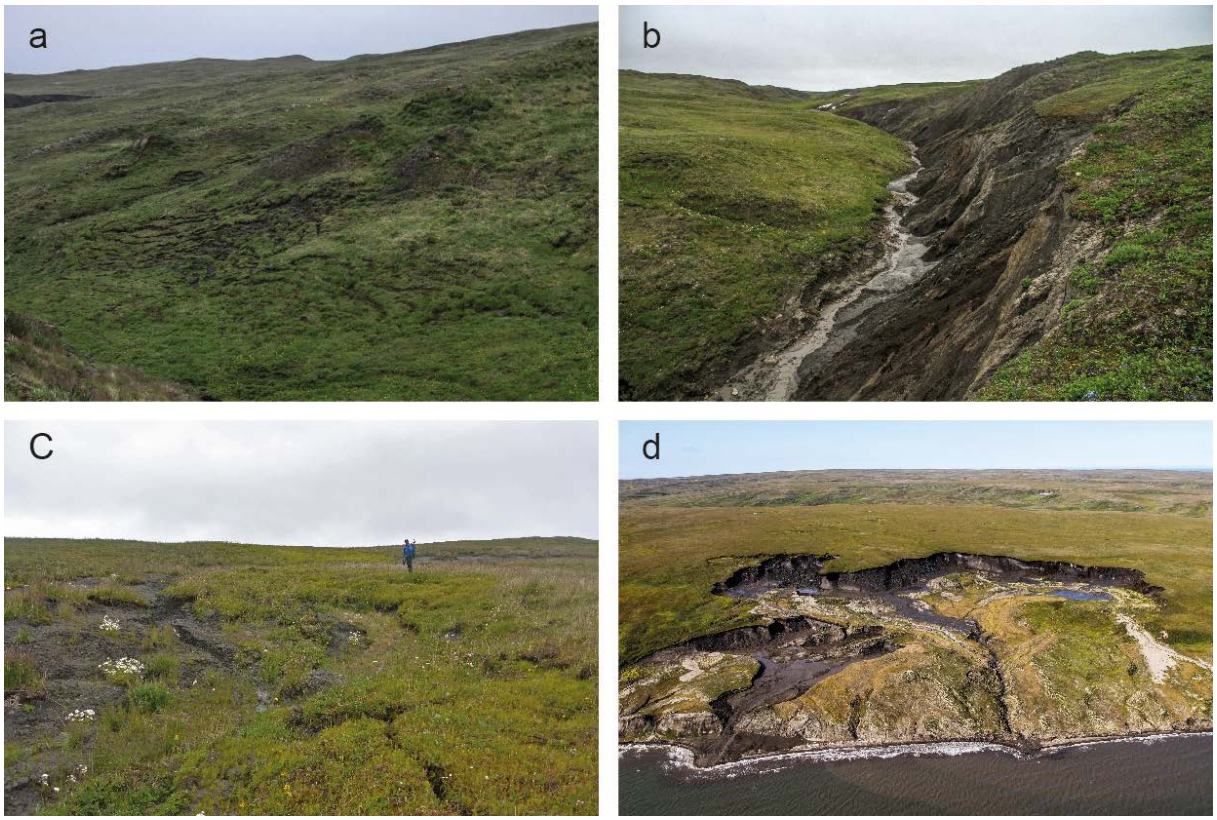

Figure 2.2: Examples of mass wasting on Herschel Island: (a) solifluction, (b) gullying, (c) active layer detachment, and (d) retrogressive thaw slumping.

Table 2.1: Basic properties of ecological units according to the field survey and Smith et al. (1989). The slope angle values in parentheses represent observed range.

Ecological unit	Name defined by Smith et al. (1989)	Topography	Geomorphic disturbance	Slope (°)	Dominant soil type	Typical vegetation
Spits and Beaches	Avadlek	beaches, spits, and other coastal accumulation forms	interchanging coastal sediment accumulation and erosion	1 (0-1)	Regosolic Static Cryosol	*Leymus mollis, Saxifraga,* and *Petasites*
Wet Polygonal Terrain	Guillemot	Level and depressional ice-wedge polygonal terrain	frost cracking and peat accumulation	2 (0-3)	Gleysolic Turbic Cryosol	*Eriophorum* and Bryophytes in drier areas (polygon rims) and *Carex* and Bryophytes in wettest areas.
Hummocky Tussock Tundra	Herschel	flat to gently sloping uplands with distinctive hummocks	absent	1 (0-4)	Orthic Turbic Cryosol	*Eriophorum* tussock tundra
Slightly Disturbed Uplands	Komakuk	gently sloping uplands to gentle slopes	slow downslope movements and gelifluction	4 (0-6)	Orthic Turbic Cryosol	*Salix arctica, Dryas integrifolia* and Fabaceae
Alluvial Fans	Orca	alluvial fans and other riverine sediment accumulations	fluvial accumulation	2 (1-6)	Regosolic Static Cryosol	*Salix richardsonii* shrub vegetation
Moderately Disturbed Terrain	Plover and Jaeger	complex slopes with unvegetated patches	moderate downslope movements, gullying and active layer detachments	5 (2-18)	Regosolic Static Cryosol	*Salix, Dryas,* Fabaceae, *Saxifraga, Petasites,* and a range of other taxa
Strongly Disturbed Terrain	Thrasher	steep slopes, cliffs, and retrogressive thaw slumps	strong gullying, active coastal erosion, slumping and other mass wasting	15 (8-26)	Regosolic Static Cryosol	Sparsely vegetated with *Salix arctica, Lupinus, Myosotis, Senecio*

Table 2.2: : Main site and core properties for cores retrieved on Herschel Island. The core locations are indicated in Figure 2.1. Ecological unit names in brackets were defined by Smith et al. (1989). The paleo-active layer depth was deducted from cryostructures below thaw depth. No. of samples indicate the number of sub-samples in a core or pit. Thaw depth was observed between 8 and 23 July 2013.

Core/pit name	Ecological unit name	Latitude (°)	Longitude (°)	Elevation (m)	Slope angle (°)	Slope exposition (°)	Total sampling depth (cm)	Observed thaw depth (cm)	Paleo-active layer depth (cm)	NDVI	SOC storage 1 m (kg m^{-2})	TN storage 1 m (kg m^{-2})	No. of samples
J01	Spits and Beaches (Avadlek)	69.56841	-138.91560	1	0	-1	40	40	> 40	0.33	5.5	0.2	8
PG2150	Wet Polygonal Terrain (Guillemot)	69.57957	-138.95726	26	0	-1	218	15	27	0.62	91.0	1.5	12
PG2151	Wet Polygonal Terrain (Guillemot)	69.57952	-138.95734	23	0	-1	250	31	63	0.60	78.9	1.0	13
PG2152	Hummocky Tussock Tundra (Herschel)	69.57148	-139.02565	57	2	70	63	34	49	0.60	45.0	0.9	5
PG2154	Hummocky Tussock Tundra (Herschel)	69.57184	-139.02545	57	2	70	198	18	19	0.67	33.9	0.5	12
PG2155	Slightly Disturbed Uplands (Komakuk)	69.57467	-139.00703	32	1	135	197	31	52	0.57	36.5	1.0	13
PG2156	Alluvial Fans (Orca)	69.57082	-138.89462	5	1	12	227	49	60	0.63	39.5	0.9	13
PG2157	Moderately Disturbed Terrain (Plover+Jaeger)	69.57179	-138.89030	15	7	158	190	46	67	0.68	28.3	0.6	12
PG2158	Strongly Disturbed Terrain (Thrasher)	69.57600	-138.89360	50	9	154	143	77	98	0.35	56.6	1.5	8
PG2159	Alluvial Fans (Orca)	69.57340	-138.99677	2	5	277	200	28	43	0.74	16.3	1.0	12
PG2162	Moderately Disturbed Terrain (Plover+Jaeger)	69.57426	-138.99422	40	8	270	70	70	> 70	0.59	11.9	0.2	6
PG2163	Hummocky Tussock Tundra (Herschel)	69.57871	-138.87083	93	4	203	230	33	46	0.69	20.9	0.6	14

2.3 Methods

2.3.1 Fieldwork and sampling

Study sites were selected to be representative of each of the ecological units (Table 2.1). We used these units as the basis for upscaling of SOC and TN content and site grouping according to geomorphic disturbance. The names of the units defined by Smith et al. (1989) are based on local landmarks or fauna. We adapted these unit names to landscape and terrain characteristics in order to enable comparison with units from other areas in the Arctic with similar characteristics.

In July 2013, we cored 11 locations (Table 2.2). At each location, a detailed terrain and vegetation survey was undertaken to characterise the ground surface. A pit was dug until the thaw depth was reached. Cores were drilled to a depth of 60 – 250 cm below the surface with a Snow, Ice, and Permafrost Research Establishment (SIPRE) permafrost coring auger barrel drill (manufactured in Jon's Machine Shop, Fairbanks, Alaska) with an inner diameter of 7.5 cm and equipped with a Stihl BT 121 engine. Where thaw depth exceeded 70 cm, a pit was dug and no permafrost core was taken because of the difficulty of digging and setting up the coring equipment. We drilled at least one core in each ecological unit, obtaining ten cores and digging two pits. The uppermost metre of the pit or core was sampled every 10 cm; below 1 m depth we sampled every 20 cm. Sampling depths were adapted to visible changes in facies or cryostructure. We obtained 7.5x7.5x5 cm samples from the active layer. Permafrost core samples were 5 cm thick and 7.5 cm in diameter.

2.3.2 Laboratory analyses

The 128 samples obtained were weighed to determine wet weight, freeze dried at -20 °C in a vacuum, and reweighed to determine dry weight. They were then ground, mixed and milled for elementary analyses, and subsampled for further analyses. Samples were separately analysed for carbon and nitrogen content in an Elementar vario EL III and for total organic carbon content using an Elementar vario MAX C manufactured by Elementar Analysensysteme GmbH, Hanau, Germany.

2.3.3 Ecological unit mapping

Ecological units were mapped from remotely-sensed imagery and a digital elevation model (DEM) using a supervised classification. The units were defined based on terrain properties, soil types, and vegetation, and thus are suitable for the study of soil properties in relation to geomorphic processes. A cloud-free and almost snowpack-free RapidEye satellite acquisition on August 15th 2010 was selected to map the units. The RapidEye image is multispectral and

has a horizontal resolution of around 6.5 m at nadir. The image was georeferenced based on ground control points taken from Lantuit and Pollard (2008) and orthorectified using a DEM derived from an IKONOS stereopair. The DEM itself was resampled from 2 m resolution to 6.5 m resolution with cubic convolution to fit to the resolution of the RapidEye image. Small artefacts (parallel stripes) were removed from the DEM dataset using a 4x4 round average filter. Preliminary results showed that SOC content correlates well with slope angle and for this reason it was added to the classification. The slope angle layer at 6.5 m resolution was calculated from the DEM. An atmospheric correction (Atmospheric and Topographic Correction (ATCOR) module in PCI Geomatica 2013) (Richter, 1996) was applied to the RapidEye image to calculate the surface reflectance values and remove the effects of low sun angle and shading.

Areas surveyed in the field were used as training units for the supervised classification. The terrain was inspected visually for vegetation and terrain properties to correctly assign the sites to the ecological units. The area boundaries were mapped in the field with a handheld Garmin Etrex H GPS. We added additional areas that we delineated on the basis of satellite imagery for the areas that had been identified during helicopter surveys (spits, alluvial fans, and polygons). In total, 21 areas were used as training units for supervised classification. An additional training unit was added to identify water bodies and separate them from the classification results. A slope layer was added as a new input band to improve the classification results.

The maximum likelihood supervised classification of the RapidEye image and slope angle added as an additional layer was performed in Exelis ENVI 5.0 (Environment for Visualizing Images) (ENVI, 2008). The result was post-processed by sieving in ENVI and by using a 4x4 circle majority filter and boundary-clean tools in ESRI ArcGIS 10.1 (ESRI, 2012) to remove isolated pixels and incorporate small unit areas into adjacent and prevalent units. The classification accuracy was assessed using ground truth points. We used coring locations and vegetation survey locations from the previous fieldwork of Myers-Smith et al. (2011). Additionally, we used ground truth points collected from other parts of the island by previous expeditions (e.g. Lantuit et al., 2012b). Photographs and vegetation data collected at the survey sites during these expeditions were inspected and assigned to an ecological unit. A total of forty ground truth points was collected to assess the classification accuracy (Figure 2.1).

2.3.4 Upscaling of SOC and TN contents

SOC and TN contents were calculated using gravimetric contents of total organic carbon (TOC) and TN in the samples. The dry bulk density was calculated using the dry weight and the volume of samples. Volumetric TOC and TN contents (kg C m^{-2} and kg N m^{-2}, respectively) were then calculated for one centimetre sample thickness (cm m^2) using the following equations:

$$SOC = cOC \times \rho \quad (2.1)$$

$$TN = cN \times \rho \quad (2.2)$$

Where cOC and cN are gravimetric contents of organic carbon and nitrogen in weight fraction and ρ is dry bulk density in g cm^{-3}. The coarse grain-size fraction (particles > 2mm) was not included in the calculations because it was either absent or present in negligible amounts. SOC and TN contents from the samples were extrapolated to apply to adjacent parts of the core that were not sampled; extrapolation extended half of the distance to the next sample along the core. The total contents of SOC and TN (in kg C m^{-2} and kg N m^{-2}, respectively) in a core were calculated by summing the content of each centimetre of the core. The values were calculated for three different depth ranges: 0-30 cm (SOC 0-30cm and TN 0-30cm), 0-1 m (SOC 0-100 cm and TN 0-100 cm), and 0-2 m (SOC 0-200 cm and TN 0-200 cm). In shorter cores, the value of the lowermost sample was extrapolated downwards. Cores and pits that did not exceed 1 m were J01, PG2152 and PG2162. Core PG2158 reached 143 cm. Extrapolation of SOC and TN for 0-2 m is less certain for these cores.

Core values were averaged across the cores for ecological units with more than one core; otherwise, the value of the single core was assigned to the ecological unit. These values were multiplied by cell area and numbers of cells from the classification to calculate stocks of SOC and TN for ecological units and for the whole island. Carbon to nitrogen (C/N) ratios for the ecological units were calculated from upscaled unit-specific SOC and TN values. We used the SOC and TN content of the uppermost metre of soil in further statistical analyses, which is standard in SOC stock quantifications (e.g. Tarnocai et al., 2009).

2.3.5 Assessing the role of terrain on site SOC and TN storage

We assessed the role of terrain on SOC and TN storage on Herschel Island by correlating them to environmental variables such as slope, soil moisture, topographical wetness index (TWI), elevation and NDVI. Geomorphic disturbance is not a linearly measurable variable because it encompasses both accumulation and mass wasting. For this reason we divided the sites into three groups according to the prevalent geomorphic processes (Table 2.1): 1) undisturbed sites (showing little or no evidence for accumulation or mass wasting; Slightly

Disturbed Uplands and Hummocky Tussock Tundra units), 2) mass wasting sites (evidence of recent or past downslope movements; Strongly and Moderately Disturbed Terrain units), 3) and accumulation sites (fluvial and peat accumulation; Alluvial Fans and Wet Polygonal Terrain units).

We related slope angle, elevation, moisture content, TWI and NDVI to SOC and TN storage in the uppermost 1 m of soil using univariate statistics. Slope angle and elevation were measured on site. TWI and NDVI site values were extracted from raster layers (Table 2.2). TWI was calculated as defined by Beven and Kirkby (1979) with upslope area calculated based on the D8 flow direction algorithm. TWI was calculated from the same DEM used for supervised classification. NDVI is a remote-sensing-derived proxy indicative of vegetation greenness and was calculated from the red and near-infrared bands of Rapid Eye imagery. The gravimetric soil moisture content was calculated from sample wet and dry mass on a wet soil basis and upscaled to cores using the same procedure as for SOC and TN contents. Slope angle, degree of disturbance, and elevation were measured in the field.

The Shapiro–Wilk test was used to test the normality of distributions. Pearson's correlation coefficients were calculated and linear regression analysis was used to calculate R-squared values in order to estimate the amount of variance within SOC and TN that is explained by the environmental variables. P-values were corrected with “False discovery rate correction” to account for any auto-correlation effects. Differences between geomorphic disturbance groups were tested with a student’s t-test. All statistical analyses were calculated using the R software (version 3.0.1). The pit from the Spits and Beaches unit was omitted from the correlation analysis because it is strongly influenced by marine processes that are not a subject of our study.

2.4 Results

2.4.1 Relation between geomorphic disturbance and site SOC and TN storage

Slope angle, TWI and moisture content were significantly correlated with SOC 0-100 cm (Figure 2.3). The strongest correlation was found between TWI and SOC 0-100 cm ($r = 0.79$, $p = 0.004$). Soil moisture content was also strongly positively correlated with SOC 0-100 cm ($r = 0.69$, $p = 0.020$). Slope angle was strongly negatively correlated with SOC 0-100 cm ($r = -0.68$, $p = 0.023$). Corrected p-values of significant correlations remained within the 95% confidence interval. Elevation ($r = -0.14$, $p = 0.690$) and NDVI ($r = 0.23$, $p = 0.630$) were not significantly correlated with SOC 0-100 cm. We found no significant correlation of any of the studied variables with TN 0-100 cm.

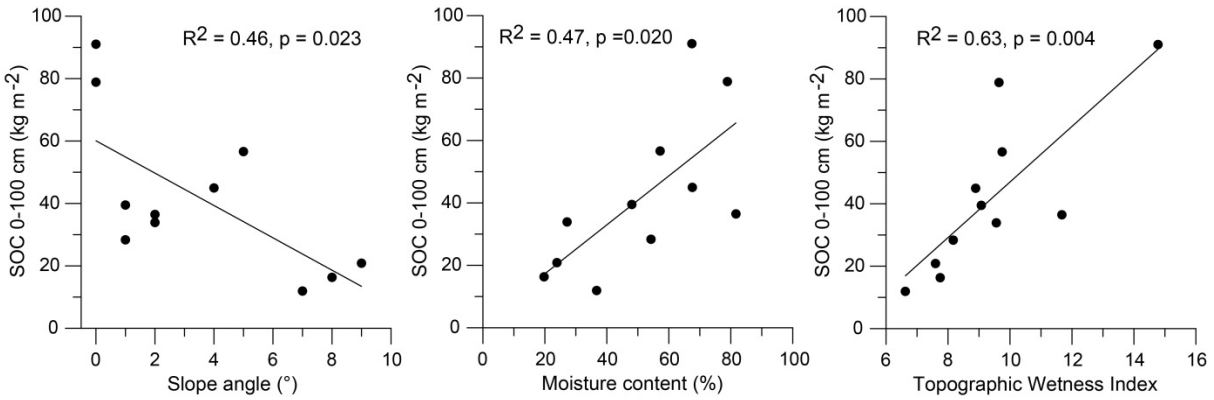

Figure 2.3: SOC 0-100 cm values plotted against slope angle, moisture content and Topographic wetness index with added linear trend line.

The comparison of means for each geomorphic disturbance group showed that SOC 0-100 cm in the mass wasting group differs significantly from undisturbed ($p = 0.002$) and accumulation groups ($p = 0.04$) (Figure 2.4). Group means of SOC 0-100 cm do not differ significantly between the accumulation and undisturbed groups ($p = 0.17$). Group means of TN 0-100 cm are not significantly different (within 95 % confidence interval) between the geomorphic disturbance groups.

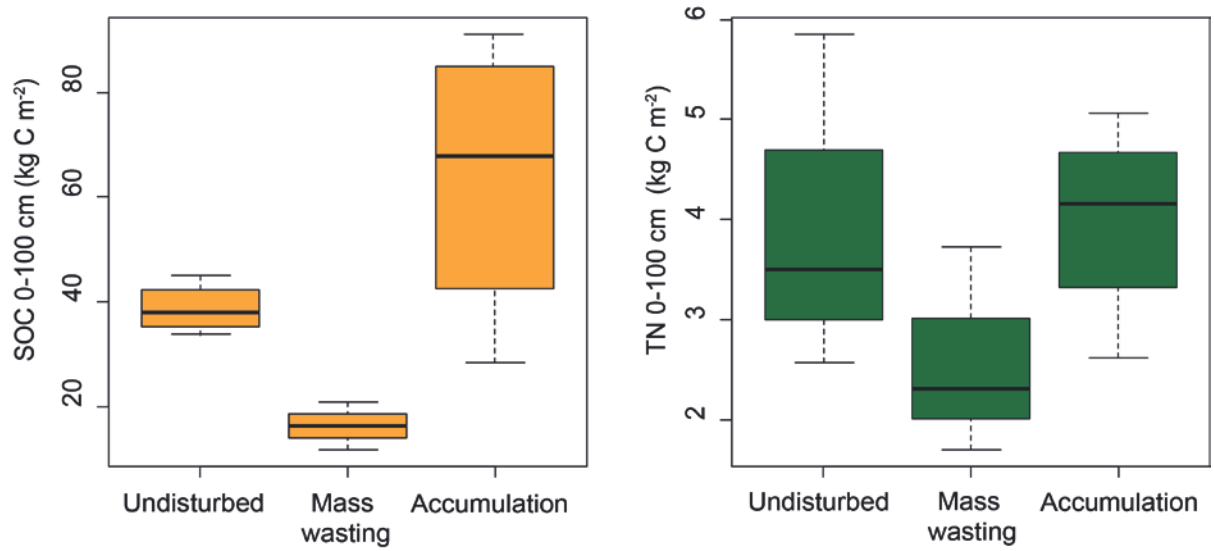

Figure 2.4: Boxplots of core SOC 0-100 cm and TN 0-100 cm storage grouped by geomorphic disturbance. Grouping of sites is described in section 2.3.5.

Down-core trend comparison showed that the majority of SOC and TN in undisturbed sites was stored in the upper 70 cm of the soil (Figure 2.5). Sites characterised by mass wasting showed low SOC contents in the upper profile and very high dry bulk densities below 50 cm depth. Sites undergoing peat and riverine accumulation showed a more homogeneous down-core distribution of SOC and TN storage.

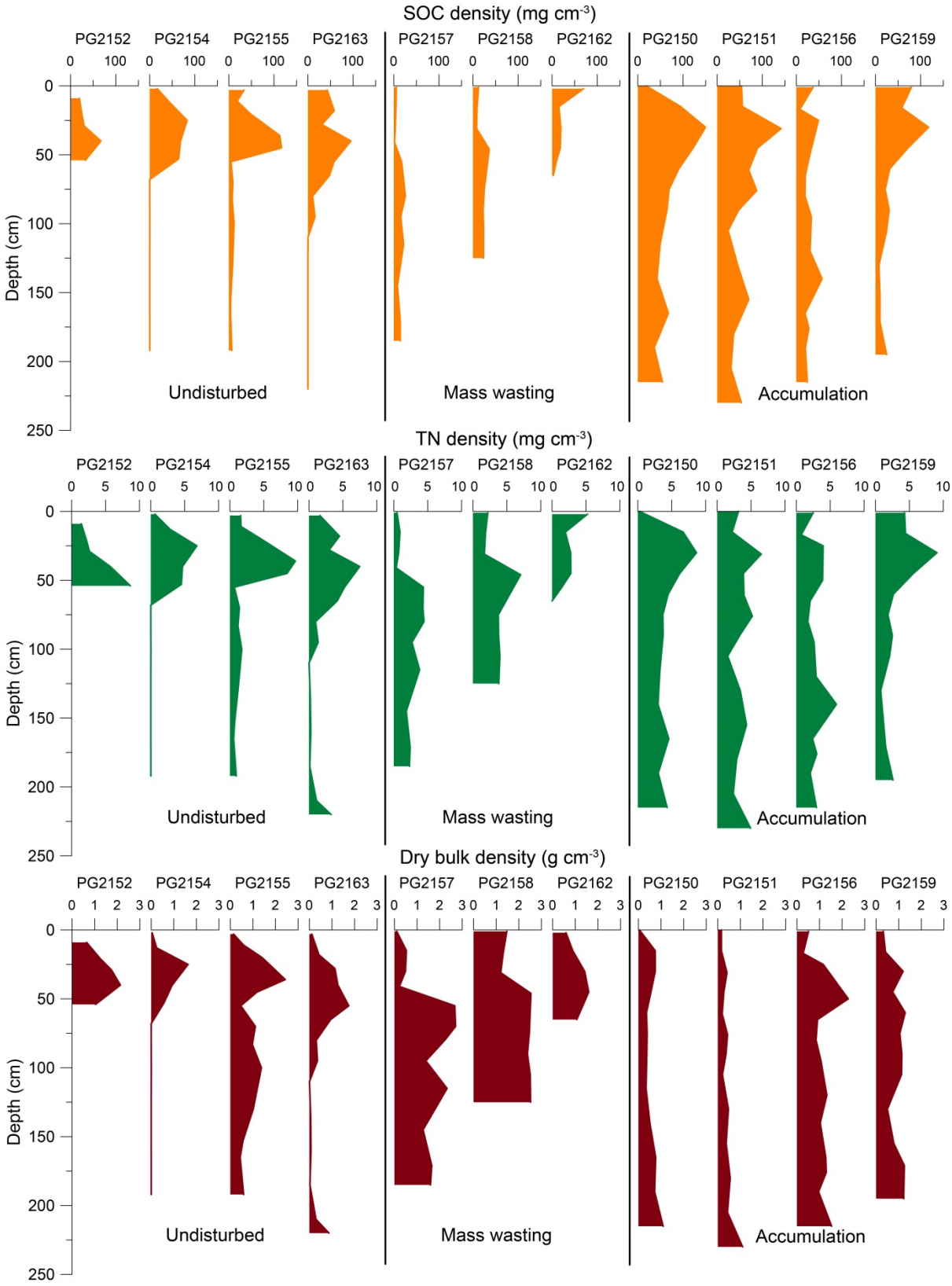

Figure 2.5: Down-core trends for SOC density, TN density and dry bulk density. Cores are grouped according to geomorphic disturbance. Cores PG2154 and PG2163 included an ice wedge ice which is indicated by their low dry bulk density in deeper soil horizons.

2.4.2 Supervised classification

According to our classification of ecological units (Figure 2.6), the Slightly Disturbed Uplands unit occupies the largest area (32 %) of the island, followed by the Hummocky Tussock Tundra (25 %) and the Moderately Disturbed Terrain (22 %) units. The Strongly Disturbed Terrain unit occupies 11 % and the Wet Polygonal Terrain unit occupies 8 %. Spits and Beaches and Alluvial Fans units each occupy 1 % of the total area.

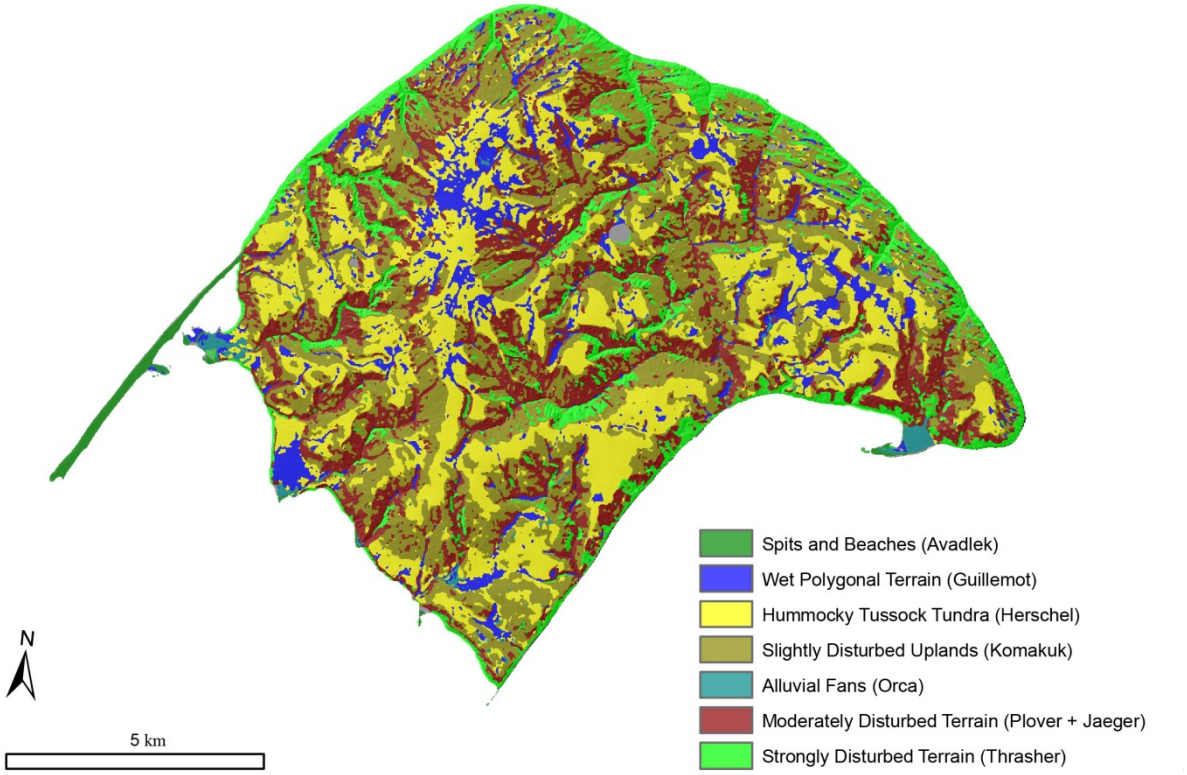

Figure 2.6: Ecological units on Herschel Island. The map is post-processed output of supervised classification. These units were used for upscaling SOC and TN.

The comparison of our ecological classification and ground truth points showed an overall 75 % classification accuracy (Table 2.3) and a kappa index of 0.70. The ecological units for which all ground truth points matched the classification output were Spits and Beaches, Wet Polygonal Terrain, and Strongly Disturbed Terrain. One mismatch each occurred for the Hummocky Tussock Tundra, Alluvial Fans, and Moderately Disturbed Terrain units. Two points out of nine of the Slightly Disturbed Uplands unit were correctly classified. Ground truth points from this unit were close to the unit boundary, which could explain the lack of classification accuracy.

Table 2.3: Contingency table of the classification accuracy between observed (ground truth points) and predicted (classification) ecological units.

Predicted\Observed	Spits and Beaches	Wet Polygonal Terrain	Hummocky Tussock Tundra	Slightly Disturbed Uplands	Alluvial Fans	Moderately Disturbed Terrain	Strongly Disturbed Terrain	Total	User's accuracy (%)
Spits and Beaches	3	0	0	0	0	0	0	3	100.0
Wet Polygonal Terrain	0	3	0	0	0	0	0	3	100.0
Hummocky Tussock Tundra	0	0	7	3	0	0	0	10	70.0
Slightly Disturbed Uplands	0	0	1	2	0	0	0	3	66.7
Alluvial Fans	0	0	0	0	4	0	0	4	100.0
Moderately Disturbed Terrain	0	0	0	2	1	7	0	10	70.0
Strongly Disturbed Terrain	0	0	0	2	0	1	4	7	57.1
Producer's accuracy (%)	100.0	100.0	87.5	22.2	80.0	87.5	100.0		

Table 2.4: SOC, TN storage and C/N ratios for different depth ranges on Herschel Island.

Ecologicl unit	Area (km^2)	SOC storage 0-30 cm ($kg\ m^{-2}$)	SOC storage 0-100 cm ($kg\ m^{-2}$)	SOC storage 0-200 cm ($kg\ m^{-2}$)	TN storage 0-30 cm ($kg\ m^{-2}$)	TN storage 0-100 cm ($kg\ m^{-2}$)	TN storage 0-200 cm ($kg\ m^{-2}$)	C/N ratio 0-30 cm	C/N ratio 0-100 cm	C/N ratio 0-200 cm
Spits and Beaches	1.1	5.5	5.5	5.5	0.2	0.2	0.2	24.6	24.6	24.6
Wet Polygonal Terrain	8.6	22.8	84.9	132.1	1.3	4.6	7.8	18.2	18.6	16.8
Hummocky Tussock Tundra	28.2	11.9	38.4	49.6	0.8	4.0	6.9	14.4	9.6	7.1
Slightly Disturbed Uplands	35.0	10.6	39.5	46.5	0.9	3.4	4.5	12.1	11.5	10.4
Alluvial Fans	1.3	15.5	42.5	66.0	1.1	3.4	5.9	14.2	12.3	11.2
Moderately Disturbed Terrain	24.1	5.8	14.1	22.7	0.6	2.0	3.3	9.9	7.0	6.9
Strongly Disturbed Terrain	12.6	3.0	20.9	44.3	0.6	3.7	7.6	5.2	5.6	5.9
Herschel Island	110.9	10.0	34.8	48.3	0.8	3.4	5.4	12.6	10.4	8.9

2.4.3 SOC and TN storage on Herschel Island

The mean storage of SOC 0-100 cm and of TN 0-100 cm for the entire island is 34.8 kg C m^{-2} and 3.4 kg N m^{-2}, respectively (Table 2.4). The highest SOC value was assigned to the Wet Polygonal Terrain unit, which contains 85 kg C m^{-2} in the uppermost 1 m of soil. The Hummocky Tussock Tundra, Slightly Disturbed Uplands, and Alluvial Fans units had SOC 0-100 cm of around 40 kg C m^{-2}. Slightly lower SOC values were found in the Strongly Disturbed Terrain and Moderately Disturbed Terrain units. The Spits and Beaches unit had the lowest SOC value of 5.5 kg C m^{-2}.

The TN storage generally followed SOC storage patterns, but with smaller differences. TN storage was high in Wet Polygonal Terrain and Hummocky Tussock Tundra (TN 0-100 cm was 4.6 and 4.0 kg N m^{-2}, respectively), lower in disturbed units (TN 0-100 cm 2.0 – 3.7 kg N m^{-2}), and lowest in Spits and Beaches (Figure 2.7 and Figure 2.8). The C/N ratio values were around 10 to 15, except for the Spits and Beaches unit, which had a higher C/N ratio.

Our estimates indicate that there are 3.9 Tg of SOC and 0.4 Tg of TN in the uppermost 1 m of soil on Herschel Island. The Slightly Disturbed Uplands unit had the highest SOC and TN stocks. The Spits and Beaches unit had the lowest SOC and TN stocks. High amounts of SOC and TN were also found in the Hummocky Tussock Tundra, Wet Polygonal Terrain, and Moderately Disturbed Terrain units. Low amounts of SOC and TN were found in the Alluvial Fans and Spits and Beaches units, mostly because of their relatively small spatial extents. The spatial distribution of TN 0-100 cm stocks mostly followed the patterns in SOC stocks.

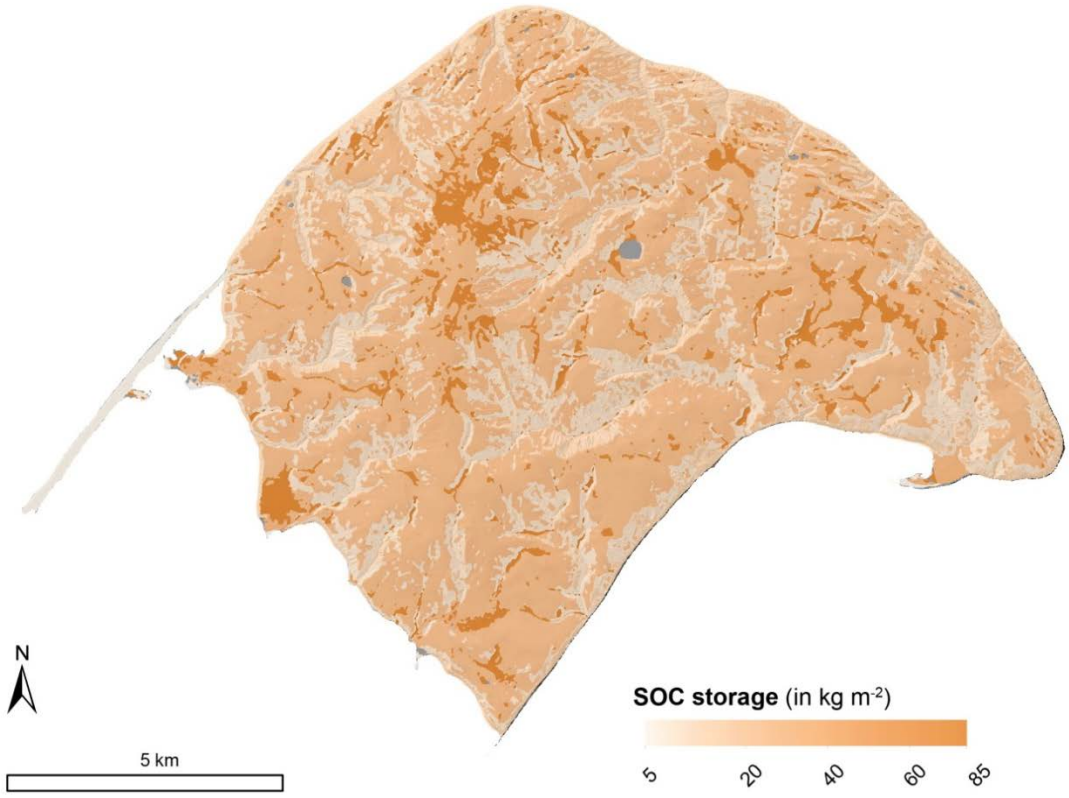

Figure 2.7: Map of SOC storage on Herschel Island for the uppermost metre of the soil. This map is the result of upscaling SOC 0-100 cm values to ecological units in Figure 2.6

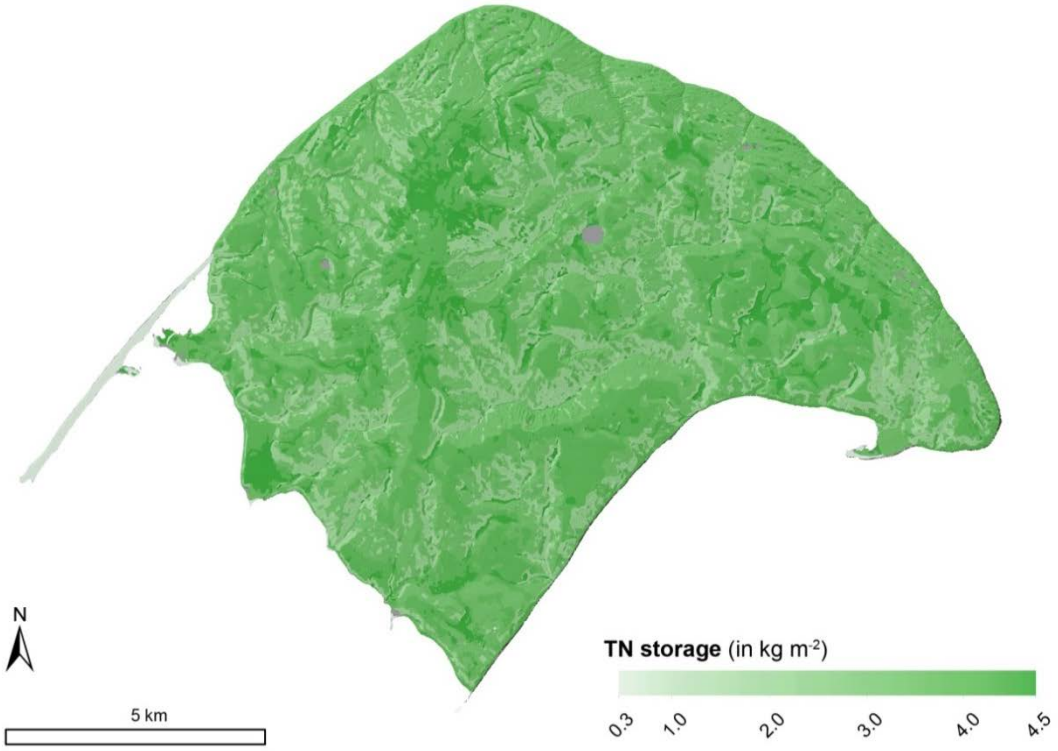

Figure 2.8: Map of TN storage on Herschel Island for the uppermost metre of soil. This map is the result of upscaling TN 0-100 cm values to ecological units in Figure 2.6

2.5 Discussion

Our results based on 11 cores and site data showed an important effect of terrain characteristics on SOC storage. The majority of SOC 0-100 cm is explained by TWI, which reflects the influence of catenary slope position and slope characteristics. Sites that are visually affected by mass wasting show significant depletion of SOC storage. We estimate the mean storage of SOC and TN in the uppermost 1 m of soil on Herschel Island to be 34.8 kg C m^{-2} and 3.4 kg N m^{-2}, respectively, with total stocks in the uppermost 1 m of soil to be 3.9 Tg C and 0.4 Tg N. Such high carbon and nitrogen storage on Herschel Island is comparable to estimates reported for other Arctic regions.

2.5.1 Effects of terrain characteristics on SOC and TN storage

The strong positive correlations between TWI, slope angle and SOC 0-100 cm indicate that terrain has an important influence on SOC storage on Herschel Island. Slope angle affects soil drainage and soil moisture content, which further affects net primary production and decomposition (Birkeland, 1984). TWI is calculated from local upslope area drainage and slope angle and is often used to quantify topographic control on hydrological processes and to predict soil organic matter distribution (Sørensen et al., 2006; Pei et al., 2010). Thus the strong correlation between TWI and SOC 0-100 cm ($R^2 = 0.63$) indicates that the majority of SOC 0-100 cm variability is explained by hydrological conditions related to catenary position and slope characteristics. Ground ice in permafrost, which was included in our moisture content calculation, may explain the weaker correlation between site measured soil moisture and SOC 0-100 cm than expected because of strong correlation between TWI and SOC 0-100 cm.

Hydrological conditions control also the water content in the active layer, and increased pore-water pressures may cause mass wasting (Matsuoka, 2001; Harris et al., 2008; Lewkowicz and Harris, 2005a). Slope angle affects not only soil drainage, but also the intensity of mass wasting (Williams and Smith, 1989). For this reason, the part of SOC 0-100 cm variation that is explained by slope angle and soil moisture, can also be attributed to mass wasting. Comparison between geomorphic disturbance groups revealed that sites with observed mass wasting contained significantly lower amounts of SOC 0-100 cm than undisturbed and accumulation sites (Figure 2.4). These groups included sites showing evidence of active or past mass wasting with various possible movement depths (from few top cm to whole active layer). Lantuit et al. (2012b) analysed the active layer in stabilised RTS areas and undisturbed areas and showed that mass wasting can alter soil moisture regime and consequently SOC storage.

The difference between geomorphic disturbance groups was also well reflected in down-core trends of SOC, TN and dry bulk density (Figure 2.5). High bulk density in mass wasting sites indicates that the material had been compacted by mass-wasting processes, which has also been observed by Lantuit et al. (2012b) on RTS. In two of the mass-wasting sites (PG2157 and PG2158) we found particularly low SOC storage in the upper 50 cm. This might indicate that mass movement such as solifluction and active-layer detachment have decreased SOC storage in these sites. Slightly higher SOC storage deeper in the core could have been caused by compaction. Very small amounts of SOC and TN in the lower parts (below 70 cm) of the cores from undisturbed sites were likely due to dilution effects in ice-rich ground.

Mass wasting may decrease SOC storage by material displacement and exposure of lower layers to aeration and increased microbial activity (Pautler et al., 2010), causing organic matter decomposition and carbon degradation (Koven et al., 2011). Pizano et al. (2014) attributed ¼ of storage loss to aerobic decomposition in material displaced by RTS activity. Mass movements that remove soil cause permafrost thaw and may deepen the active layer. Leaching of particulate organic carbon also has the potential to decrease SOC storage. Woods et al. (2011) demonstrated that dissolved organic carbon delivered from watersheds with slope disturbances is more labile than dissolved organic carbon from undisturbed watersheds. Lamoureux and Lafrenière (2014) demonstrated that slope disturbances can activate old particulate organic carbon from formerly undisturbed watersheds. Repeated mass wasting can also hinder plant growth and thus decrease accumulation of organic matter.

The insignificant correlation between terrain variables and TN 0-100 cm could be the consequence of low nitrogen concentrations and low sample size or could indicate that TN storage is less influenced by terrain than SOC storage. The higher loss of carbon in comparison to nitrogen during organic material decomposition results in decreasing soil C/N ratios with decomposition (Meyers, 1994; Kuhry and Vitt, 1996). C/N ratios for 0-100 cm (Table 2.4) show significantly lower C/N ratios in sites characterised by mass wasting than in other sites. Down-core trends (Figure 2.5) show that mass wasting sites have, in comparison with other sites, significantly lower SOC contents, whereas TN storage is comparable to other sites. This might indicate that mass wasting promotes decomposition and carbon loss, but has a reduced impact on nitrogen storage. Low C/N ratios that we observed on Herschel Island can be explained by the presence of marine algae in organic matter (Meyers, 1994), which originates from the marine sediment that was glacially reworked. C/N ratios below 9 in Strongly and Moderately Disturbed Terrain can be due to abundance of this material exposed by mass wasting. Very low C/N ratios could also result from measured inorganic nitrogen that could have been present in the samples.

Most of the variance in SOC 0-100 cm storage in our study was explained by TWI. Nevertheless, geomorphic disturbances such as mass wasting show an important effect on soil properties and decrease in SOC storage. The effect of mass wasting on SOC storage might increase in the future under a warming climate (Grosse et al., 2011) with increasing retrogressive thaw slumping (Lantz and Kokelj, 2008) and an increase in active-layer detachment activity (Lewkowicz and Harris, 2005a). Continuous and slow mass wasting such as solifluction and soil creep can cause a significant relocation of material across the landscape (Lewkowicz and Clarke, 1998). The effect of this slow, continuous geomorphic disturbance on SOC and TN storage needs to be studied in detail because it is one of the most widespread processes of soil movement in periglacial environments (French, 2013) and the area affected by such disturbances across the circumpolar Arctic is likely much larger than the limited area affected by active-layer detachments and RTSs (Grosse et al., 2011).

2.5.2 Suitability of ecological classification for SOC upscaling

Upscaling SOC to units derived from multispectral satellite imagery is a commonly used procedure in analysis of Arctic landscapes. We found that slope angle is an important determinant of SOC for the diverse terrain of Herschel Island. Adding a slope angle layer to spectral bands of satellite imagery significantly improved the accuracy of our supervised classification of ecological units, and ultimately of SOC estimations. Horwath Burnham and Sletten (2010) used NDVI classes for SOC upscaling in the High Arctic of Greenland. The lack of correlation between NDVI and SOC found in our study suggests that using NDVI would not increase the accuracy of our SOC estimation. Adding information about slope angle, soil moisture and catenary slope position could improve SOC storage estimates in areas with diverse terrain similar to that of Herschel Island.

Our classification accuracy is according to ground truth points agreement (75 %) comparable to accuracies reported from other studies (78 %: Hugelius et al., 2012 and 77 %: Zubrzycki et al., 2013).. The accuracy of our classification was high in Spits and Beaches, Strongly Disturbed Terrain, and Wet Polygonal Terrain units. The units affected by disturbance were characterised by lower accuracy, which likely reflects the transitional nature of these classes observed in the field. These units often change gradually from one into another without a clearly established boundary.

2.5.3 SOC and TN storage and stocks

The SOC and TN storage found in our ecological units is comparable or higher than the storage reported from bog peatlands, shrub tundra and floodplain terraces in similar circum-Arctic studies (Table 2.5). There are no units comparable to our moderately- and strongly-

disturbed units in the literature estimating SOC and TN storage, suggesting that the effect of mass wasting on SOC and TN storage was not included in existing storage estimations.

Table 2.5: Comparing SOC 0-100 cm storage in our ecological units to storage in comparable units from other studies.

Herschel Island		Comparable studies			
Ecological unit	SOC 0-100 cm sorage (kg m^{-2})	Comparable unit in other studies	Study Area	SOC 0-100 cm sorage (kg m^{-2})	Reference
Wet Polygonal Terrain	85	bog peatlands	Central Canadian Arctic Alaska	80 94-82	Hugelius et al. (2010) Michaelson et al. (1996)
Hummocky Tussock Tundra and Slightly Disturbed Uplands	40	shrub tundra	Western Siberia Central Canadian Arctic	10-40 21-40	Hugelius et al. (2011) Hugelius et al. (2010)
Alluvial Fans	42	holocene floodplain terrace	Lena River Delta	30	Zubrzycki et al. (2013)

The mean SOC 0-100 cm storage on Herschel Island is estimated to be 34.8 kg C m^{-2}. Hugelius et al. (2010) calculated a value of 33.8 kg C m^{-2} for the Tulemalu Lake area (central Canadian Arctic) and Hugelius et al. (2011) calculated one of 28.1 kg C m^{-2} for the Usa basin (European Russian Arctic). Zubrzycki et al. (2013) calculated 25.7 kg C m^{-2} for the Holocene part of the Lena River Delta. The same authors reported TN 0-100 cm storage in the Holocene part of the Lena River Delta (northern Siberia) to be 1.1 kg N m^{-2}, which is three times lower than on Herschel Island (3.4 kg N m^{-2}). In general, SOC storage on Herschel Island is similar to values reported in comparable environments elsewhere. In the Northern Circumpolar Soil Carbon Database, Hugelius et al. (2013a) reported 55.3 kg C m^{-2} of SOC 0-100 cm storage for the whole of Herschel Island, which overestimated the SOC 0-100 cm storage by 59 %.

The highest SOC and TN storage in the uppermost 1 m occurs in the Wet Polygonal Terrain unit. This is largely because peat has probably been accumulating in the thermokarst depressions and flat valley bottoms since the beginning of the Holocene (Fritz et al., 2012). In these parts of the landscape, wet anoxic conditions favour the preservation of organic carbon and nitrogen (Hobbie et al., 2000). The second largest SOC and TN storage was observed in slightly disturbed or undisturbed ecological units with mineral soil that has undergone cryoturbation or has been influenced by accumulation of fluvial sediment (Smith et al., 1989).

2.6 Conclusions

We found that terrain has an important influence on SOC storage on Herschel Island. The majority of variance in SOC storage (63 %) was explained by TWI, an indication of catenary position and slope characteristics. We also inferred that sites characterised by different geomorphic disturbances result in different SOC storage. Mass wasting sites showed material compaction and decreased SOC storage, particularly in the upper 50 cm. Increased mass wasting could lead to enhanced mobilization of carbon and nitrogen stocks, which could have

important impacts on both the terrestrial and marine components of this Arctic coastal ecosystem. While studies dealing with decreased SOC and TN in permafrost environments due to mass wasting that occur as single rapid event (e.g. RTS) exist, the importance of slow, continuous mass wasting such as solifluction has not yet been taken into account. We estimated average SOC 0-100 cm and TN 0-100 cm on Herschel Island to be 34.8 kg C m^{-2} and 3.4 kg N m^{-2}. High-resolution studies such as ours will help to improve circum-Arctic storage estimates and projections of future fluxes of carbon and nitrogen with warming.

3 Manuscript #2 – Dynamics of permafrost coasts along the Canadian Beaufort Sea based on annual airborne LIDAR elevation data

Jaroslav Obu[1,2], Hugues Lantuit[1,2], Guido Grosse[1], Frank Günther[1], Torsten Sachs[3], Veit Helm[4] and Michael Fritz[1]

[1]Department of Periglacial Research, Alfred Wegener Institute Helmholtz Centre for Polar and Marine Research, Telegrafenberg A43, 14473 Potsdam, Germany

[2]Institute of Earth and Environmental Science, University of Potsdam, Am Neuen Palais 10, 14469 Potsdam, Germany

[3]GFZ German Research Centre for Geosciences, Telegrafenberg, 14473 Potsdam, Germany

[4]Alfred Wegener Institute Helmholtz Centre for Polar and Marine Research, Am Handelshafen 12, 27570 Bremerhaven, Germany

Submitted for publication to Geomorphology journal, periglacial geomorphology special issue.

Abstract

Erosion of permafrost coasts has received increasing scientific attention because of rapid land loss and the mobilisation potential of old organic carbon. The majority of permafrost coastal erosion studies focus on time periods from a few years to decades. Most of these studies emphasize the spatial variability of coastal erosion, but the intensity of inter-annual variations, including intermediate coastal aggradation, remains unexplained. We used repeat airborne Light Detection And Ranging (LIDAR) elevation data from 2012 and 2013 with 1 m horizontal resolution to study coastal erosion. Study sites included the major geomorphological coastal features of the Yukon Coast and on Herschel Island. We studied elevation and volume changes and coastline movement and compared the results between geomorphic units. Our results showed that 78 % of the coastline length was affected by elevation decrease. Most of the extremes were recorded in study sites with active slumping (e.g. 22 m of coastline retreat and 42 m of coastline progradation). Results showed simple uniform coastal erosion from low coasts and a highly diverse erosion pattern along coasts with higher backshore elevation. This variability was particularly pronounced in the case of active retrogressive thaw slumps, which can decrease coastal erosion or even cause

progradation by sediment release. Coastline progradation also results from the accumulation of block failure material. These occasional events can significantly affect the coastline position on a specific date and can affect coastal retreat rates as estimated by coastline digitalisation from air photos and satellite imagery. These deficiencies can be overcome by airborne LIDAR measurements, which provide detailed and high-resolution information about quickly changing elevations in coastal areas. An important advantage of an annual coastal erosion study is the possibility to relate short-term erosion observations to controlling factors in view of the rapid ongoing environmental change in the Arctic.

3.1 Introduction

About 34 % of the Earth's coasts are affected by permafrost; 35 % of these coasts in the Arctic are lithified, while 65 % are unlithified (Lantuit et al., 2012a) and particularly vulnerable to coastal erosion. Where excess ground ice is present, coastal erosion is especially efficient because of the thermal impact of sea water and the loss of volume upon thaw. Permafrost coastal erosion is limited to the ice-free summer season and during this period, coasts retreat three to four times faster than non-permafrost coasts, with extreme rates being much greater (Are, 1988). Lantuit et al. (2012a) reported an average Arctic coastal erosion rate of 0.5 m a^{-1}; 3 % of the Arctic coastline was retreating faster than 3 m a^{-1}. Jones et al. (2009) reported an extreme 25 m erosion event that occurred during one year at Drew Point, a particularly ice-rich site on the Alaskan Beaufort Sea coast. Permafrost coastal erosion has attracted much scientific attention because of the large amounts of sediment released to the Arctic Ocean (Rachold et al., 2000), the mobilisation of old organic carbon (Vonk et al., 2012), and the release of nutrients which affect elemental budgets and biogeochemical cycles in the coastal zones of the Arctic Ocean (Ping et al., 2011).

High erosion rates can occur within a short time period at specific locations (Dallimore, 1996; Barnhart et al., 2014a), while average erosion rates for longer coastal segments or long observation periods are generally much lower (Solomon, 2005). This spatial and temporal variability is caused by a wide spectrum of factors acting at different spatio-temporal scales. Regional factors acting on a larger scale are storminess, waves and storm surges, ice-free season duration, sea level, and summertime sea surface temperature. Local factors controlling erosion are sediment properties (cohesiveness and grain size), cryostratigraphy (amount, type, and distribution of ground ice), and geomorphology (cliff height and slope, exposure, underwater shore slope, presence of barrier islands and spits and littoral sediment supply, and coastal hinterland topography) (Héquette and Barnes, 1990; Solomon, 2005; Jones et al., 2009). Dallimore et al. (1996) emphasised the importance of storm events in connection with ground ice for coastal erosion in the Canadian Beaufort Sea. Barnhart et al. (2014a) indicated the importance of the sea-ice-free season, wave exposure, and sea water temperature in the

Alaskan Beaufort Sea, while Günther et al. (2015) demonstrated the importance of the temporal concurrence of open water with warm summer air temperatures in the southern Laptev Sea.

A standard approach of coastal erosion estimation is the digitisation of coastlines from historic and current satellite imagery or aerial photographs. This approach provides horizontal measures of coastal retreat. Timespans between different datasets used in previous studies usually ranged from 50 to 10 years, the shortest being 5 years in Jones et al. (2009). Studies that attempted to quantify volumetric change used digital elevation models (DEMs) derived from tacheometric surveys (on shorter timespans) and stereophotogrammetry (on longer timespans) (Lantuit and Pollard, 2005; Leibman et al., 2008; Günther et al., 2012; Günther et al., 2015). In contrast to the methods used in these studies, airborne Light Detection And Ranging (LIDAR) scanning enables short term mapping of small objects and surfaces with very little texture and contrast and offers new applications for coastal erosion studies. White and Wang (2003) and Young and Ashford (2006) studied volume changes of non-permafrost coasts using repeat airborne LIDAR data. One of the first studies using airborne LIDAR data to determine volumetric changes of permafrost coastal areas, covering a period of four years, was by Jones et al. (2013) for a stretch of the Alaskan Beaufort Sea.

Most existing studies on permafrost coastal erosion estimate the erosion rates over time periods from a few years to decades. Many of the factors influencing coastal erosion (e.g. storms, mass movements) are discrete events in time and space and can significantly vary between years. The signal of their specific influence gets smoothed over time and can no longer be traced. For this reason the exact role of the different factors influencing the erosion of unconsolidated permafrost coasts remains poorly and fractionally understood. Studies capturing processes on a yearly basis are needed to evaluate the exact contributions of different factors to coastal erosion at regional and local scales.

The aim of this study is to characterise coastal erosion and other related geomorphic processes in the immediate coastal hinterland based on repeat LIDAR DEM datasets from 2012 and 2013 for various segments of the Canadian Beaufort Sea coast. Our objectives are to (1) quantify coastal erosion for a one-year period in order to better understand coastal erosion variability, (2) quantify coastal erosion and volumetric changes in different geomorphic units, and (3) discuss the importance of local and regional factors on coastal erosion during the observation period.

3.2 Study area

The Yukon Coastal Plain (Canada) is situated between the Mackenzie Delta to the east and the Alaskan border to the west, and extends north of the British and Richardson mountains towards the Beaufort Sea. Its coastline is approximately 280 km long. East of the Firth River the area was glaciated by an extension of the Laurentide Ice Sheet (Figure 3.1) (Mackay, 1959; Hughes, 1972). Much of the area within the maximum glacial limit is covered by moraines. Herschel Island was formed as an ice-thrust moraine (Mackay, 1959). Glacial sediments were reworked by thermokarst processes and other surficial sediments are of lacustrine, fluvial, or glaciofluvial origin (Rampton, 1982). The sediment composition ranges from organic fine-grained mixtures of clay, silt, and sand in lacustrine deposits to fine-grained marine deposits and tills with pebbles and cobbles in moraines (Bouchard, 1974; Rampton, 1982; Fritz et al., 2012). These sediments are commonly unconsolidated with considerable amounts of ground ice. Ice wedges, segregated ice, and massive ice are common and lead to the occurrence of thermokarst landforms. Where massive ground ice occurs along the coast, retrogressive thaw slumps (RTSs) actively develop (Lantuit and Pollard, 2005).

The backshore elevations range from a few meters to 30 m and do not exceed 50 m except at Kay Point, where the elevation reaches 80 m, and on Herschel Island where it exceeds 100 m. The coast is mostly erosional, except where it is protected by barrier islands, spits, and beaches; these landforms mostly occur where there is riverine material supply or strong longshore drift, as is the case between Catton Point and Komakuk Beach (Figure 3.2).

The polar climate has a strong continental character with pronounced anticyclonic influence in winter and maritime influences in summer during the open-water season (Wahl et al., 1987). The mean annual air temperature (1971–2000) is −11.0°C at Komakuk Beach, the closest weather station ~40 km west of Herschel Island, with an average July maximum of 7.8°C (Environment Canada, 2000). Mean annual precipitation is between 161 mm a^{-1} at Komakuk Beach and 254 mm a^{-1} at Shingle Point (~100 km southeast of Herschel Island) and is almost equally apportioned between rain and snow (Environment Canada, 2000).

Storms, which are frequent in late August and September, come predominantly out of the west and northwest, with a secondary mode from the east to the southeast (Hudak and Young, 2002; Solomon, 2005). Winds blowing over open waters can generate significant wave heights of 4 m or more (Pinchin et al., 1985). The coastal areas of the Beaufort Sea are ice-covered for 8 to 9 months of the year, with complete sea-ice cover from mid-October through June (Solomon, 2005). The sea is usually frozen to the seabed in water depths less than 2 m (Solomon et al., 1994).

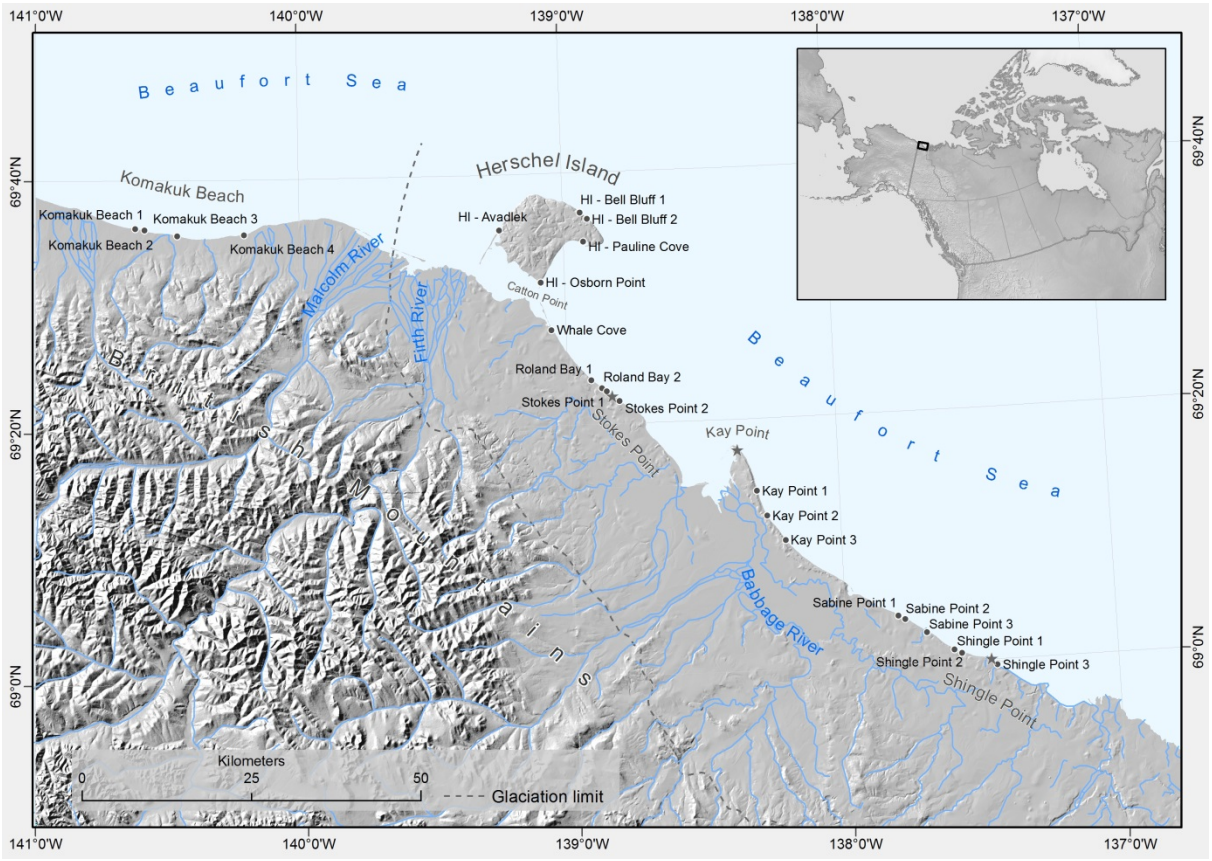

Figure 3.1: Map of study area (Yukon Coastal Plain and Herschel Island) with study sites. The base layer was provided by Geomatics Yukon.

3.3 Methods

3.3.1 Airborne LIDAR data

LIDAR scanning of the Yukon Coast and Herschel Island took place during the AIRMETH (AIRborne studies of METHane emissions from Arctic wetlands) campaigns (Kohnert et al., 2014) on 10 July, 2012 and on 22 July, 2013. Point cloud data were acquired with a RIEGL LMS-VQ580 laser scanner instrument on board the Alfred Wegener Institute's POLAR-5 science aircraft. The laser scanner was operated with a 60° scan angle at a flight height of around 200 m above ground in 2012 and 500 m in 2013. This resulted in a scan width from 200 (2012) to 500 m (2013) and a mean point-to-point distance of 0.5 to 1.0 m.

Raw laser data were calibrated, combined with the post-processed GPS trajectory, corrected for altitude, and referenced to the EGM (Earth Gravitational Model) 2008 geoid (Pavlis et al., 2008). The final georeferenced point cloud data accuracy was determined to be better than 0.15 +/- 0.1 m. The loss of accuracy varies along the flight track because of the vertical accuracy of the post-processed GPS trajectory. The GPS data were acquired in 50 Hz resolution with a Novatel OEM4 receiver on board POLAR-5. The GPS trajectory was post-

processed using precise ephemerides and the commercial software package Waypoint 8.5 (PPP [precise point positioning] processing). For the interpolation to the final DEM an inverse distance weighting (IDW) algorithm was applied using all cloud points within a 10 m radius of each point. Finally, the DEMs from the different acquisition years were interpolated to raster grids of 1 m horizontal resolution (Figure 3.2).

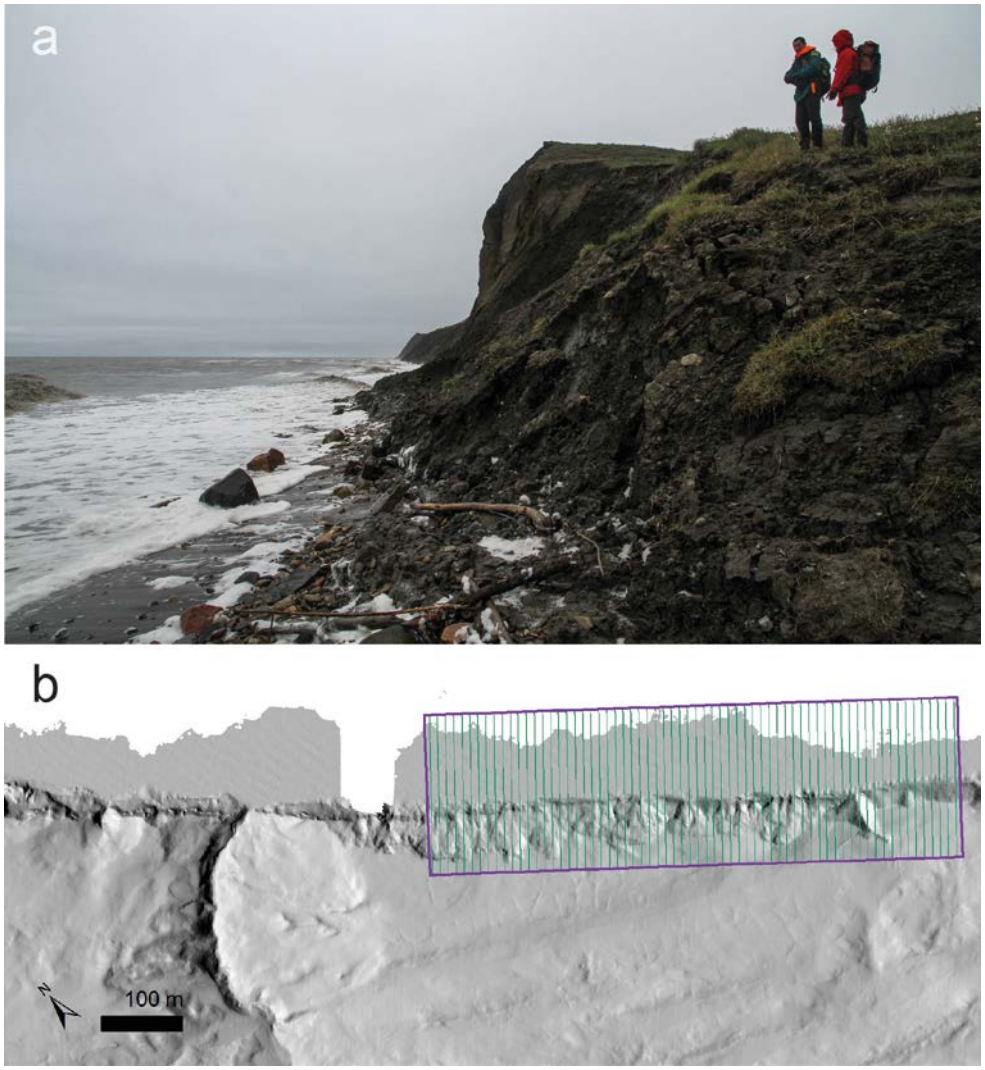

Figure 3.2: Photography and LIDAR DEM of Bell Bluff, on Herschel Island: (a) a view towards the east from a gully between bluffs as high as 30 m, (b) LIDAR DEM displayed as hillshade and transects perpendicular to the coastline with 10 m spacing at the Bell Bluff 2 study site.

To quantify vertical change that is significant at the 99% confidence interval, we followed the procedures used by Jones et al. (2013). A threshold that describes elevation change between both datasets was calculated using the equation:

$$threshold = 3 \times \sqrt{(2012 \text{ vertical accuracy})^2 + (2013 \text{ vertical accuracy})^2} \quad (3.1)$$

Vertical accuracies for both datasets were estimated to be 0.15 m, which results in the threshold of 0.64 m for significant vertical elevation change.

The accuracy of the datasets was additionally tested at locations characterised by the presence of anthropogenic features that presumably remain stable and are not affected by vertical movements because of artificial embankments underneath (Figure 3.3). The first feature was a gravel road near an oil tank facility at Shingle Point. The second feature was an airstrip at Stokes Point on beach accumulation features which are unlikely to be underlain by near-surface ice-rich permafrost (Smith et al., 1989). The differences between both DEM datasets were assessed along profiles and were within the previously-stated 0.15 m uncertainty.

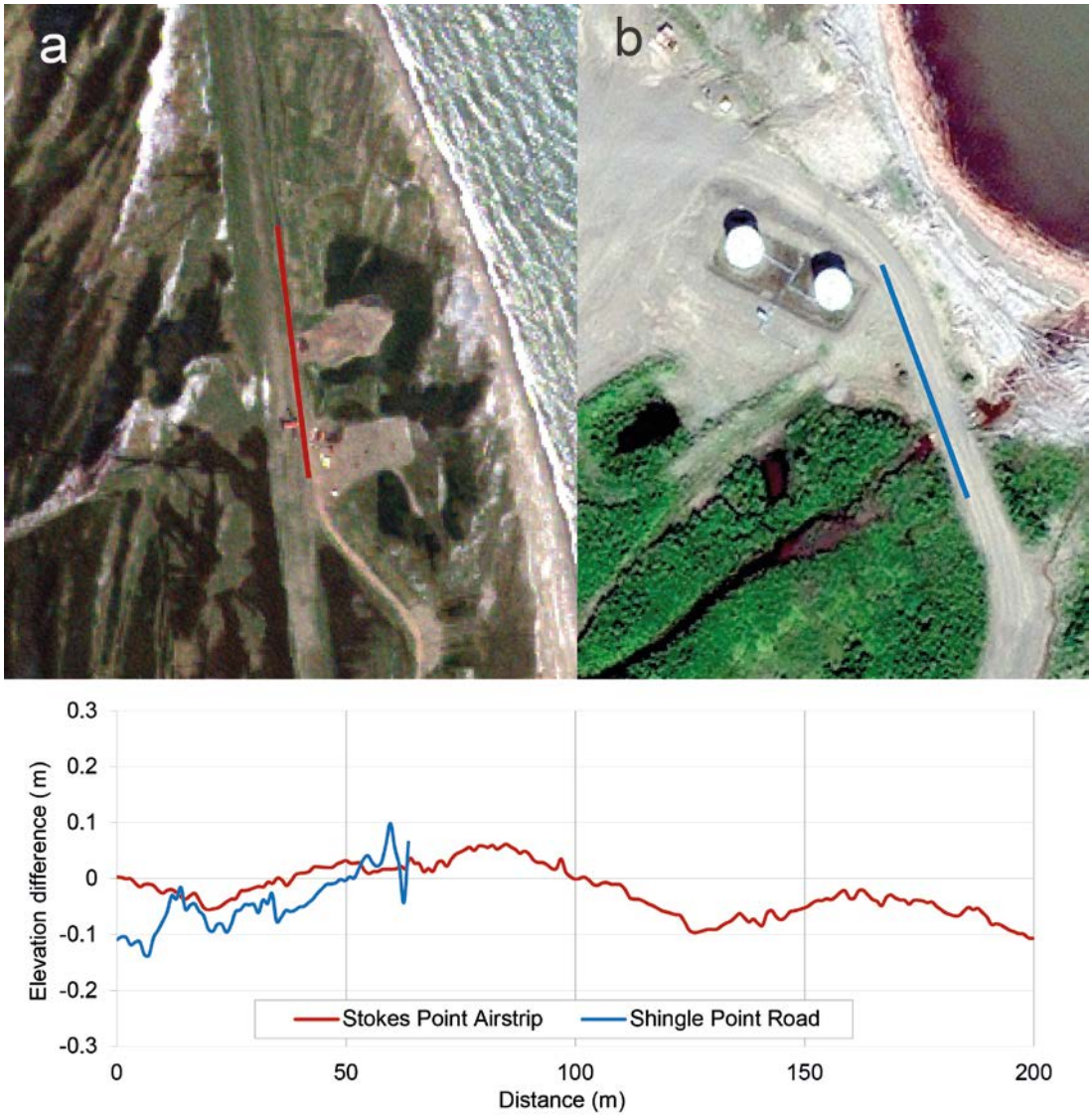

Figure 3.3: Comparison of elevations between both LIDAR DEM datasets from 2012 and 2013. The airstrip near Stokes Point (a) and the road near an oil tank facility at Shingle Point (b) are likely protected from vertical movements over the course of one year. The elevation difference is 0.03 ± 0.05 m, inside the ±0.15 m elevation uncertainty stated for the entire dataset.

3.3.2 Study sites selection and classification

Study sites were chosen along the Yukon Coast and Herschel Island so that all major geomorphologic coastal types were represented. The erosion of unconsolidated permafrost coasts is accompanied by a variety of mass-wasting processes such as retrogressive thaw slumping, active-layer detachment sliding, gully erosion, and landsliding. We use the term slumping for all mass movements, ranging from very-small-scale mass movement features to major RTSs. The study sites were classified to assess the differences in coastal erosion. Slumping, bluff height, and presence of beach were the main criteria for classification. According to prevalent geomorphic processes we classified sites as low bluffs, active slumps, stabilised slumps, high bluffs with no slumping, or beach-protected coasts (Table 3.1). There was little or no evidence of slumping on bluffs lower than 10 m so only coastal bluffs higher than 10 m were classified as active or stabilised slumps. Altogether, 23 coastal sections from 200 to 500 m length and 200 to 250 m width were chosen as study sites (Table 3.2). Barrier islands, spits, and other depositional features were not included in the study because of their low annual change rate.

Table 3.1: Classification of study sites according to prevailing geomorphic processes and morphology.

Geomorphic unit	Description
Low bluff	coastal bluffs < 10 m height
Active slumps	coastal bluffs > 10 m, evidence of active slumping
Stabilised slumps	coastal bluffs > 10 m, evidence of stabilised slumps
High bluff with no slumping	coastal bluffs > 10 m, no evidence of active or past slumping
Beach-protected coast	coast with well-expressed protecting beach

Table 3.2: Study sites on Herschel Island and the Yukon Coast (see also Figure 3.1). Sites were selected on the basis of prevalent geomorphic processes. Volumetric percentages of excess ice were taken from Couture (2010) for the whole Yukon Coast.

Site name	Abbreviation	Geomorphic unit	Maximal bluff height (m)	Section length (m)	Site area (m^2)	Ice content (%)	Excess ice content (%)
Roland Bay 2	RB2	Active slumps	12 - 20	490	97900	53.8	0.8
Kay Point 2	KP2	Active slumps	10 - 20	497	99400	38.2	0.0
Shingle Point 1	ShP1	Active slumps	15 - 30	500	99900	46.2	0.0
Sabine Point 3	SaP3	Active slumps	20 - 30	442	132400	32.2	0.0
Herschel Island - Avadlek	HIAV	Active slumps	10 - 25	510	102000	51.3	4.5
Herschel Island - Bell Bluff 1	HIBB1	Active slumps	35	288	57600	50.2	2.2
Herschel Island - Bell Bluff 2	HIBB2	Active slumps	30 - 35	668	133600	50.2	2.2
Komakuk Beach 4	KB4	Beach-protected coasts	5	236	47100	57.7	22.2
Whale Cove	WC	Beach-protected coasts	1 - 2	478	95700	57.3	16.7
Sabine Point 1	SaP1	Beach-protected coasts	20 - 22	497	99400	30.4	0.0
Kay Point 3	KP3	High bluff with no slumping	12 - 30	460	91900	38.2	0.0
Sabine Point 2	SaP2	High bluff with no slumping	21	490	98100	59.7	20.1
Shingle Point 3	ShP3	High bluff with no slumping	10 - 20	331	66100	40.4	0.0
Komakuk Beach 2	KB2	Low bluff	6	394	78800	52.3	11.8
Komakuk Beach 1	KB1	Low bluff	3	334	66700	52.3	11.8
Komakuk Beach 3	KB3	Low bluff	7	379	75900	57.7	22.2
Stokes Point 2	SP2	Low bluff	4 - 15	456	91200	53.2	0.0
Roland Bay 1	RB1	Low bluff	2 - 5	461	92300	51.5	0.0
Stokes Point 1	SP1	Low bluff	9	365	73100	53.2	0.0
Kay Point 1	KP1	Stabilised slumps	20 - 30	497	99400	38.2	0.0
Shingle Point 2	ShP2	Stabilised slumps	20 - 27	477	95500	46.2	0.0
Herschel Island - Osburn Point	HIOP	Stabilised slumps	20 - 30	545	109000	55.5	13.0
Herschel Island - Pauline Cove	HIPC	Stabilised slumps	15 - 20	397	79500	55.5	13.0

3.3.3 Quantification of erosion rates and volume change

We created indicators of coastal dynamics using the elevation models derived from the LIDAR data. These indicators included elevation change, volume change, coastline movement, and hinterland erosion length. We then distinguished between erosion and progradation change for the first three indicators. For erosion, changes were termed elevation decrease, volume decrease, and coastline retreat. For progradation, changes were termed elevation increase, volume increase, and coastline progradation (for details see next paragraph). The 2012 elevation dataset was subtracted from the 2013 dataset to calculate the elevation difference. The observation period was one year and 12 days; thus, the values presented in this paper overestimate yearly rates by 3 %. Elevation changes greater than the uncertainty threshold (0.64 m) were included in the analyses. All elevation changes that were caused by changes in water surfaces (e.g. sea waves) between the two data acquisitions were excluded from further analyses. Indicators were separately calculated for each study site and for each geomorphic unit which consists of several study sites Table 3.3, Figure 3.4).

Descriptive statistics on elevation change and volume change were calculated from pixels within the extent of the study site. Values were calculated separately for elevation decrease and elevation increase with ArcGIS 10.1. We calculated volume decrease in m^3 as the sum of elevation decrease of pixels within the extent of the study site ($dV_s = \sum_{i=1}^{n} dE_d$). The same

procedure was separately applied for volume increase ($dV_i = \sum_{i=1}^{n} dE_i$). Volume change was then normalised to 100 m of coast to allow comparison among the sites and with other studies. The exact extent of RTSs was digitised in the Roland Bay 2, Kay Point 2, Sabine Point 3, and Shingle Point 1 units. Volume change properties were calculated separately for these RTSs to highlight their volume change characteristics.

Coastline movements and hinterland erosion length were calculated using parallel transects with 10 m spacing stretching across the entire study site perpendicular to the coast. Every pixel of the DEM difference raster was analysed along these transects. Values along each transect were extracted in ArcGIS 10.1 from the elevation difference dataset and from both the 2012 and 2013 elevation datasets, and then analysed using R software (version 3.0.1). The coastline was defined as the 1 m contour of the DEM to exclude tidal variations of 0.5 m in the area (Solomon, 2005). Coastline movement along transects was calculated as the distance between the coastline positions in 2012 and 2013. Hinterland erosion indicates how far inland the effect of coastal erosion stretched. This parameter is meant to encompass the erosional processes acting upon the lower part of the cliff and the denudational processes acting on its upper part. We defined hinterland erosion as the maximum continuous length along a transect that underwent elevation decrease during the study period.

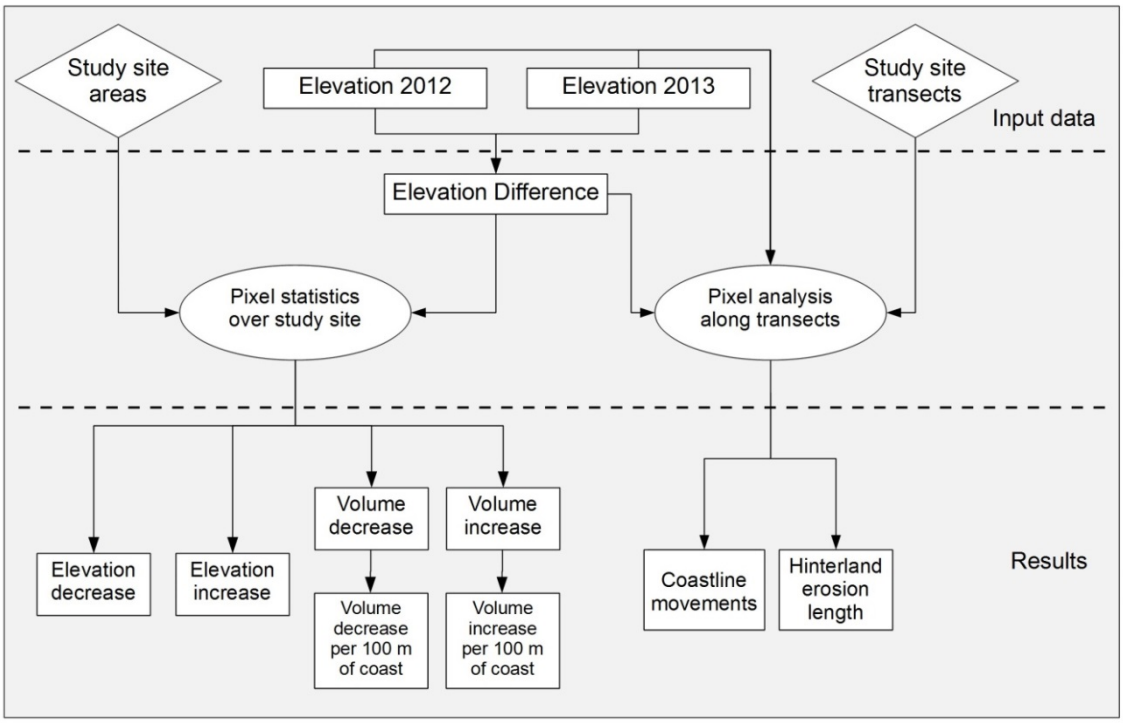

Figure 3.4: Diagram showing the process of indicator calculation. Elevation and volume changes were calculated as zonal statistics for the study sites and geomorphic units. Coastline movements and hinterland erosion length were calculated from elevation changes along transects in the study sites.

3.4 Results

We analysed coastline and backshore areas over a total coast length of 10.2 km and classified the coast into five geomorphic units. Among them, 33% belonged to the unit of active slumps, 23% to low bluffs, 19% to stabilised slumps, 13% were high bluffs with no slumping, and 12% belonged to the unit of beach-protected coasts. The percentage of coastline length (percentage of transects) affected by coastal erosion was 78 %. The studied coastal site areas were mostly affected by elevation decrease (76 %), while a smaller portion was affected by elevation increase (24 %). The most extensive elevation decrease occurred in the active-slumps geomorphic unit (13.2 % of coastal area). The elevation of beach-protected coasts was relatively stable; only small areas were affected by elevation decrease (1.5 %) or increase (5.1 %).

3.4.1 Elevation and volume changes

The maximum elevation decrease was recorded in an active-slumps unit (13.2 m, Sabine Point 2) but this coastal type also showed strong elevation increase (9.1 m, Bell Bluff 1) where the eroded material was re-deposited from block failure (Table 3.3). A high mean elevation decrease was recorded in the active-slumps and high-bluffs units (3.1 and 3.0 m, respectively). Mean elevation decrease was lower in the three other units (1.1 - 1.8 m). The highest volume decreases were observed in the active-slumps unit, followed by low bluff, high bluff with no slumping, stabilised slumps, and beach-protected coast. The volume decrease in active slumps was two times larger than in the low-bluff unit and three times larger than in stabilised slumps. The largest positive volume changes (i.e. volume increase) were observed in beach-protected coasts and stabilised slumps followed by active slumps, while low bluffs underwent the lowest volume accumulation. The only unit where volume increase was greater than decrease was beach-protected coasts. RTSs alone were characterised by a volume decrease of 117 554 m^3 and a volume increase of 6480 m^3, meaning that 5.5 % of mobilised material re-accumulated.

Table 3.3: Elevation change at the study sites grouped by geomorphic unit. Statistics for elevation decrease and elevation increase were calculated separately. Yearly rates account for 97% of the values given in the table, because the duration of observation period was one year and 12 days.

Elevation decrease					
Unit	Number of sections	Mean (m)	STD (m)	Maximum (m)	Volume decrease per 100 m of coastline (m^3/100m)
Low bluff	6	1.8	1.8	9.6	4235
High bluff with no slumping	3	3.0	2.4	13.4	3519
Beach-protected coasts	3	1.1	0.4	2.6	310
Active slumps	7	3.1	2.8	18.6	8833
Stabilised slumps	4	1.4	0.8	5.3	2686
All sites	23	2.4	2.4	18.6	4918

Elevation increase					
Unit	Number of sections	Mean (m)	STD (m)	Maximum (m)	Volume increase per 100 m of coastline (m^3/100m)
Low bluff	6	0.9	0.4	2.6	83
High bluff with no slumping	3	0.8	0.2	2.3	401
Beach-protected coasts	3	1.0	0.2	2.4	1012
Active slumps	7	1.0	0.7	9.1	840
Stabilised slumps	4	1.3	0.8	5.7	1074
All sites	23	1.1	0.6	9.1	672

3.4.2 Coastline movements

Both coastline retreat and progradation occurred along the studied transects (Table 3.4). Mean coastline movement was 0.1 ± 9.0 m of progradation, while the median exhibits no net coastline movement. Coastal retreat was prevalent along low bluffs and stabilised slumps with a mean retreat of 4.5 m and 2.6 m, respectively. Progradation was observed along beach-protected coasts (5.2 m), active slumps (2.2 m), and high bluffs with no slumping (1.7 m). The mean progradation for the active-slumps unit was greatly affected by the values from the Sabine Point 3 site. Mean retreat of 0.8 m was observed for the other six active-slump sites. Relatively high standard deviations (Table 3.3) and non-normal distribution of variables (Figure 3.5) show that extreme values significantly influenced the averages. The maximum coastline retreat and progradation occurred in the active-slumps unit (22 m and 42 m, respectively). High maximum retreat rates occurred in the low-bluff unit (21 m) and along coasts with stabilised slumps (17 m). The second highest progradation was recorded in the beach-protected coast unit. Hinterland erosion was greater in active slumps, low bluffs, and stabilised slumps (hinterland erosion length was around or above 20 m) and less in high bluffs with no slumping and beach-protected coasts. The effects of coastal erosion stretched 15.8 ± 15.8 m inland, on average, across all sites.

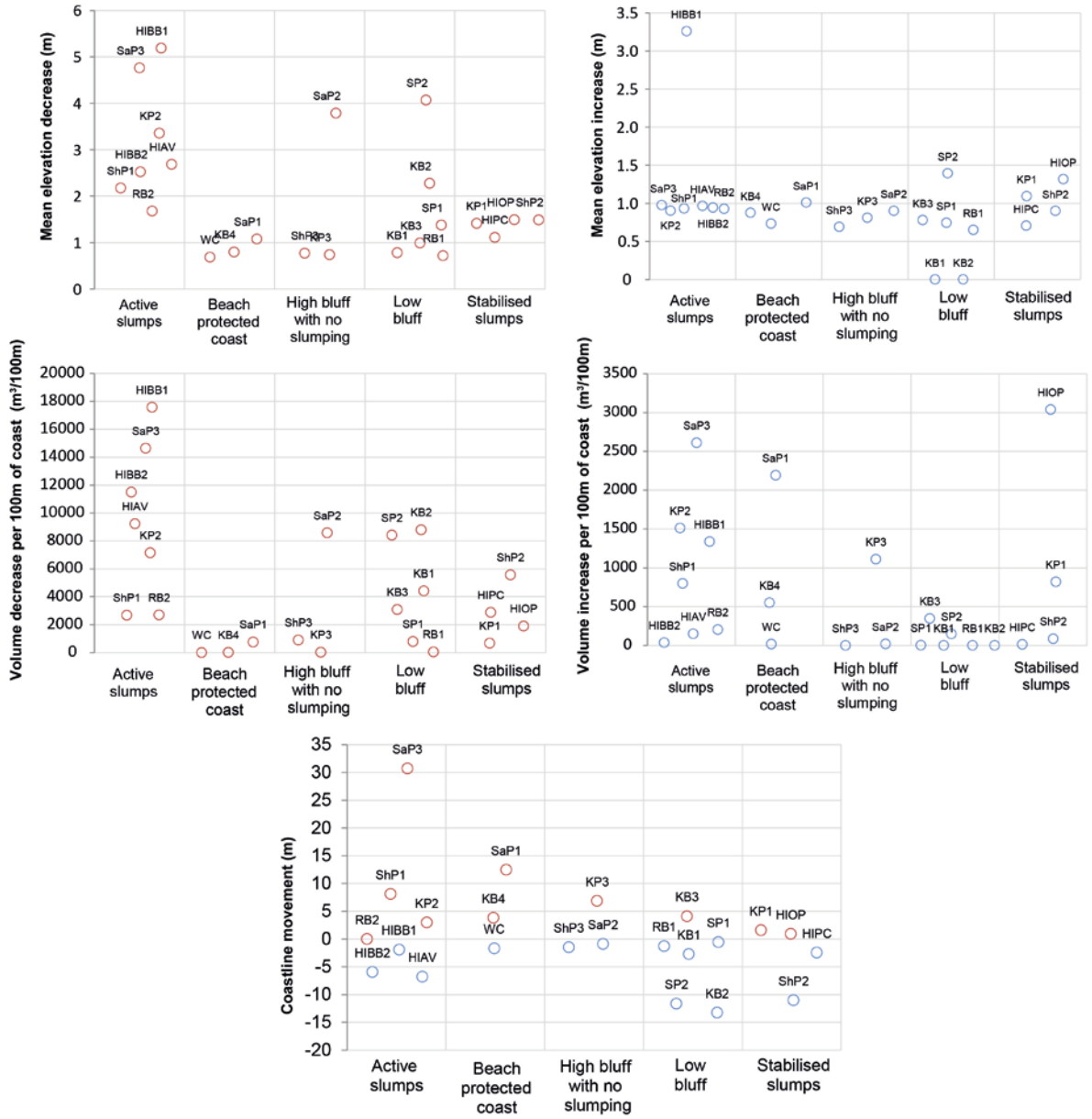

Figure 3.5: Plots of study sites grouped in geomorphic units plotted against mean elevation decrease and increase, volume decrease and increase per 100 m of coast, and coastline movement. For coastline movement, retreat is shown as negative values.

Table 3.4: Coastline movements and hinterland erosion lengths for study sites grouped by geomorphic unit type. Statistics were calculated based on transects with 10 m spacing in study sites.

		Shoreline movement (m)					Hinterland erosion length (m)			
Unit	Number of transects	Mean	Median	STD	Max. retreat	Max. progradation	Mean	Median	STD	Max
Low bluff	236	**-4.5**	-3	6.9	-21	10	**16.9**	17	14.0	68
High bluff with no slumping	128	**1.7**	0	4.3	-7	11	**9.8**	5	10.3	30
Beach-protected coasts	120	**5.2**	2	7.6	-5	20	**2.2**	0	4.6	25
Active slumps	337	**2.2**	0	11.4	-22	42	**23.3**	23	19.0	113
Stabilised slumps	188	**-2.6**	-1	5.6	-17	8	**14.0**	14	10.7	48
All sites	1009	**0.1**	0	9.0	-22	42	**15.8**	14	15.8	113

3.5 Discussion

This study provides insights into the spatial erosion variability of permafrost coastal dynamics in the Canadian Beaufort Sea on the temporal scale of 1 year. High variability of coastal erosion intensity between different geomorphic units and also within study sites suggests that, even at a local scale, coastal erosion processes were highly heterogeneous. This is a result of combined local and regional factors which either hinder or intensify coastal erosion.

3.5.1 Coastal erosion and its variability

A maximum coastline retreat rate of 22 m was recorded on Herschel Island, at the Avadlek site. Similar maximum erosion rates were reported from other investigations in the Canadian and Alaskan Beaufort Sea and from the Laptev Sea region (Solomon, 2005; Jones et al., 2009; Günther et al., 2013). Maximum coastline progradation was 42 m and was a consequence of beach progradation by the material delivered from an RTS (Figure 3.6, Sabine Point 3). A high progradation of up to 20 m was observed on Herschel Island (Figure 3.6, Bell Bluff 1), where material accumulated from slope failure. Solomon (2005) reported maximum yearly progradation rates of up to 7 m a^{-1} for a few locations in the Beaufort-Mackenzie region. In our study, 78 % of the coast underwent an elevation decrease. We recorded an average coastline movement of +0.1 m but it is characterised by high variability, as shown by the standard deviation of 9.0 m. Hinterland erosion stretched inland, on average, by 15.8 m and is also highly variable with a standard deviation of 15.8 m. This shows the uneven spatial distribution of geomorphic processes on the coast and in the backshore area. Elevation decreases of more than 10 m were recorded at sites with active erosion and denudation processes at high backshore elevations. Overall, a maximum elevation decrease of 18 m was recorded in an RTS at the Sabine Point 3 site.

Elevation decrease, volume change, and coastal retreat are variable inside geomorphic units and across them (Table 3.3 and Figure 3.4). The variability in the active-slumps unit can be explained by the different intensity of mass-wasting processes. The highest elevation changes

in this unit occurred at the site with an actively evolving RTS (Figure 3.6, Sabine Point 3) and at the NE side of Herschel Island, which is the most exposed to waves and storm surges (Figure 3.6, Herschel Island – Bell Bluff 1). High variability within the low-bluffs unit occurred because it includes inactive bluffs and bluffs eroding by up to 20 m per year (Figure 3.6, Stokes Point 2). High spatial and temporal variability is a basic characteristic of arctic coastal erosion (Are, 1988, Lantuit et al., 2012a). Solomon (2005) reported local variations up to 17 m a^{-1} of coastline retreat and progradation rates up to nearly 7 m in the Mackenzie Delta region. Lantuit and Pollard (2008) reported variation of erosion rates at contiguous locations by factors of 2–8 for Herschel Island. Our study showed that not only coastline movements but also volume changes are very spatially heterogeneous. High volume losses do not always coincide with coastline retreat. Considerable volume losses occurred at the Stokes Point 1 and Sabine Point 3 sites despite high coastline progradation. High temporal variability occurs at the Shingle Point 2 site, where we observed coastline retreat of 11.0 ± 3.3 m, but Hynes et al. (2014) recorded coastline movement rates between 0.6 m a^{-1} and -0.3 m a^{-1} between 1953 and 2004.

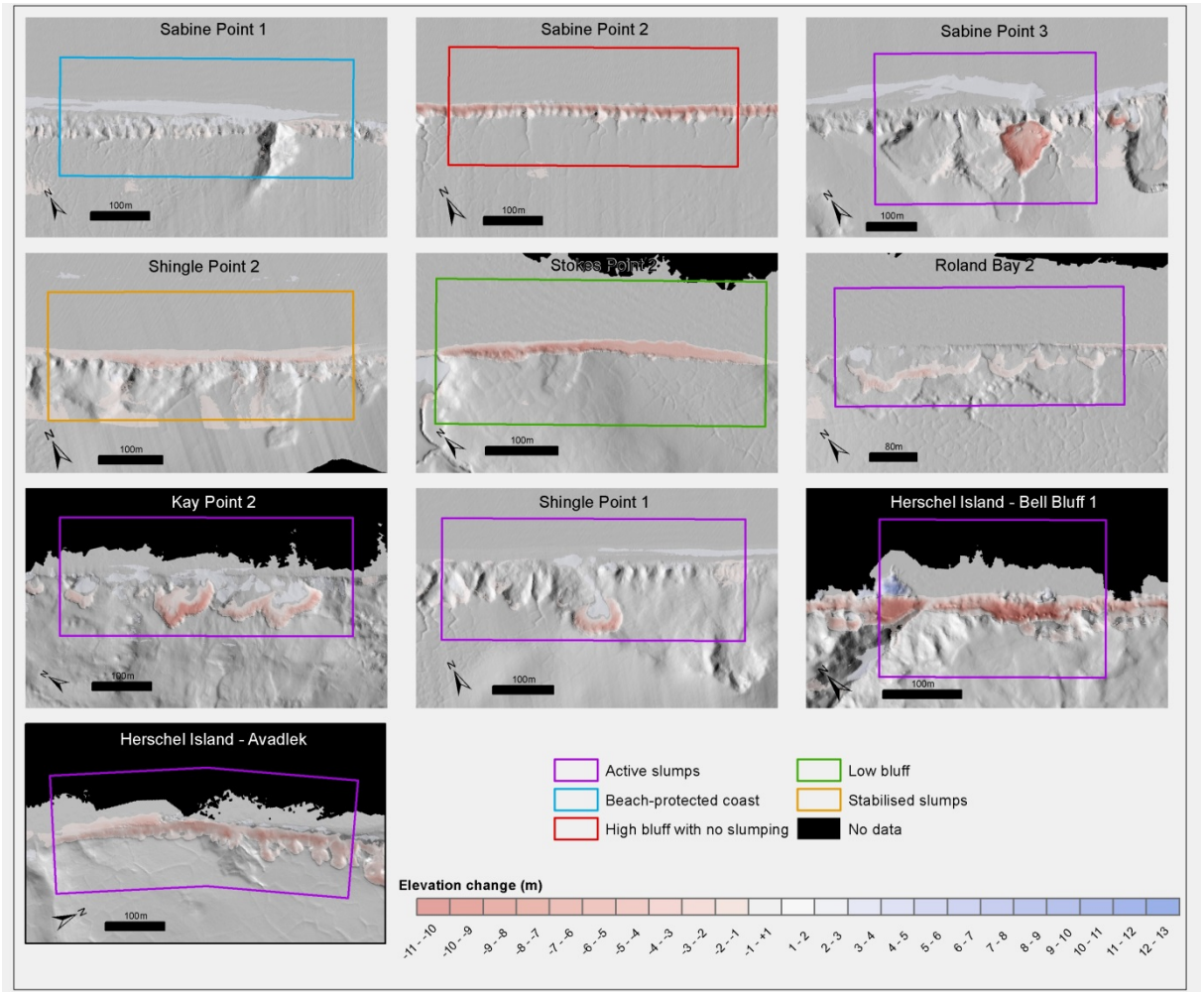

Figure 3.6: Examples of study sites comprising all geomorphic units. Red colour shows erosion and blue accumulation.

3.5.2 Coastal erosion in different geomorphic units

Coasts with low backshore elevations (< 10 m) showed simple and linear coastal retreat, while coasts with high backshore elevations showed more diverse denudation processes. Mean coastline retreat was the highest and volume decrease was second-to-greatest within the low-bluff unit. High coastline retreat indicates that coastal erosion is efficient enough to remove all material provided from the hinterland by processes, causing volume decrease in this unit. To the contrary, mean coastline progradation on three active-slumps unit sites along the Yukon Coast, which have undergone the highest volume decrease, indicates that coastal erosion was not efficient enough to remove all of the mobilised material. This suggests intermediate accumulation of eroded material after mobilisation. Sites from the same unit on the western and northern part of Herschel Island have conversely undergone considerable coastline retreat (on average 1.9 to 5.9 m at different sites) despite high volume decreases, presumably because of more exposure to storm waves and surges. Lantuit and Pollard (2008) calculated average coastal retreat rates of 0.6 to 1.6 m a^{-1} between 1952 and 1970 and 0 to 1.6

m a^{-1} between 1970 and 2000 for the same sites. The stabilised slumps, where slumping was temporarily not active, showed the second highest coastal retreat and moderate volume loss. The high bluffs with no slumping showed relative erosional inactivity in the hinterland and along the coastline and average coastal progradation, because the active bluffs higher than 10 m that were characterised by coastal erosion and slumping were classified as other geomorphic units. Héquette and Barnes (1990) indicated that erosion rates are insignificantly correlated to bluff height. The diversity of denudation processes on bluffs higher than 10 m could be the reason for this insignificance. Small thermo-erosional niches were observed in bluffs with low backshore elevations and absent in bluffs with high backshore elevations, presumably because of very active thermal denudation.

3.5.3 Factors influencing coastal erosion

3.5.3.1 Role of slumping

Coastal dynamics can be greatly influenced by slumping events directly in situ and further along the coast. The term “slumping” in our study encompasses all mass movements from very small scale to RTSs. Slumping was very common on the Yukon Coast and Herschel Island and occurred where the bluffs were higher than 10 m. Sites with active slumping included most of the extreme values of erosion, accumulation, and coastline movements among the geomorphic units (Figure 3.5). This indicates the importance of slumping, especially within RTSs, for altering the linear behaviour of coastal erosion. The effect of RTSs is evident at the Sabine Point 1 and 2 sites. The first site is located west of an active RTS and has experienced a strong sediment accumulation regime, whereas the second site, east of an RTS, has undergone strong erosion. The occurrence of slumping can hinder or temporarily stop coastal erosion on the coasts adjacent to RTSs because of the sediment supply to the shore.

Lantuit and Pollard (2008) and Leibman (2008) suggested that RTS activity amplifies coastal erosion, because of massive ice presence and ground settlement. Our results, however, show that short-term coastline retreat rates are lower in the units of active and stabilised slumps than in the low-bluff unit. The occurrences of RTSs can even result in high coastline progradation rates, because of beach accumulation by sediment released from RTSs. However, this material, transported by mass wasting, can again be removed within a few days during strong wave activity and within a few weeks during lower wave activity as observed by Leibman et al. (2008) on the Yugorsky Peninsula. Our LIDAR acquisitions, therefore, represent snapshots of the coastal situation on the acquisition day, which could result in a recording of elevation increase and coastal progradation due to the presence of short-lived mass wasting depositional features. High progradation rates were also observed because of

material accumulated from slope failure (Bell Bluff 1 site), where the material persisted for a longer time because it was less reworked.

Volume increase that was recorded inside RTS areas over the study period accounted for 5.5 % of the volume decrease, meaning that at least 5.5 % of the material that has been activated is stored inside RTSs and not directly transported to the sea. The excess ice percentage at our slump sites was zero or negligible (Couture, 2010), so the same volume which has been eroded can potentially be accumulated. The percentage of stored sediment can be higher, because activated material can be slowly moved towards the RTS outlet without volume increases, which we recorded. The fraction that stayed within the slump during one year is relevant for the quantification of carbon output from RTSs, because material that is not directly transported to the sea is exposed to aerobic processes and therefore increased microbial activity (Pautler et al., 2010). This can decrease the amount of stored carbon and increase direct CO2 emissions from RTSs to the atmosphere (Vonk et al., 2012).

3.5.3.2 Role of beaches and accumulation

Coasts protected by beaches show relative stability or even accumulation. The results in Table 3.3 and Table 3.4 indicate that this unit has undergone the lowest erosion, but significant material accumulation and coastline progradation. The volume decrease made up only 8 % of the volume increase in this unit, meaning that material originates from elsewhere and is transported by longshore drift. Rampton (1982) associated beaches with coarse-grain sediments, because silty sediment is easily suspended in the water, transported offshore, and therefore unlikely to accumulate on the beach (Are, 1988). To relate occurrence of beaches to grain size in our study area, detailed mapping of sediments would be required. Sediment transported as longshore drift can originate from mass wasting, coastal erosion, or distributary streams. Lantuit and Pollard (2008) reported that bluffs on SE Herschel Island are affected by beach armouring because of distributary streams. When the sediment supply ceases, the accumulated beach can undergo high coastline retreat rates, since unconsolidated beach sediment can be rapidly eroded (Shingle Point 2 site).

3.5.4 Suitability of the airborne LIDAR dataset for coastal erosion studies

Airborne LIDAR datasets provide highly accurate information about coastline variations. The coastline has often been defined as the land-ocean interface (Solomon, 2005; Lantuit and Pollard, 2008; Jones et al., 2009). This definition includes beaches, which in our study showed considerable variations in the vicinity of RTSs (up to 40 m of prograded coast). The collapsed material and material that was moved by mass wasting sometimes resulted in progradation of the coastline to a distance of up to 20 m. These occasional events can significantly affect the coastline digitalisations and can present a source of variations in the

estimations of retreat rates. Thus the digitalisation of cliff bottom line (as done by Günther et al., 2013) might be more suitable for the estimation of coastal retreat rates in permafrost regions.

Use of airborne LIDAR datasets is limited in the case of overhangs, because the volume underneath cannot be recorded. These overhangs were present in some low-bluff coastal study sites (e.g. Stokes Point 2), but did not exceed 1 m in width (Figure 3.7). Assuming that overhangs are continuously developing, the volume calculation uncertainty originating from their presence in our datasets can be neglected because it is similar in both datasets.

A possible perspective on detecting short-term and inter-annual changes in permafrost coastal erosion is to relate observed changes to local and regional factors. This can improve our understanding of process, modelling accuracies, and subsequent prediction of the future development of Arctic coastal erosion under increasing air temperatures and lengthening open-water season duration (Barnhart et al., 2014b). The major advantage of repeat airborne LIDAR elevation data compared to stereophotogrammetry is the unique high accuracy and the possibility of multiple short observation periods.

Figure 3.7: Thermo-erosional niches building an overhang at Stokes Point where the coast retreated by up to 20 m between 2012 and 2013.

3.6 Conclusion

Our study indicates considerable spatial variability in short-term coastline erosion and progradation, which cannot be resolved by long-term observation. This variability is significantly related to a wide spectrum of denudation processes acting on permafrost coasts. Comparison between geomorphic units revealed that erosion behaviour is simple and relatively linear at low-elevation coasts and becomes diverse at higher-elevation coasts, where denudation is more active. Among these denudation processes, retrogressive thaw slumping is particularly important. Its occurrence affects not only the coastal processes in situ, but, as we have demonstrated, also nearby coasts with sediment input and cessation of erosion. Most of the erosion and deposition extremes were recorded at sites with slumping activity. On average at least 5.5% of the eroded material was temporarily accumulated again inside RTSs, meaning that material was exposed to aerobic conditions which could activate stored organic carbon before material is transported to the sea. Our study also showed that short-term coastline movements, such as beach progradation or block failures, can be intensive but are generally short-lived features along permafrost coasts; they must be considered when digitising coastlines from air photos or satellite imagery. An important advantage of spatially-detailed, single-year studies is the possibility to relate short-term erosion to factors controlling coastal erosion on an annual basis. Our study can serve as a baseline for further studies and coastal erosion modelling that can reveal the exact relationships between factors controlling erosion along permafrost coasts. These coasts are becoming more vulnerable to erosion as Arctic Ocean sea-ice coverage decreases and Arctic air temperature increases.

4 Manuscript #3 – Relation between planimetric and volumetric erosion of permafrost coasts: a case study from Herschel Island, western Canadian Arctic

Jaroslav Obu[1,2], Hugues Lantuit[1,2], Michael Fritz[1], Wayne H. Pollard[3], Torsten Sachs[4], and Frank Günther[1]

[1]Department of Periglacial Research, Alfred Wegener Institute Helmholtz Centre for Polar and Marine Research, Telegrafenberg A43, 14473 Potsdam, Germany

[2]Institute of Earth and Environmental Science, University of Potsdam, Am Neuen Palais 10, 14469 Potsdam, Germany

[3]Department of Geography, McGill University, 805 Sherbrooke Street West, Montreal, Canada

[4]GFZ German Research Centre for Geosciences, Telegrafenberg, 14473 Potsdam, Germany

Submitted for publication to Polar Research journal.

Abstract

Ice-rich permafrost coasts often undergo rapid erosion and result in land loss, release of considerable amounts of sediment, organic carbon and nutrients impacting the near-shore ecosystems. Arctic coastal erosion studies typically report on planimetric erosion due to the lack of volumetric erosion data. Our aim is to explore the relationship between planimetric and volumetric coastal erosion and update the coastal erosion rates on Herschel Island in the Canadian Arctic. We used high-resolution digital elevation models to compute sediment release and compare volumetric data to planimetric coastline movements digitised from satellite imagery. Our results show that volumetric erosion is locally less variable and likely corresponds better with environmental forcing than planimetric erosion. Average sediment release volumes are of the same range as sediment release volumes calculated from coastline movements combined with cliff height. However, the differences between both estimates are significant on small coastal section basis. We attribute the differences between planimetric and volumetric coastal erosion to mass wasting, which is abundant along the coasts of Herschel Island. The average recorded coastline retreat on Herschel Island was 0.68 m a^{-1} for

the period 2000 – 2011. Erosion rates increased by more than 50 % in comparison to the period 1970 – 2000, which is in accordance with a recently observed increase along the Alaskan Beaufort Sea. The estimated annual sediment release was 28.2 m^3 m^{-1} with resulting fluxes of 590 kg C m^{-1} and 104 kg N m^{-1}.

4.1 Introduction

Coastal erosion rates in the Arctic are among the highest measured despite the fact that the erosional processes are limited to the short ice-free season (3-4 months) (Are 1988; Overduin et al., 2014). Coastal erosion rates can locally, in exposed sites, exceed 20 m a^{-1} (Jones et al., 2009; Günther et al., 2013; 2015). Lantuit et al. (2012a) reported an average erosion rate of 0.5 m a^{-1} for the entire Arctic; three per cent of the Arctic coastline is retreating faster than 3 m a^{-1}. Particularly vulnerable are unconsolidated and ice-rich coasts, which are subject to a combination of mechanical and thermal action by waves (Are, 1988). The projected increase of Arctic air temperatures is expected to result in increased sea-surface temperatures and a lengthening of the open-water season that will likely increase erosion rates (Overeem, 2011; Stocker et al., 2014; Günther et al., 2015).

Erosion of permafrost coasts can cause rapid land loss, which can lead to a loss of habitat, natural resources, and archaeological sites as well as endangering modern infrastructure and communities (Johnson et al., 2003; Mars and Houseknecht 2007). Jones et al. (2008) used aerial photography to identify cultural and historical sites on the Alaskan Beaufort Sea coast that are threatened or had already been eroded by coastal erosion. According to Mars and Houseknecht (2007) the threat of land loss can be reasonably well resolved from coastline retreat rates derived from satellite imagery.

Soils and unconsolidated deposits in the northern circumpolar region store large quantities of soil organic carbon (Hugelius et al., 2014). Considerable proportions of this carbon are released together with other elements by coastal erosion (Rachold et al., 2004). Lateral fluxes of organic carbon and nutrients can change water and environment quality and significantly alter Arctic coastal ecosystems (Ping et al., 2011). Vonk et al. (2012) estimated that approximately two thirds of the eroded organic carbon in Arctic Siberia escapes to the atmosphere as carbon dioxide, suggesting that coastal erosion is also an important source for greenhouse gas release. In order to estimate mass fluxes of sediment, volumetric erosion data is required.

Previous studies on Arctic coastal erosion were mostly based on linear coastline movements (planimetric coastal erosion) and land loss observations, with few studies estimating actual volume losses (volumetric coastal erosion). This shortcoming is mostly due to the absence of high-resolution digital elevation models (DEMs) for remote polar regions. Recent volumetric

erosion studies used stereo-photogrammetrically- or LIDAR-derived DEMs (Jones et al., 2013; Günther et al., 2015). Coastal carbon flux calculations were based mainly on the combination of planimetric coastline movement rates and average cliff heights (e.g. Jorgenson and Brown, 2005; Ping et al., 2011; Günther et al., 2013) and assumed that coastline retreat correlates with sediment release. The paucity of volumetric data significantly limits the accuracy of estimates for sediment fluxes by erosion. The use of high-resolution DEM data offers new possibilities to address this knowledge gap. The most recent information of coastal erosion for the Canadian Beaufort Sea is from 2000 (Solomon, 2005; Lantuit and Pollard, 2008) and given the recent sea-ice minima needs updating.

The aim of our study is to explore the relationship between planimetric and volumetric coastal erosion measurements and the corresponding estimates of sediment release rates for Herschel Island. The specific objectives of this study are to:

- quantify rates of planimetric erosion based on coastline positions digitised from satellite imagery,
- quantify volumetric erosion rates derived from DEM elevation differences used to convert volume change into estimated sediment release based on excess ground ice data and to estimate organic carbon and nitrogen fluxes,
- explore the relationship between rates of sediment release, coastline movement, and sediment release calculated from coastline movement rates combined with cliff height,
- update the recent coastline movement rates on Herschel Island and compare them to the existing baseline (1970-2000) calculated by Lantuit and Pollard (2008).

4.2 Study Area

Herschel Island is located a few kilometres off the northwestern Yukon Coast (Canada) in the southern Beaufort Sea. The island is situated at 69°34'N and 138°55'W, is 13 x 15 km in size and covers an area of 110 km^2 (Figure 4.1). Mean annual temperature is -9°C and daily averages rise above 5°C in July and August (Burn 2012). Yearly precipitation is between 150 and 200 mm. Permafrost is continuous with mean annual ground temperature of -8 °C at the depth of zero annual amplitude and active layer depths range between 40 and 60 cm (Burn and Zhang 2009). Storm events generate high winds from predominantly westerly and northwesterly directions, with a secondary set of storm events coming from the east to southeast (Hudak and Young 2002; Solomon 2005). Storms are frequent in late August and September and can generate significant wave heights of 4 m and higher (Pinchin et al., 1985). Coastal areas of the southern Beaufort Sea are ice-fast for 8 to 9 months of the year, with complete sea-ice cover from mid-October through June (Solomon 2005). The trend of open water season lengthening around Herschel Island is 1.5 day a^{-1} (Barnhart et al., 2014b).

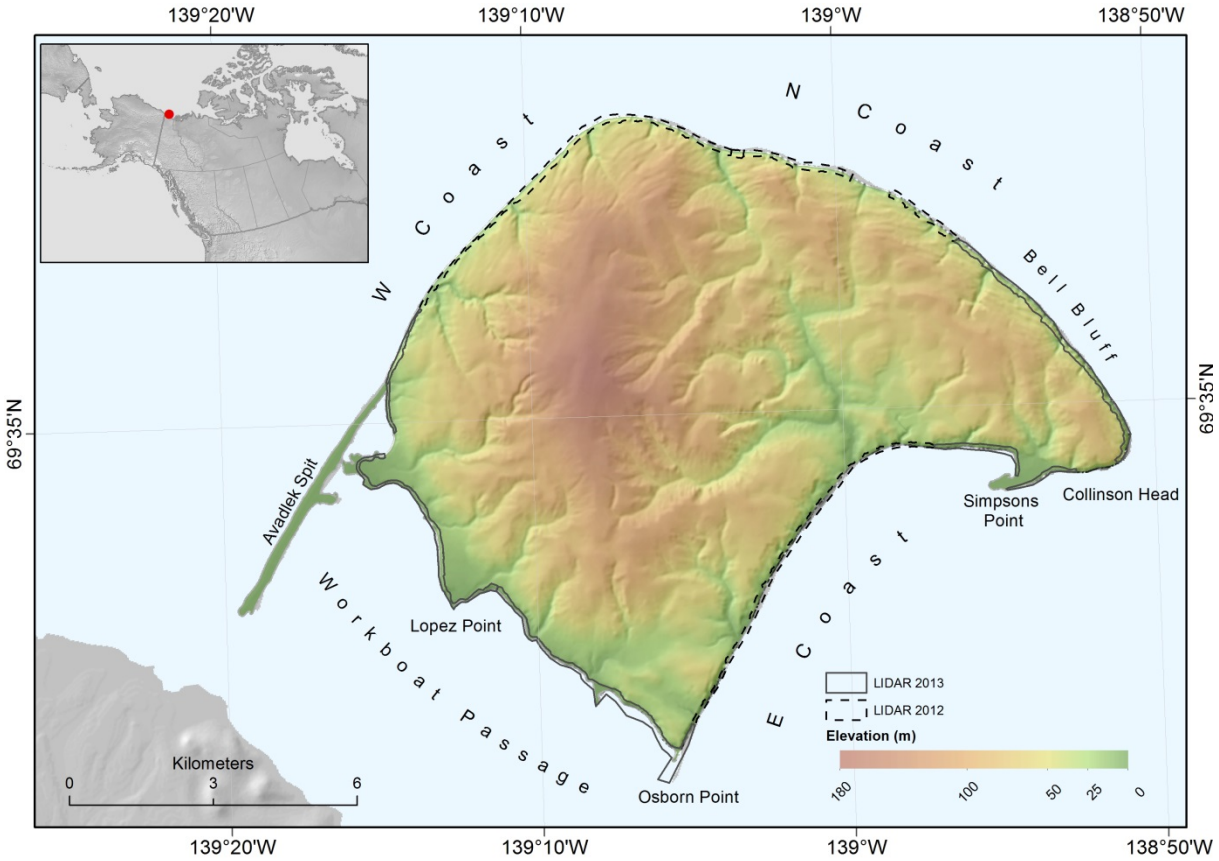

Figure 4.1: Hypsometric tint map of Herschel Island in the Canadian Arctic with place names. Coastal areas are marked with the year of LIDAR DEM acquisition used for calculations. Displayed are also four coastal units (east, north, and west coast and Workboat Passage).

Sea-bed topography, sediment structures and ground ice origin suggest that Herschel Island is a push moraine that was formed by the Laurentide ice sheet progression (Mackay 1959; Bouchard 1974; Fritz et al., 2012). The island is therefore made of unconsolidated and mostly fine-grained marine sediment and is characterised by a massive ground ice of glacial and intrasedimental origin (Bouchard 1974; Pollard 1990; Fritz et al., 2011). Herschel Island rises to a maximum height of 180 m a.s.l., its terrain is diverse and characterised by numerous valleys, gullies, steep coasts, and thermokarst phenomena (Lantuit and Pollard, 2005; 2008). Mean soil organic carbon and total nitrogen storage for the uppermost 1 m on Herschel Island are estimated to be 34.8 kg C m^{-2} and 3.4 kg N m^{-2} (Obu et al., in press).

Steep cliffs undergoing erosion and mass-wasting processes are prevalent on the Herschel Island coasts (Lantuit and Pollard, 2008). Mass wasting may proceed in a cascade-like manner where the slope undergoes several stages from undercutting to levelling or rapid block failure. Thawed material can be transported to the coast as mudflows from retrogressive

thaw slumps or as active layer detachment landslide (Lantuit and Pollard, 2005; Lantuit et al., 2012b). The highest and the steepest cliffs are found on north and west coasts. The cliff height gradually increases from 30 to 50 m from Collinson Head towards the northernmost part of the Island and decreases to 30 m from the northern part towards the Avadlek Spit at the southwest corner. The east coast is less steep and with low cliffs ranging between 20 to 30 m high. Cliffs along Workboat passage are relatively low and gentle, around 10 m high but up to 20 m close to Osborn point. Sedimentation features resulting from longshore drift include three sand/gravel spits, including; Simpson, and Osborn Point and Avadlek Spit. Ground ice contents by ice type were estimated by Couture (2010). Percentage of excess ice is the highest in Workboat passage (35 %) and along the east coast (13 %). North and west coasts have estimated excess ice volumes between 2 and 5 %.

4.3 Methods

4.3.1 Processing of satellite imagery and coastline mapping

Satellite imagery from different points in time was used to determine the coastline positions. An Ikonos satellite image was acquired on 18 September 2000 and two GeoEye images were acquired on 31 August and 8 September 2011. The raw imagery was processed with Geomatica 2014 Ortho Engine and georeferenced using ground control points collected by Lantuit and Pollard (2008). Additional ground control points that were used to georeference the Ikonos image were based on the GeoEye image to ensure a good spatial match between both datasets. GeoEye images were processed with Rational Function and mosaicked to 0.5 m pixel spacing. The Ikonos image data was lacking rational polynomial coefficients and was therefore processed using a physical sensor model (Toutin, 2011) to final 0.6 m pixel spacing. All images were ortho-rectified to mean sea level as the reference plane for a correct coastline position. Residual mean square (RMS) for the Ikonos image was 0.74 m and 1.77 m for GeoEye. The Ikonos image did not completely cover the western part of Herschel Island and consequently the coastline movement was not estimated for this data gap.

We defined the coastline according to Bird (2011) as “the edge of the land at the limit of normal high spring tides”. In the case of steep coasts with no accumulations at the shore the cliff base was mapped and in case of low coasts or accumulations the first beach ridge was mapped. Coastlines were digitised as shapefiles in ESRI ArcGIS 10.3 and used to evaluate planimetric coastal erosion. While the majority of studies on Arctic coastal erosion were based on planimetric erosion, we differentiate coastline movements as both coastline retreat and progradation, and volume of sediment change (sediment release and accumulation).

4.3.2 DEMs and volume change

High resolution DEMs from 2004, 2012 and 2013 were used to calculate volumetric changes in the coastal area. A DEM from 2004 is a PhotoSat product created from an Ikonos stereopair from 18 September, 2004 with a 2 m pixel spacing and estimated vertical resolution of 0.5 m (Short et al., 2011). DEMs from 2012 and 2013 were acquired from airborne LIDAR scanning that took place during the AIRMETH (AIRborne measurements of METHane fluxes) campaigns (Kohnert et al., 2014) on 10 July, 2012 and on 22 July, 2013. Point cloud data were interpolated to raster DEMs with 1 m pixel spacing with inverse distance weighting algorithm. Vertical accuracy was estimated to be 0.15 m. A detailed LIDAR DEM creation procedure is described by Obu et al. (under review). All DEM elevations were referenced to EGM (Earth Gravitational Model) 2008 geoid (Pavlis et al., 2008) in order to exclude errors originating from geoid differences.

DEMs were subtracted to calculate elevation differences. Elevation increase and elevation decrease were analysed separately. DEM calculations were conducted with ESRI ArcGIS 10.3. Volume change was calculated as a sum of the elevation change multiplied by cell size:

$$V = \sum_{i=1}^{n} A \cdot \Delta h \quad (4.1)$$

Where V is the recorded volume change, A is the pixel area and Δh is the elevation difference between two DEM pixels.

In areas of continuous permafrost ground ice may accumulate far in excess of normal soil moisture conditions. The volume of supernatant water present if a vertical column of frozen sediment were thawed is referred to excess ice (French, 2013). The volume of sediment upon thaw of excess ice is therefore less than the total eroded volume (Are, 1988). Couture (2010) calculated excess ice percentage for the six terrain units of Herschel Island. Released sediment volumes were calculated using the method of Lantuit and Pollard (2005), which took into account the excess ice percentage under the overburden material, which is very low of excess ice, using the following equation:

$$V_s = \sum_{i=1}^{n} [Ai \cdot (\Delta h - Zo)(1 - \theta) + (A \cdot Zo)] \quad (4.2)$$

Where Vs is the volume of released sediment, Zo is mean overburden depth and θ is the fraction of the excess ground ice. The same authors reported mean overburden material thickness of 1.5 m on Herschel Island. Volumes were corrected only for erosion (elevation decrease), but not for accumulation (elevation increase), because we assume that after sediment relocation the material is free of excess ice.

4.3.3 Accuracy assessment

Uncertainty in the coastline position can be due to the satellite imagery positioning. Accuracy of coastline position was assessed from the georeferencing uncertainty (δr) and geometric resolution of dataset (δp) adapting the method of Günther et al. (2013). The threshold for considered coastline changes was calculated using:

$$\delta x = \sqrt{\delta_r^2 + \delta_p^2} \quad (4.3)$$

$$\delta cr = \frac{\sqrt{\delta x_1^2 + \delta x_2^2}}{t_2 - t_1} \quad (4.4)$$

Where δx is the cumulative uncertainty in coastline position, δcr is the change rate uncertainty and t_1 and t_2 are the dataset acquisition years. The coastline change rate threshold was 0.18 m a^{-1}.

Elevation change accuracy was estimated using the approach of Jones et al. (2013). Vertical accuracies of the Ikonos derived and LIDAR DEM datasets were used to calculate the threshold of considered elevation changes:

$$\delta z = 3 \times \sqrt{\delta_{DEM1}^2 + \delta_{DEM2}^2} \quad (4.5)$$

Where δz is the elevation change uncertainty and δ_{DEM} is the vertical accuracy of the DEM datasets. Threshold for the significant elevation change was 1.57 m.

4.3.4 Coastline movement, sediment release, organic carbon and nitrogen flux estimation

Coastline movements and sediment release were analysed using a series of belt transects. These are 50 m wide and 400 m (in inland direction) long sections of coast. In total, 963 belt transects were generated for the 48 km of coastline studied.

Coastline movements (planimetric erosion) were analysed along 36 km of coast in the Ikonos and GeoEye image overlap area. Digitised coastlines were combined to generate polygons, which indicate the coastline retreat or progradation area. These polygons were clipped by the belt transects to calculate the area of retreat and/or progradation that occurred inside each transect belt. These areas were divided by the belt transect base width (50 m) to get an average coastal retreat or progradation for each belt transect. Average coastline movement for the whole coastline was calculated as total retreat and progradation area divided by total studied coastline length. Total retreat distances were divided by the number of years to determine annual retreat rates. Standard deviations were estimated from the rates calculated for the belt transects.

Volumetric erosion was calculated from volume change that was recorded inside the belt transects. Only volume change that was a direct consequence of coastal erosion was considered; land loss and mass movement directly on the coast, but not gully erosion and volume changes inside retrogressive thaw slumps. The swath of the LIDAR surveys did not always cover the whole coastal zone along the track due to flight constraints. To achieve the best quality in the volume change data we included LIDAR datasets from 2012 and 2013 in the volume change analyses and selected the acquisition year according to the best coastal zone coverage (Figure 4.1). There was only 3.1 km of coastline with insufficient coverage by both LIDAR DEMs at Bell Bluff, Collinson Head, Simpson Point and Orca Cove. Volume change was also not calculated for Avadlek Spit because the elevation uncertainties were too high. Volume change rates were calculated according the year of the DEM dataset that was chosen for a belt transect.

In order to estimate the sediment released for the entire Herschel Island coastline and four island units (Figure 4.1), the sediment release was interpolated for the parts of the island where volumetric erosion data were missing (Bell Bluff, Collinson Head and in Orca Cove) as an average of the 20 adjacent transects. Organic carbon and nitrogen fluxes were calculated by multiplying sediment release and carbon and nitrogen storage estimates from Obu et al. (in press) for Herschel Island. They reported storage of 20.9 kg C m^{-3} and 3.7 kg N m^{-3} in the strongly disturbed terrain, which is actively undergoing material removal. This storage is for this reason reflecting the organic carbon and nitrogen contents of the parent material that is being eroded at the cliffs.

Sediment release was also calculated using planimetric erosion rates to compare it with sediment release calculated from DEMs. The coastline retreat rates were combined with cliff heights, which is an established method for organic carbon fluxes calculation (Lantuit et al., 2009; Ping et al., 2011). We used the following equation:

$$V_{sc} = R \cdot l_t(h - Zo)(1 - \theta) + (R \cdot l_t \cdot Zo) \quad (4.6)$$

Where *Vsc* is the volume of sediment release estimated from the planimetric retreat rates, *h* is the cliff height, *R* is the coastline retreat rate and l_t is the transect width. This equation takes into account the ground-ice content and overburden thickness in the same principle as equation 4.2. Mean cliff height of each transect belt was averaged from DEM elevations.

4.3.5 Update of coastline retreat rates

Lantuit and Pollard (2008) calculated erosion rates on Herschel Island for two periods (1952-1970 and 1970-2000). To estimate the recent change in coastal erosion rates, we updated the rates for the period 2000-2011 using the same survey points. Coastline movement was

measured as the distance between the coastline digitised by Lantuit and Pollard (2008) and the ones digitised in the present study.

4.4 Results

4.4.1 Planimetric erosion

Net annual rate of coastline retreat along the analysed 36 km of Herschel Island coast was 0.68 ± 2.48 m a^{-1}. Average annual coastline retreat rate was 0.88 m a^{-1} and the average coastline progradation rate was 0.20 m a^{-1}. Percentage of analysed coastline that underwent retreat was 72 % and coastline aggradation was 11 %. The rest of coastline did not experience any net change. The strongest retreat rate of 5.2 m a^{-1} was recorded at a low cliff coast at Simpson Point (Figure 4.2). Belt transects with coastline retreat rates between 0 to 0.5 m a^{-1} were the most common (Figure 4.3) and frequency was gradually decreasing towards higher retreat rates. Coastline retreat rates above 3 m a^{-1} occurred at the Simpson Point alluvial fan and at Collinson Head.

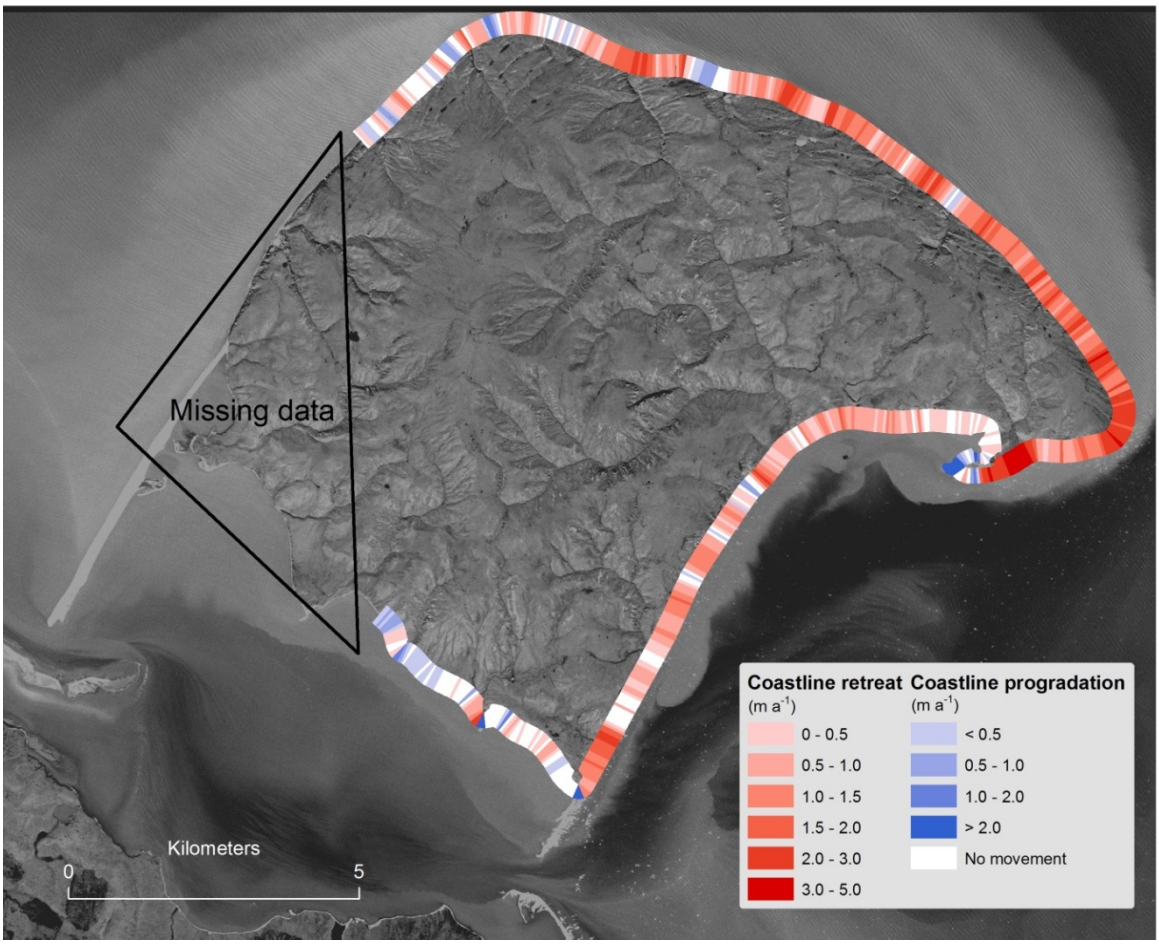

Figure 4.2: Map of planimetric erosion inside belt transects on Herschel Island. Net rates of coastline movement between 2000-2011 were calculated from digitised coastlines. Red colour indicates coastline retreat and blue indicates coastline progradation.

Coastline retreat rates were the highest along the north coast (Table 4.1, Figure 4.2). They were considerably lower in the western and eastern coast and were lowest in Workboat Passage unit. Coastline progradation occurred sporadically and was most common in Workboat Passage. Coastal retreat rates showed high variability also within these four Herschel Island units. The analysed spits (Simpson and Osborn point) were characterised by sedimentation and spit aggradation and resulted in high coastline progradation rates above 20 m a^{-1}.

Table 4.1: Coastline movement, volume decrease, sediment release and carbon and nitrogen fluxes in different units of Herschel Island. Volume decrease and sediment release rates include interpolated data for gap-filling.

Islands' unit	Mean coastline retreat rate ($m\ a^{-1}$)	Mean coastline progradation rate ($m\ a^{-1}$)	Mean net coastline movement rate ($m\ a^{-1}$)	Mean volume decrease rate ($m^3\ m^{-1}\ a^{-1}$)	Total volume decrease rate ($m^3\ a^{-1}$)	Mean sediment release rate ($m^3\ m^{-1}\ a^{-1}$)
East coast	0.85 ± 0.95	0.19 ± 3.74	-0.66 ± 3.93	6.9 ± 10.8	89 000	6.2 ± 9.7
North coast	1.22 ± 0.75	0.02 ± 0.10	-1.20 ± 0.79	73.1 ± 30.3	1 111 000	71.6 ± 29.7
West coast	0.30 ± 0.42	0.16 ± 0.33	-0.13 ± 0.62	23.6 ± 24.5	189 000	23.0 ± 23.9
Workboat Passage	0.16 ± 0.35	0.72 ± 0.77	0.56 ± 0.84	1.1 ± 3.1	13 000	0.9 ± 2.6
Herschel Island	0.88 ± 0.86	0.20 ± 2.26	-0.68 ± 2.48	29.0 ± 37.2	1 404 000	28.2 ± 36.2

(table continued)

Islands' unit	Total sediment release rate ($m^3\ a^{-1}$)	Organic carbon flux ($kg\ C\ m^{-1}\ a^{-1}$)	Nitrogen flux ($kg\ N\ m^{-1}\ a^{-1}$)	Total organic carbon flux ($Tg\ C\ a^{-1}$)	Total nitrogen flux ($Tg\ N\ a^{-1}$)
East coast	80 000	130.1	23.0	1.7	0.30
North coast	1 088 000	1495.7	264.8	22.7	4.02
West coast	185 000	480.4	85.0	3.9	0.68
Workboat Passage	11 000	19.3	3.4	0.2	0.04
Herschel Island	1 364 000	589.8	104.4	28.5	5.05

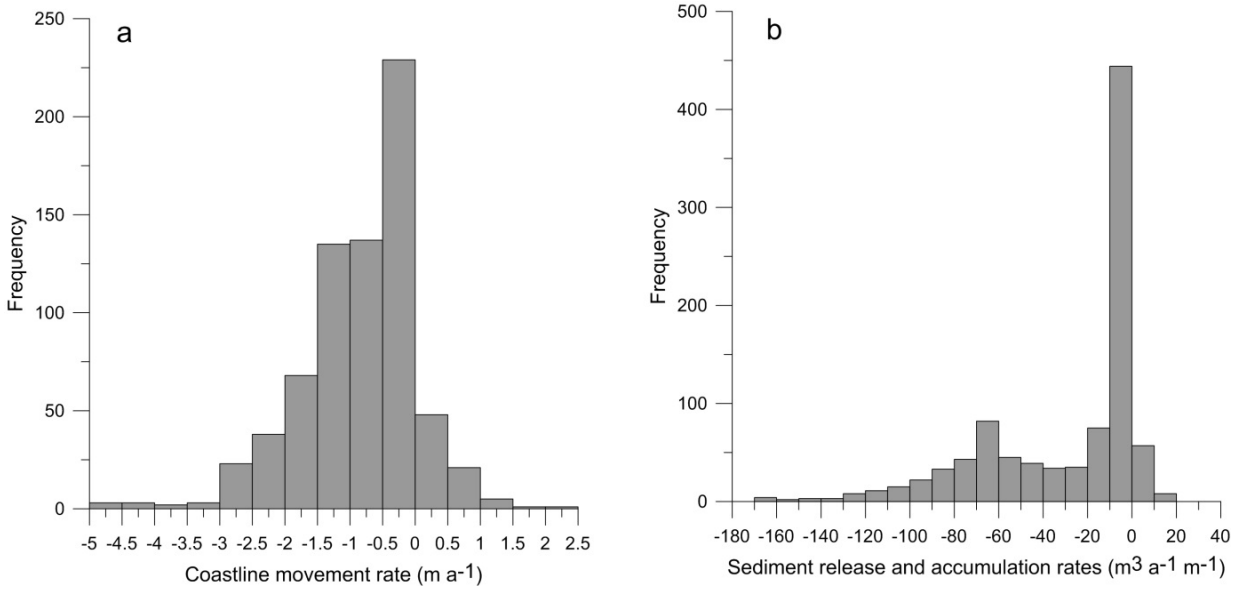

Figure 4.3: Frequency distribution for (a) coastline movement and (b) net rates of sediment release and accumulation. Negative values represent coastline retreat and sediment release, whereas positive values indicate coastline progradation and sediment accumulation.

4.4.2 Volumetric erosion, organic carbon and nitrogen fluxes

Along the entire coastline, the average volume decrease was 29.0 m^3 m^{-1} a^{-1} and the resulting sediment release was 28.2 m^3 m^{-1} a^{-1}. In contrast to coastline movement, the sediment release showed less variability within the four units. Sediment release rates were high in the whole northern part of Herschel Island (Figure 4.4) and were considerably lower along the east and west coasts. The lowest sediment release was recorded in Workboat Passage. The annual net sediment release for the entire island was 1 364 000 m^3 a^{-1}. The resulting organic carbon and nitrogen fluxes were 590 kg C m^{-1} a^{-1} and 104 kg N m^{-1} a^{-1}. Sediment release rates showed a bimodal frequency distribution. The most frequent rate was between 0 and 10 m^3 m^{-1} a^{-1} (Figure 4.3), while a second, less pronounced frequency peak occurred between 60 and 70 m^3 m^{-1} a^{-1}.

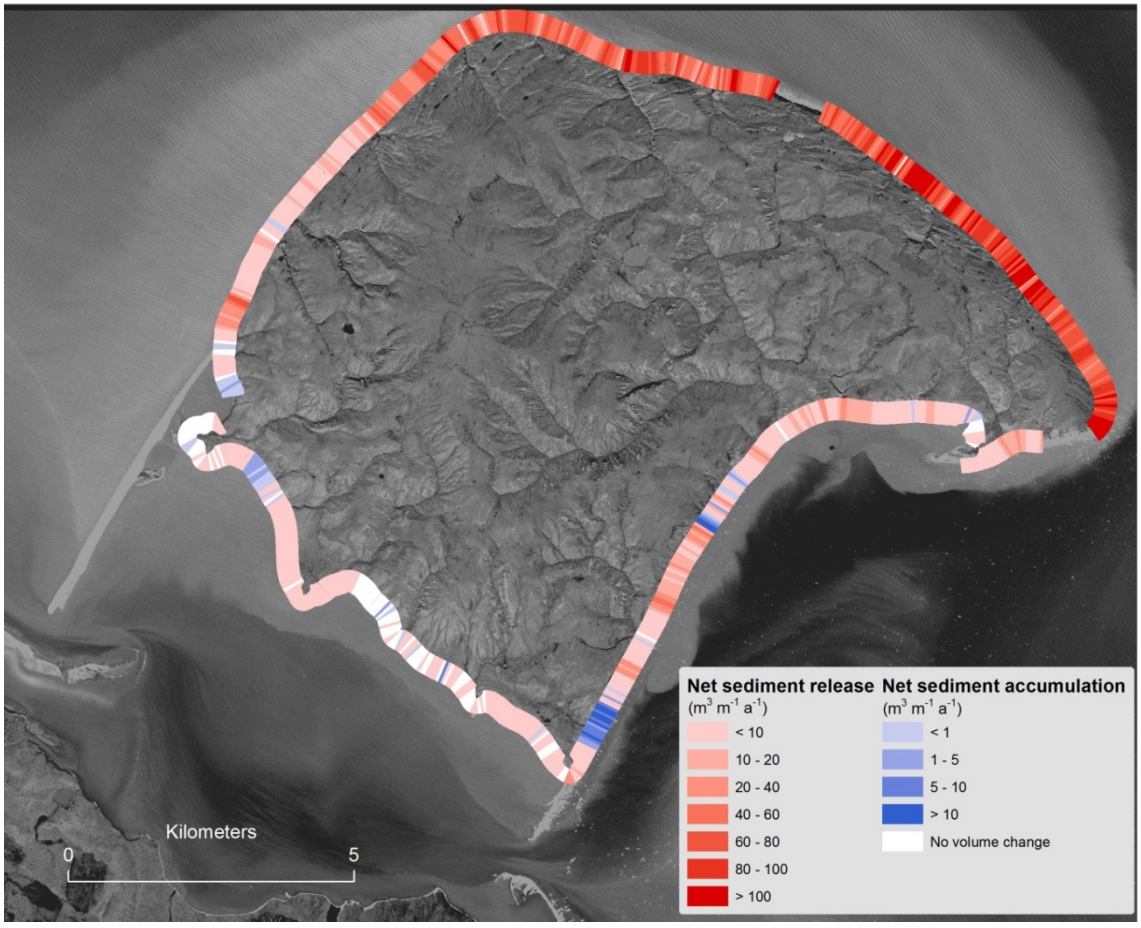

Figure 4.4: Map of volumetric erosion inside belt transects on Herschel Island. Net sediment release rates between 2000-2011 are based on DEM elevation changes. Red colour indicates sediment release and blue indicates sediment accumulation.

The average sediment release rate based on planimetric erosion that was calculated from planimetric coastline retreat rates and cliff heights was 31.3 m^3 m^{-1} a^{-1}. Calculations based on DEMs for the same transect belts (only overlapping data) gave an average sediment release rate of 35.7 m^3 m^{-1} a^{-1}. This comparison shows that the method using planimetric coastline retreat rates underestimated the average sediment release rate. Although both average release rates are similar, the estimates vary significantly among belt transects. The correlation between both rates inside belt transects is statistically significant (p-value < $2.2e^{-16}$) but low (Figure 4.5).

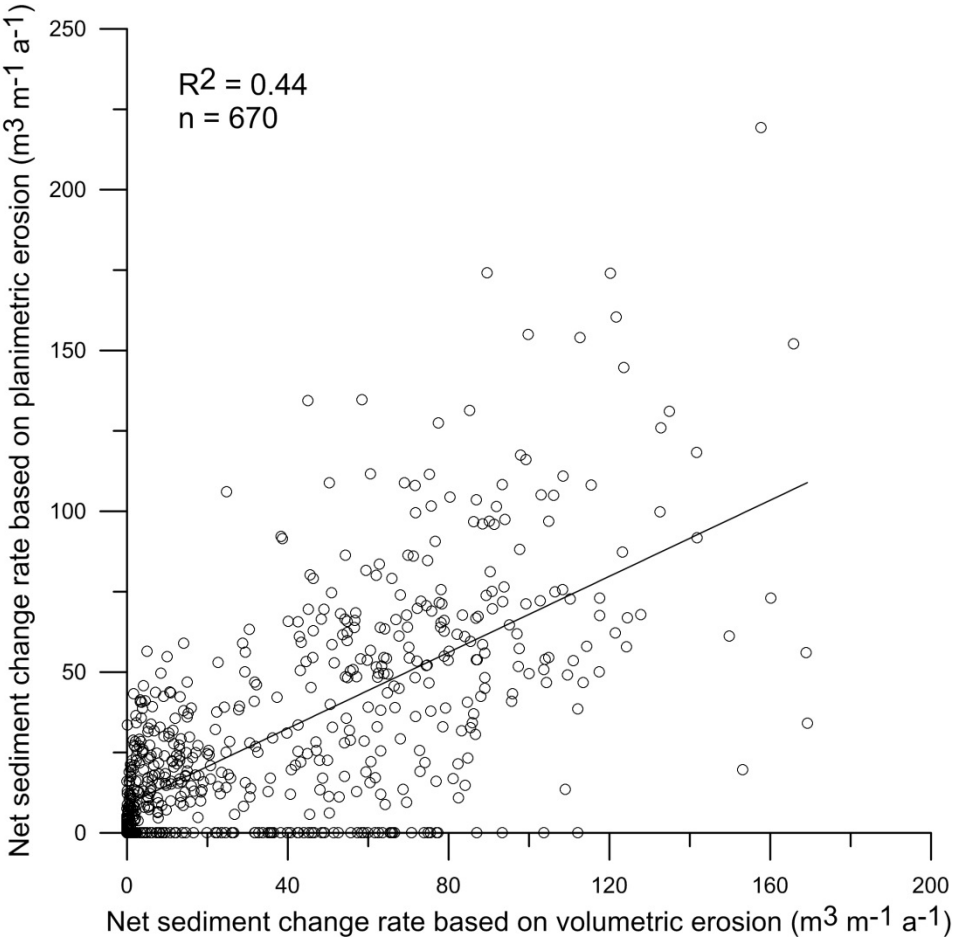

Figure 4.5: Scatterplot with linear best fit showing sediment release rates based on DEM elevation change compared to sediment release calculated from coastline retreat and cliff height.

4.4.3 Relation between planimetric and volumetric erosion

Estimated planimetric erosion over 11 years (2000-2011) and volumetric erosion over a period of 8 to 9 years (2004-2012, 2013) overlap for 7 years; meaning that 54 to 58 % of the study time span. The majority of transects that experienced coastline retreat also underwent

sediment release. There are also many transects that underwent coastline progradation (negative planimetric erosion) but sediment release (volumetric erosion). Few transects were subject to both coastline progradation and sediment accumulation or coastline retreat and sediment release.

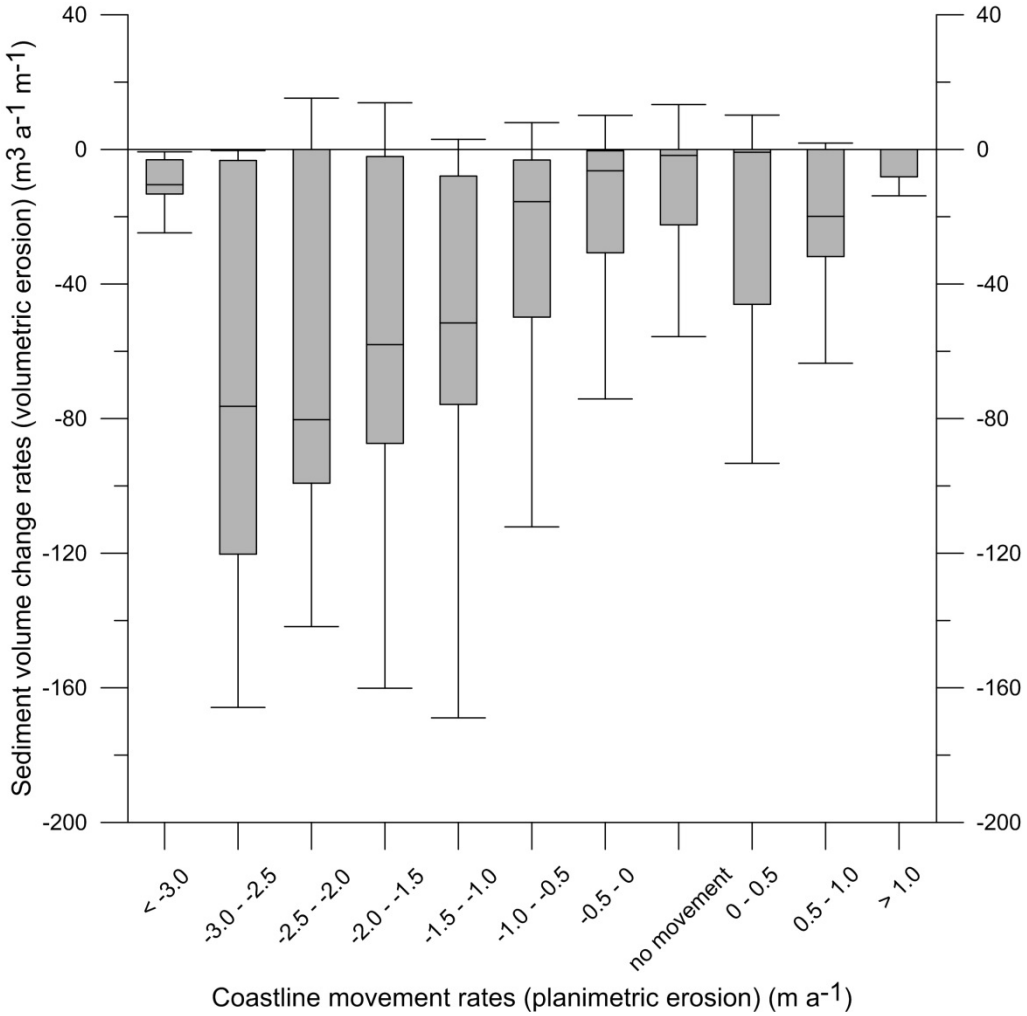

Figure 4.6: Boxplot showing sediment release or accumulation rates for different classes of coastline movement.

Figure 4.6 shows that volumetric erosion and its variability increase with planimetric erosion rate. Both the sediment release and its variability decrease where coastline retreat rates are higher than 3 m a^{-1}. Volume decrease is prevalent also where coastlines prograded. High sediment release occurred mostly in transects with a maximum cliff height above 30 m (Figure 4.7). Considerable sediment release and coastline progradation were recorded together where cliff heights were above 40 m. The highest coastline retreat was accompanied by relatively low sediment release in transects with low cliffs (below 20 m).

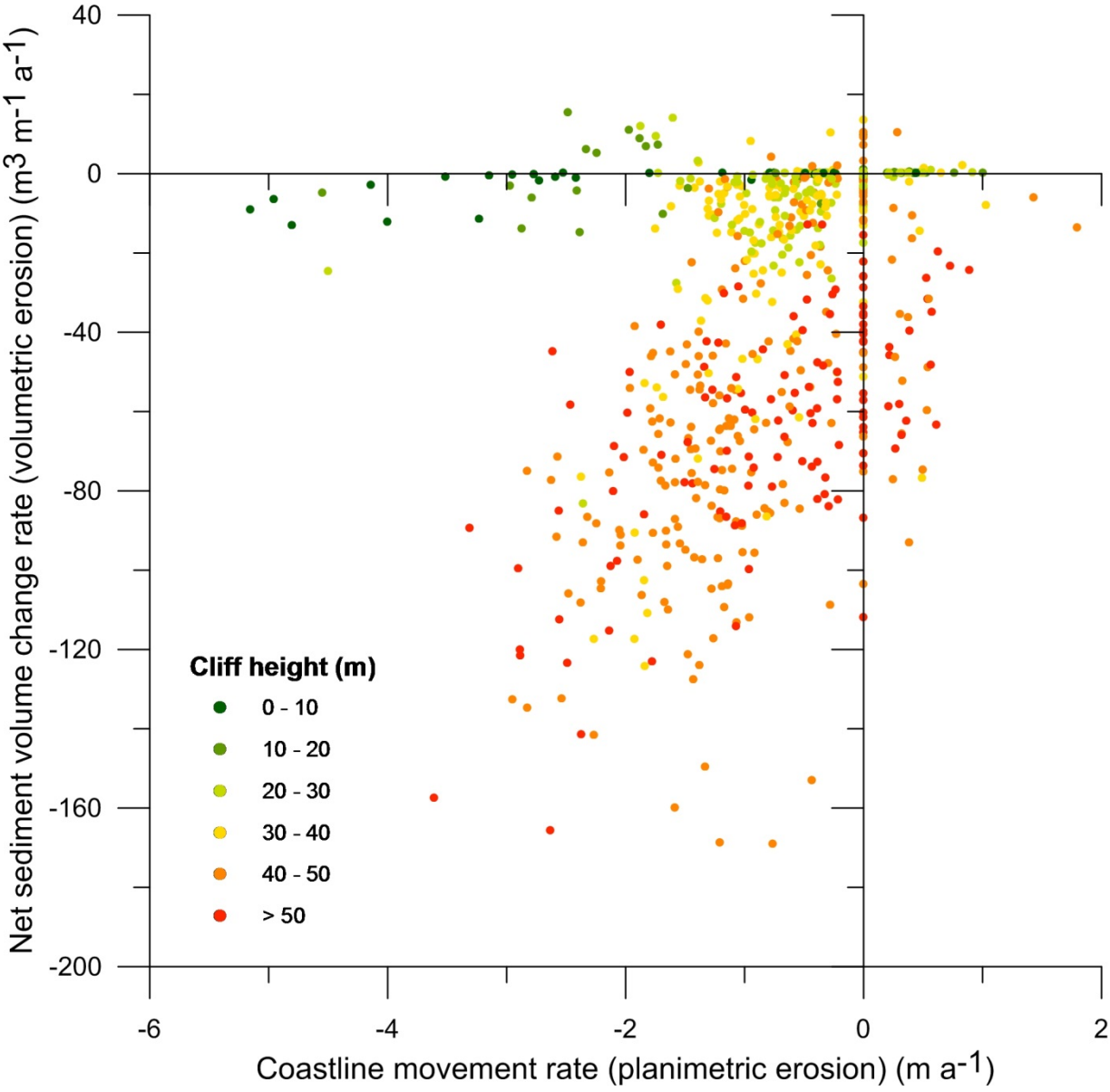

Figure 4.7: Scatterplot showing the relationship between coastline movement rate and net sediment change grouped according to cliff heights.

4.4.4 Update of coastline retreat rates (2000 – 2011)

A coastline retreat rate of 0.92 m a^{-1} was recorded for the period 2000-2011 using the same method and transects used by Lantuit and Pollard (2008). They reported 0.73 m a^{-1} of annual coastline retreat rate for the period 1952-1970 and 0.54 m a^{-1} for 1970-2000. The coastline retreat rate increased by 0.38 m a^{-1} and was statistically significant ($p = 0.001$). The correlation between individual coastline movement rates from 1970-2000 and 2000-2011 was very low with ($R^2 = 0.0027$) and values show scattered distribution (Figure 4.8). The majority of compared coastline transects showed a recent increase in the rate of coastal erosion. None

of the transects were characterised by coastline progradation during both analysed periods. Retreat rates have increased at Collinson Head, Bell Bluff and at the southern part of the east coast. The increase was mostly recorded where Lantuit and Pollard (2008) recorded a decreasing retreat rate.

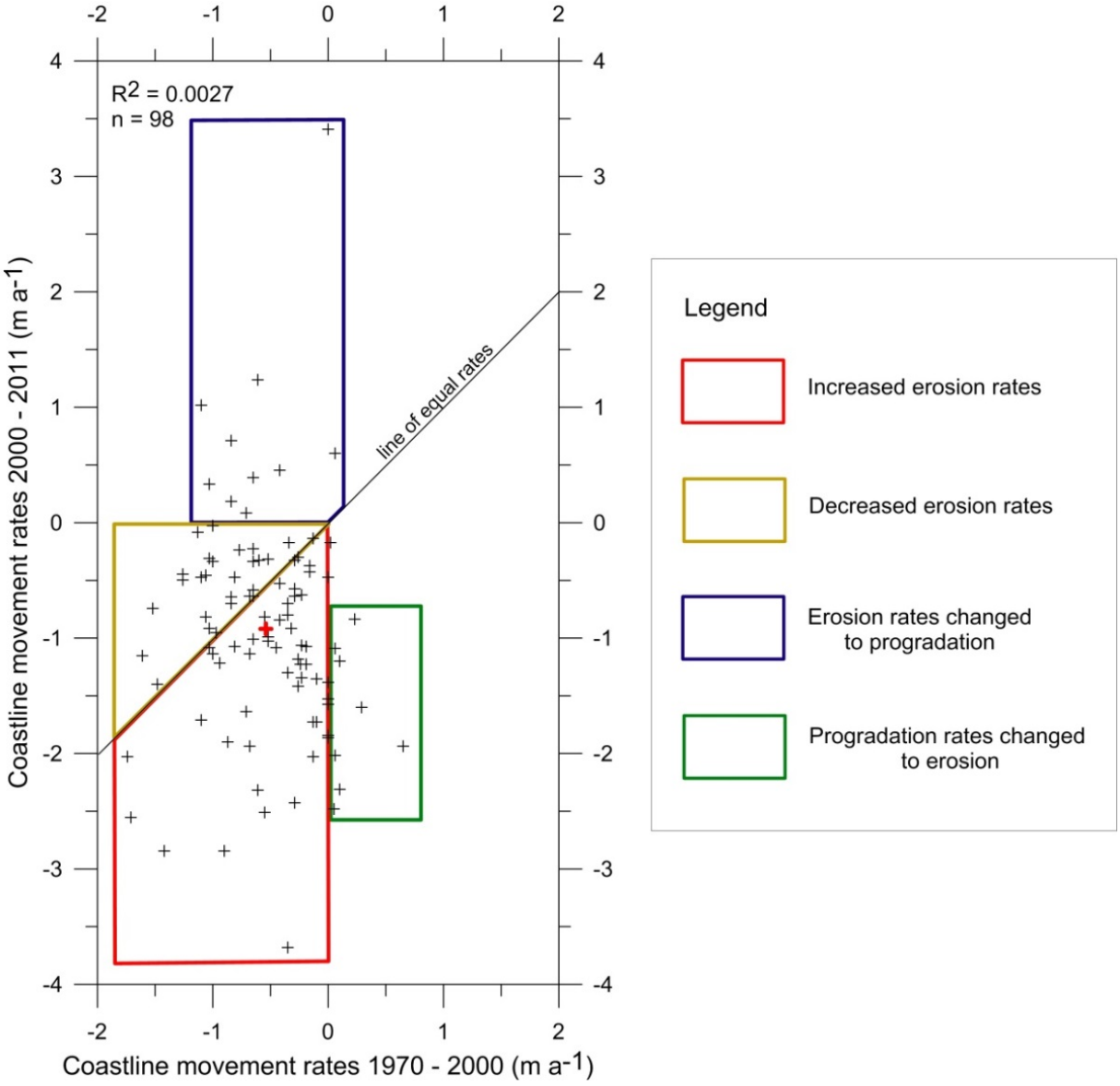

Figure 4.8: Scatterplot with coastline movement rates from period 1970-2000 and 2000-2011. Crosses that are below the line of equal rates underwent coastline retreat rate increase. The red cross represents the average coastline movement rates. The coloured sectors highlight different changes in coastline movement rate.

4.5 Discussion

4.5.1 Planimetric erosion

We recorded an average coastline retreat rate 0.68 m a^{-1}, which is similar in magnitude with the rates that were reported for the Beaufort-Mackenzie region (Solomon 2005). Compared to modern coastal erosion rates reported from low-lying thermokarst coasts along the Dmitry Laptev Strait (Günther et al., 2013) or from the coastal lowlands with ice-rich cliffs of the Alaskan Beaufort Sea coast (Jones et al., 2009), erosion rates on Herschel Island are low. However, they are comparable to the results of Lantuit et al. (2011) for high cliff coasts on the Bykovsky Peninsula, where the material removal and sediment beach dynamics are more similar to Herschel Island (Günther et al., 2013). Coastline movement rates were not estimated for the part of Workboat Passage and the west coast where coastline movement rates are lower (Lantuit and Pollard, 2008). Thus, we assume that the average coastline retreat would be slightly lower when including the missing section of coastline.

The high standard deviation in coastline movement is a consequence of high progradation rates measured on spits, where accumulation occurred (Simpson and Osborn point). Excluding transects with spits, the coastline retreat rate would be 0.80 m a^{-1} with 0.95 m of standard deviation. Solomon (2005) and Lantuit et al. (2011) reported a high spatial and temporal coastal erosion rate variability for other parts of Canadian Beaufort Sea and Laptev sea. Obu et al. (under review) showed that high short term coastline variability rates can occur due to sediment accumulation. Our results suggest that sedimentation of spits can change rapidly and can influence the average coastline retreat up to 0.10 m a^{-1}.

4.5.2 Volumetric erosion and soil organic carbon and nitrogen fluxes

The volumetric erosion shows different erosion patterns in comparison to planimetric. Planimetric erosion shows higher variability and alternation between coastline retreat and progradation, whereas volumetric erosion is more uniform (Figure 4.2 and Figure 4.3). The latter is characterised by high rates along the north coast, lower rates along the east and west coast, and low rates at Workboat Passage. Both planimetric and volumetric erosion were the highest along the north coast, but volumetric is considerably higher in comparison to other parts of Herschel Island. The west coast underwent low planimetric erosion, but considerable volumetric erosion due to the high cliffs. In contrast, the east coast underwent higher planimetric erosion rate than the west coast, but the volumetric erosion was considerably lower along the east coast. The north and west coast have the longest fetch and are the most exposed to predominant storm winds, waves and storm surges (Hudak and Young, 2002; Atkinson 2005). For this reason, we assume that volumetric erosion likely corresponds better with environmental forcing, than planimetric erosion.

Organic carbon and total nitrogen fluxes on Herschel Island are higher than reported from other parts of the Beaufort Sea region. Ping et al. (2011) estimated organic carbon fluxes of 73 kg C m^{-1} a^{-1} for the different coastal types of the Alaskan part of the Beaufort Sea coast, which is considerably lower than our estimate for Herschel Island of 590 kg C m^{-1} a^{-1}. We attribute this difference to considerably lower cliff height (1.9 m in average) compared to Herschel Island (18 m), because coastline retreat rates and carbon storage are similar in both regions. The estimate for exposed bluff (3.2 m cliff height) organic carbon flux (163 kg C m^{-1} a^{-1}) for the Alaskan coast was in a range of our organic carbon flux estimations for the east coast of Herschel Island. Organic carbon fluxes from different parts of Laptev Sea varied between 70 to 850 kg C m^{-1} a^{-1} (Günther et al., 2013) and are more in range of the fluxes calculated in our study area.

4.5.3 Relation between planimetric and volumetric erosion

Our results suggest that the relationship between planimetric and volumetric coastal erosion is complex and non-linear. Rates of volumetric erosion are not necessarily increasing with planimetric erosion rates. The average sediment release is increasing until the coastal retreat rates reach ~3 m a^{-1}. Further increase in coastal retreat rates results in considerably lower sediment release. Transects with these high retreat rates are located along relatively low cliff coast (Radosavljevic et al., unpubl. ma.), such as the alluvial fan at Simpsons Point, which results in low sediment release rates. In contrast, high sediment release occurs where the cliffs are higher and coastline retreat rates were not necessarily high. The simultaneous occurrence of sediment release and coastline progradation at high cliffs suggests that these coasts are subject to intermittent transport of material to the shore, where it can cause coastline progradation, despite a net sediment release. Volume increase that occurred together with coastline retreat at some places on the east coast could be explained as a sediment accumulation event that occurred at the coast after 2011, when coastline movement was not recorded due to an incomplete planimetric and volumetric dataset overlap.

Although the average sediment release estimated from planimetric coastline movement (combined with cliff height) compared to sediment release derived from DEMs is similar, the differences between the same belt transects are significant. The reason is likely the complex relationship between planimetric and volumetric erosion, which is shown by a low correlation between both estimates (Figure 4.5). Elevation classes show weak clustering according to planimetric and volumetric erosion (Figure 4.7). Lantuit et al. (2009) have shown that estimated sediment release from coastal erosion rates and cliff height are too uncertain to be a reliable method for Arctic-wide estimation of sediment release. Our study has shown that the same estimations can be uncertain also on the local scale, because weak relationship between coastline retreat and sediment release (as in case of Herschel Island).

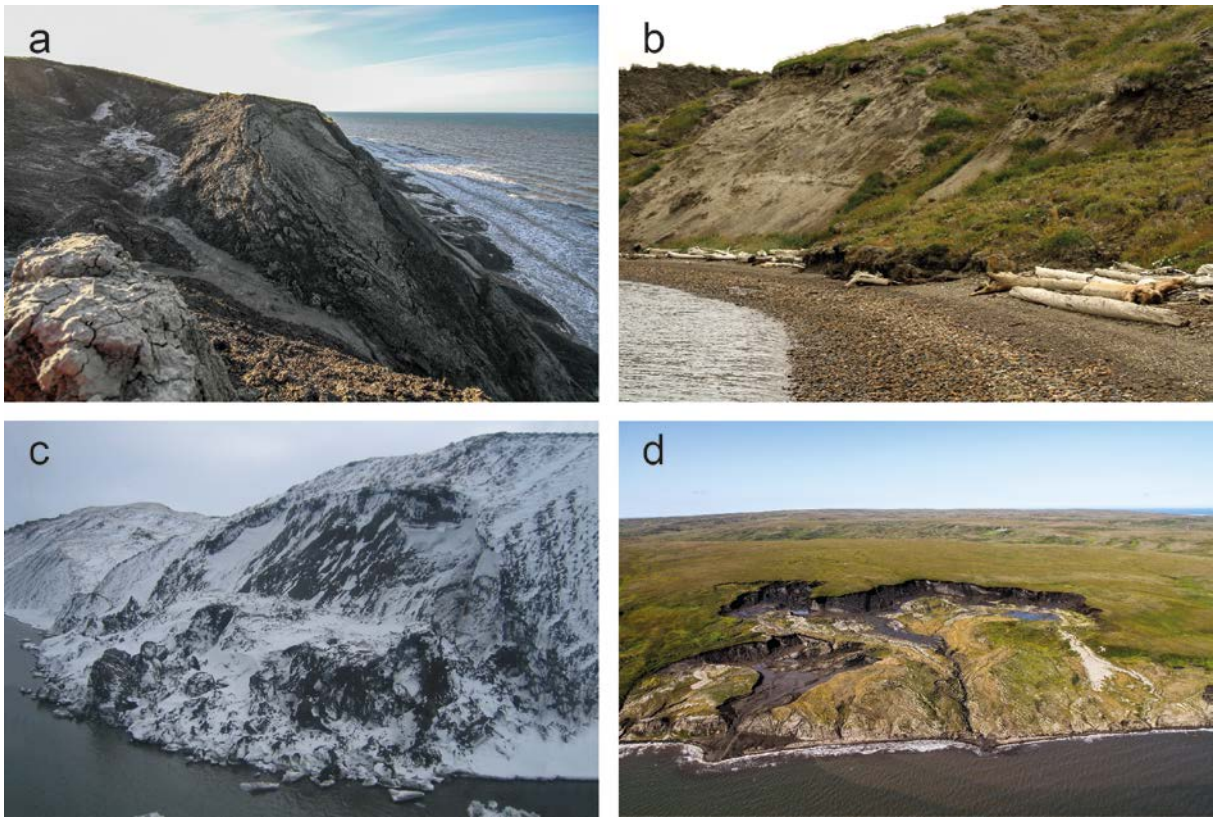

Figure 4.9: Coasts of Herschel Island can undergo a series of mass wasting and accumulation processes. Material is being transported as mudflows, landslides and block failures before reaching the shore. (a) Slumping, mudflows and shore accumulations on Bell Bluff; (b) active layer detachment on the east coast; (c) block failure on the north coast; (d) retrogressive thaw slump on the east coast.

We assume that the main reason for non-linear and complex relationships between coastline movement and sediment release is related mass wasting that occurs along coasts of Herschel Island (Figure 4.9). Lantuit and Pollard (2005; 2008) reported numerous active layer detachments and retrogressive thaw slumps. Obu et al. (under review) demonstrated that slumping can cause significant short term coastline variations on Herschel Island and along Yukon Coast. Lantuit et al. (2012a) and Leibman et al. (2008) indicated that material that is accumulated along the shoreline can inhibit coastal erosion until it is removed from the cliff toe. Constant supply of material to the shore either as liquefied sediment or collapsed material is likely slowing coastline retreat or causing even progradation, while the sediment is being constantly released. For this reason, modelling efforts trying to relate coastal erosion based on coastline movements to different environmental and local factors, should consider the effect of material transported to shore by mass wasting. Furthermore, studies that estimate sediment release and carbon fluxes based on coastline movement rates and cliff height should take into account different modes of sediment transport to the coast. The estimates of sediment release

based on cliff bottom and cliff top line movements as carried out by Günther et al. (2013) and Kizyakov et al. (2013) likely better capture the coastal erosion complexity due to mass wasting.

Some of the differences between planimetric and volumetric coastal erosion and consequent sediment release might originate from incomplete temporal overlap of our datasets, because several studies have shown a high temporal variability of permafrost coastal erosion (Obu et al., unpubl. ma.). As one of the first studies comparing the planimetric and volumetric Arctic coastal erosion it can serve as a baseline for further studies that explore this relationship in Arctic environments, where spatial data availability and field-work possibilities are limited.

The relationship between planimetric and volumetric erosion might be less complex in other Arctic coastal environments. In regions with low coasts and high planimetric erosion rates sediment release estimates based on planimetric erosion would likely be more suitable. As for example those observed on coastal sections of Alaska studied by Jones et al. (2009), where coastal erosion successfully removes the released material. The relationship is probably also more complex in ice-rich coasts with higher elevation as studied by Hoque and Pollard (2009) and Günther et al. (2013 and 2015) where thermoerosional-niche collapses modify simple erosion relationships between planimetric and volumetric erosion. Increasing availability of high-resolution elevation datasets in the future might offer more opportunities to study volumetric coastal erosion and sediment release. This would ultimately improve estimates of carbon and nutrient fluxes to the Arctic Ocean and their impact on coastal ecosystems.

4.5.4 Update of coastline retreat rates

We observed an increase of 52 % in coastline retreat rates during a period of 2000-2011 in comparison to the period 1970-2000. Günther et al. (2013) reported a similar increase for East Siberian coasts and Jones et al. (2009) for parts of the Alaskan Beaufort Sea for a period from 2002 to 2007. The latter attribute this increase to (1) increasing effectiveness of winds from easterly direction, (2) an increase in open water extent and, (3) Arctic Ocean surface warming and sea-level rise. Increased erosion rates on Collinson Head and a decrease in erosion rates on west coast (Figure 4.10) is in accordance with increasing effectiveness of easterly winds. The general increase of erosion rates on the north coast might be due to increased open water extent (Barnhart et al., 2014b) and later formation of land fast ice (Mahoney et al., 2014). Scattered values (Figure 4.8) and the low correlation between the current and rates from period 1970-2000 show that the recent erosion rates have undergone a significant change in spatial patterns. This indicates that the spatial distribution of coastline retreat can significantly vary over time.

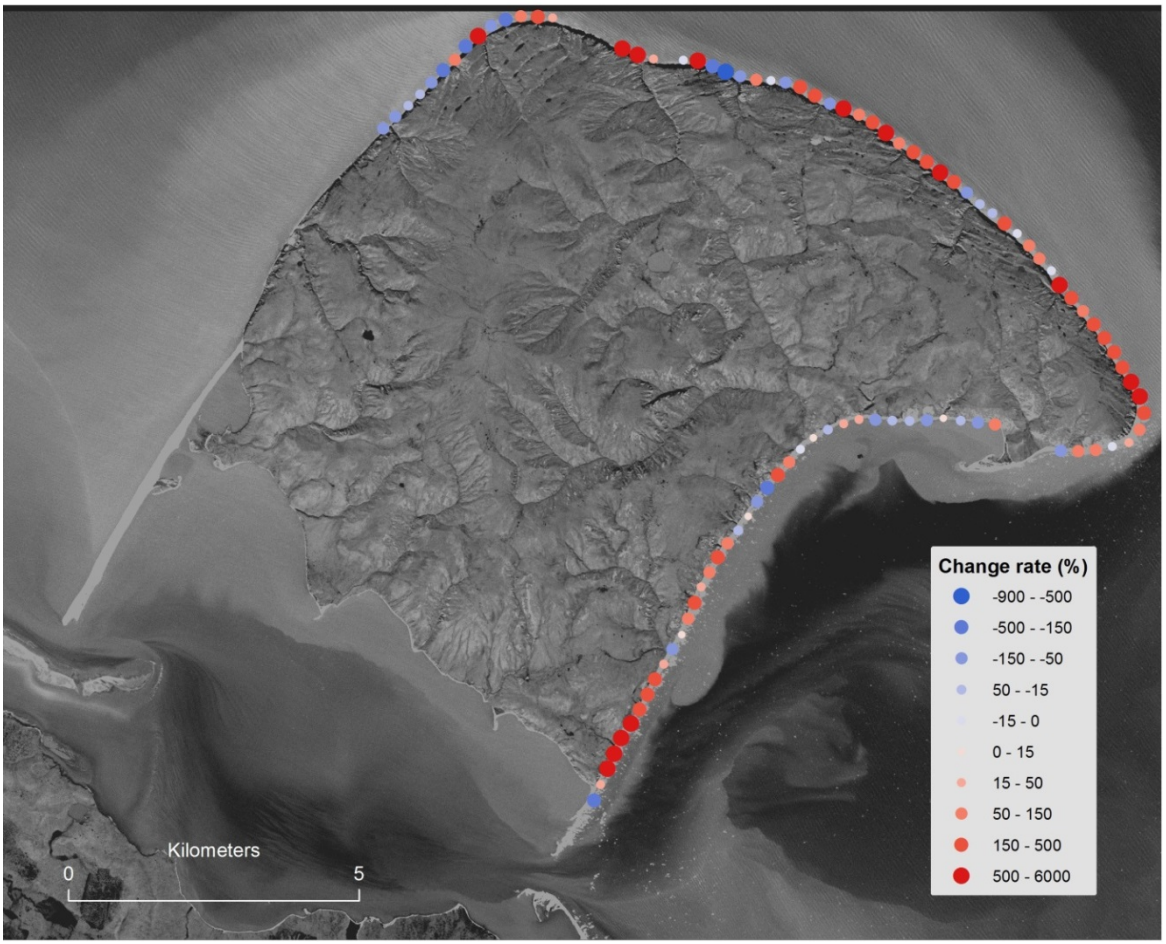

Figure 4.10: Rate of change in coastline movement between 1970-2000 and 2000-2011 based on the study from Lantuit & Pollard (2008). Positive values (red) show an increase in retreat rates.

4.6 Conclusions

Our study has demonstrated a complex relationship between planimetric and volumetric coastal erosion based on observations from Herschel Island. Two important implications are: (1) spatial patterns of volumetric erosion appear to be less variable than planimetric and correspond better with the exposure of island's coasts to wave action. We therefore suggest that volumetric erosion corresponds better with environmental forcing and could provide better coastal erosion modelling results. (2) Sediment release calculated from DEMs on a transect basis show a low correlation with sediment release calculated from planimetric erosion (combining coastline movement and cliff height). Organic carbon fluxes estimated from DEM are consequently considerably more accurate. We attribute the complexity of the relationship to frequent mass wasting that is occurring on Herschel Island's coasts, which is causing temporary coastline progradations, while sediment is being continuously removed. The observed recent increase in coastal retreat rates on Herschel Island is in agreement to increases observed along the Alaskan Beaufort Sea and the East Siberian coasts.

5 Discussion

The manuscripts in previous chapters dealt with SOC storage and coastal erosion on Herschel Island and along Yukon Coast. The results indicated important influence of mass-wasting on SOC storage and coastal erosion.

5.1 Effect of mass wasting on stored SOC

We showed in the Manuscript 1 that the ecological units exposed to mass wasting are characterised by lower SOC storage than other units. This implies that processes occurring during or after the mass wasting events are responsible for the storage decrease. In this section, we discuss possible mechanisms that follow the mass wasting events influence the SOC storage.

Material movements induced by mass wasting can considerably change ground and soil conditions in two ways: (1) Removal of thawed material above the permafrost table results in formation of a new active layer and permafrost degradation, which, in turn, leads to the degradation of the thawed OM. (2) Change in moisture regime can induce a shift to oxic conditions on the sites where material was removed, which can lead to more favourable conditions for OM decomposition (Koven et al., 2011; Preis et al. 2012). SOC and TN storage can then be altered by increased microbiological activity, leaching (wash) processes and direct transport of material to the sea. However, the moved material can often re-accumulate below the disturbance site.

5.1.1 Carbon degradation due to microbial activity upon ground disturbance

Oxic conditions increase microbial activity (Dyckmans et al., 2006), thus the material aeration following mass wasting can increase microbial activity, which in turn accelerates OM degradation. The material movement induced by solifluction is the fastest at the ground surface (Williams and Smith, 1989), where its impact is the greatest. Although this process is relatively slow, the material movement can disturb the vegetation cover or even cause overturning of surficial soil (Matsuoka, 2001). Exposure of the upper ground material to aeration may therefore increase microbial activity in freshly exposed material.

ALDs can, on the other hand, form instantly or within a few days and relocate the whole active layer (Lewkowicz, 2007). This induces oxic condition on the slide plane and causes permafrost degradation. Pautler et al. (2010) demonstrated that increased microbial activity following ALDs occurrence was due to these oxic conditions and also to the availability of new nutrients in freshly thawed material.

The material released from RTSs is usually transported through the collapse of material on headwalls and mudflows, which can accumulate in mud pools (Lantuit and Pollard, 2005). This material accumulation can, in some cases, temporarily cause an elevation increase (Manuscript 2). This material is eventually transported to the slump outlet if not temporarily stabilised on the slump floor. Either during slow transport or stabilisation, the material moved by RTSs can undergo OM degradation due to the occurrence of oxic conditions, increased availability of nutrients and resulting increase in microbial activity.

5.1.2 Depletion of SOC storage due to leaching

Mass wasting can change the hydrological conditions of the location that underwent disturbance and expose the material to surface wash and throughflow. Kokelj and Lewkowicz (1999) demonstrated that leaching redistributes dissolved solids such as salts after different mass movement processes. Similarly, the OM could be subject to leaching process. In the case of solifluction, the action might be limited, due to the lack of large mechanical disturbance, which would expose the stored OM. Nevertheless, solifluction movements can expose small amounts of cryoturbated OM to the surface and leaching.

A comparison between undisturbed and disturbed (with ALDs) watersheds in a study by Woods et al. (2011) indicated the presence of photochemically- and biologically-labile dissolved organic carbon (DOC) in disturbed watersheds. DOC likely originates from sequestered permafrost organic carbon. Lamoureux and Lafrenière (2014) observed release of old particulate organic carbon (POC) from the same disturbed watersheds, which also indicates release old organic carbon from marine sediments. DOC and POC carbon fluxes observed from these disturbed watersheds likely originated from freshly exposed material and thawed permafrost following the occurrence of the ALDs.

Preliminary results from our study area show that meltwater sampled at the RTS outflow contains considerable amounts of DOC and POC (Weege, personal communication). We assume for this reason that surface- and meltwater leaching can effectively deplete SOC storage of material that is being activated by RTSs.

Additionally, RTS headwalls and ALD depressions often act as a snow traps (Kokelj and Lewkowicz, 1998). The accumulated snow can contribute to surface runoff and wash erosion during the snowmelt and consequently also increase the rate of SOC leaching.

5.1.3 Direct transport of material to the sea

The material released by RTSs and ALDs directly at the coast is to a great extent subject to immediate removal by wave action and transported to near-shore zone. In the case of block failures, the released material is being removed before undergoing thawing processes and OM

degradation. However, the material that remains exposed on the coastal cliffs can experience a degradation of significant portion of labile organic carbon before being eroded by coastal erosion (Vonk et al., 2012). We can therefore assume that material directly transported to the sea by block failure contribute more labile carbon to near-shore zone than material from other mass-wasting processes.

5.1.4 Mobilised material accumulation

If mobilised material is not a subject to removal, it accumulates. In the case of solifluction, the moved material can form solifluction lobes or sheets (Matsuoka, 2001). In the case of ALD, the moved active layer accumulates at the toe of the disturbance in form of overthrust material (Lewkowicz, 2007). On RTSs, accumulation processes are more complex; vegetation and upper organic-rich soil parts can be buried in two ways: (1) mudflows can cover vegetated parts of RTS, and (2) turf falling from the headwall can accumulate in mud pools (Lacelle et al., 2010; Lantuit et al., 2012b).

An increase in material thickness on the site of accumulation can cause permafrost aggradation and preservation of OM and therefore increase the stored SOC and TN. Accumulated material is usually compacted (Manuscript 1, Lantuit et al., 2012b) and has reduced pore space. Therefore, the aeration and consequent microbial activity are reduced. If accumulated material is subsequently subject to water throughflow (in case displaced material is deposited in a stream), the wash and erosion of material is likely to have an impact on stream nutrient fluxes (Lamoureux and Lafrenière, 2009). The erosion of accumulated material would consequently cause increased transport of DOC and POC, which would decrease SOC storage of the accumulated material.

5.2 Effect of mass movements on coastal erosion

As demonstrated in Manuscript 2 and 3, mass movement can cause significant short-term material accumulations and coastline movements. These events can significantly change the coastal erosion characteristics, which are considerably different from the ones where mass wasting does not occur. In this section, we discuss the effects and implications of mass wasting on coastal erosion.

5.2.1 Effect mass wasting on coastline position

Mass wasting can reshape the coastal area and challenge the definition of the coastline (i.e. cliff bottom and cliff top lines). This is especially true in the case of ALDs, RTSs and combined slumping and mudflows (Manuscript 3, Figure 4.9a.). ALDs transport active-layer material to the coast, where it temporarily accumulates. As observed on Herschel Island

(Manuscript 3, Figure 4.9b), removal of material caused by ALDs above and on a bluff likely levels out both cliff bottom and cliff top line, making them hard to identify and define. The occurrence of polycyclic RTSs can on the other hand result in the occurrence of several headwalls (Manuscript 2, Figure 3.6), which can have distinct upper and lower edge. Defining the RTS headwall as a cliff bottom and top line would not be in accordance with their established definitions (Günther et al., 2013). Coastline position defined as an edge of the land at the limit of normal high spring tides is for this reason the most suitable to study planimetric coastal erosion in case of the coasts in our study area, which are characterised by mass wasting.

The coastline as defined above is inevitably subject to fluctuations caused by mass wasting. Block failures result in immediate material accumulation and a progradation of the coastline. Accumulated material may persist for longer, depending on the size of block failure. ALDs can also transport material to the shore, but in comparison to block failures they produce less material which is already thawed and easily eroded. RTSs produce mudflows, which accumulate on the shore, but are also generally relatively quickly eroded (Lantuit and Pollard, 2008; Günther et al., 2013). These mudflows are highly variable in time and the coastline position is consequently also highly variable. Mass-wasting processes can therefore cause coastline position fluctuations and when coastal erosion is measured by planimetric coastline retreat, the results are influenced accordingly.

5.2.2 Effect of mass wasting on volume loss

Permafrost coasts are eroded by both thermal and mechanical action of waves. The frozen sediment has to be thawed before it can be removed and suspended (Are, 1988). Mass movements located at the coast often transport material that has already been thawed. In the case of RTSs, the material is being thawed on the headwall and in the slump floor and then transported to the shore as a mudflow (Lantuit and Pollard, 2005). Thawed material (active layer) can also be transported to the shore with ALDs. In both cases, the material is thawed under the atmosphere and the sea-water energy is not required to thaw material before it is being eroded. ALD and RTS activity can thus likely increases volumetric coastal erosion. In addition, Lantuit and Pollard (2008) indicated that mudflows on RTSs could efficiently remove fine-grained material from the slump floor. The remaining coarse-grained sediment that is lacking cohesion can easily be eroded afterwards.

5.2.3 Differences between planimetric and volumetric erosion

As shown in Manuscript 3, the planimetric coastal erosion approach along coasts characterised by mass wasting may be sufficient for studying land and habitats loss, but is insufficient for estimating sediment release and nutrient fluxes. We attribute this to the mass-

movement-induced coastline fluctuations that affect the planimetric erosion measures, which considerably differ from volumetric erosion measures. Mass wasting does not only affect coastline position in situ, but also in the vicinity due to the sediment that can be transported as longshore drift along the coastline and cause additional coastline fluctuations (Manuscript 2).

The residence time of the material accumulated due to mass-wasting processes can vary considerably. Barnhart et al. (2014b) and Leibman et al. (2008) reported, based on observations from northern Alaska and western Siberia, that the material originating from ice-rich block failures generally remains on the shore from a few days to weeks. The time that is required for the less ice-rich block failures observed on Herschel Island to be eroded has however not been reported yet. The mudflow lobes accumulated at the RTSs outlets and the active layer material released by ALDs are likely short-living features, although no systematic observation of these features has been conducted yet. The rate of eventual removal depends on the exposure of material to coastal erosion. Repeated mass wasting events can result in frequent coastline fluctuations. We assume that their impact on planimetric coastal erosion is in the range of a few years to a decade. The fluctuations recorded by planimetric erosion due to mass-wasting processes are probably less pronounced during longer time spans (several decades), when the overall coastline retreat is several orders of magnitude greater than coastline fluctuations due to mass wasting.

6 Summary

We showed that mass wasting has a significant influence on SOC storage. The sites where mass-wasting processes are active show depletion of SOC. The possible mechanisms responsible for the SOC storage are associated with an increased microbial activity and leaching. We also showed that the overall storage can be increased at sites where mobilised material accumulates because of the burial of organic-rich material and the aggradation of the permafrost. We also demonstrated several possible impacts of mass-wasting processes on coastal erosion. Temporary accumulations of mobilised material can occur at the mass wasting site or can be transported to the adjacent coast by longshore drift. Unfortunately, traditional observations of coastline movement through planimetric coastline movement rates do not resolve the occurrence of mass movements and cannot accurately depict the actual sediment loss. Mass-wasting processes can also accelerate coastal erosion due to transport of already thawed material that lacks cohesion. Predicted increase of mass-wasting activity due to Arctic temperature increase will accelerate the SOC activation due to described mass-wasting processes. Organic carbon fluxes due to coastal erosion may also increase, although the volumetric erosion data would be required to record it completely.

References

This list of references includes references of introduction, all manuscripts and discussion sections.

Anisimov, O. & Reneva, S. 2006. Permafrost and changing climate: the Russian perspective. *AMBIO: A Journal of the Human Environment* 35: 169–175.

Are, F.E. 1988. Thermal abrasion of sea coasts. *Polar geography and geology* 12: 2.

Atkinson, D.E. 2005. Observed storminess patterns and trends in the circum-Arctic coastal regime. *Geo-Marine Letters* 25: 98–109.

Barnhart, K.R., Anderson, R.S., Overeem, I., Wobus, C., Clow, G.D. & Urban, F.E. 2014a. Modeling erosion of ice-rich permafrost bluffs along the Alaskan Beaufort Sea coast. *Journal of Geophysical Research: Earth Surface* 119: 1155–1179. DOI: 10.1002/2013JF002845

Barnhart, K.R., Overeem, I. & Anderson, R.S. 2014b. The effect of changing sea ice on the physical vulnerability of Arctic coasts. *The Cryosphere* 8: 1777–1799.

Beven, K.J. & Kirkby, M.J. 1979. A physically based, variable contributing area model of basin hydrology/Un modèle à base physique de zone d'appel variable de l'hydrologie du bassin versant. *Hydrological Sciences Journal* 24: 43–69.

Bird, E. 2011. *Coastal geomorphology: an introduction*, John Wiley & Sons.

Birkeland, P.W. 1984. *Soils and geomorphology.*, Oxford University Press.

Bockheim, J.G. 2007. Importance of cryoturbation in redistributing organic carbon in permafrost-affected soils. *Soil Science Society of America Journal* 71: 1335–1342.

Botch, M.S., Kobak, K.I., Vinson, T.S. & Kolchugina, T.P. 1995. Carbon pools and accumulation in peatlands of the former Soviet Union. *Global Biogeochemical Cycles* 9: 37–46. DOI: 10.1029/94GB03156

Bouchard, M. 1974. *Géologie des dépôts meubles de l'île Herschel, Territoire du Yukon*. MSc Thesis. Montréal: Université de Montréal.

Brown, J., Ferrians Jr., O.J., Heginbottom, J.A. & Melnikov, E.S. 1997. Circum-Arctic map of permafrost and ground-ice conditions, USGS Numbered Series.

Burke, E.J., Jones, C.D. & Koven, C.D. 2013. Estimating the permafrost-carbon climate response in the CMIP5 climate models using a simplified approach. *Journal of Climate* 26: 4897–4909.

Burn, C.R. 2012. *Herschel Island Qikiqtaryuk A Natural & Cultural History*, Calgary: University of Calgary Press.

Burn, C.R. & Lewkowicz, A.G. 1990. Canadian Landform Examples-17 Retrogressive Thaw Slumps. *The Canadian Geographer/Le Géographe canadien* 34: 273–276.

Burn, C.R. & Zhang, Y. 2009. Permafrost and climate change at Herschel Island (Qikiqtaruq), Yukon Territory, Canada. *Journal of Geophysical Research: Earth Surface* 114: F02001. DOI: 10.1029/2008JF001087

Canada Soil Survey Committee 1978. *The Canadian system of soil classification*, Research Branch, Canada Department of Agriculture.

Ciais, P., Sabine, C., Bala, G., Bopp, L., Brovkin, V., Canadell, J., Chhabra, A., Ruth, D., Galloway, J., Heimann, M., Jones, C., Le Quéré, C., Myneni, R.B., Piao, S. & Thornton, P. 2014. Carbon and Other Biogeochemical Cycles. In *Climate Change 2013 - The Physical Science Basis*. Intergovernmental Panel on Climate Change, ed. Cambridge: Cambridge University Press, pp. 465–514.

Couture, N.J. 2010. *Fluxes of soil organic carbon from eroding permafrost coasts, Canadian Beaufort Sea*. PhD Thesis. Montreal: University of Montreal.

Dallimore, S.R., Wolfe, S.A. & Solomon, S.M. 1996. Influence of ground ice and permafrost on coastal evolution, Richards Island, Beaufort Sea coast, NWT. *Canadian Journal of Earth Sciences* 33: 664–675.

De Krom, V. 1990. *Retrogressive thaw slumps and active layer slides on Herschel Island, Yukon*. M. Sc. Thesis, Montréal, Quebec.

Dyckmans, J., Flessa, H., Lipski, A., Potthoff, M. & Beese, F. 2006. Microbial biomass and activity under oxic and anoxic conditions as affected by nitrate additions. *Journal of Plant Nutrition and Soil Science* 169: 108–115.

Euskirchen, E.S., McGuire, A.D., Kicklighter, D.W., Zhuang, Q., Clein, J.S., Dargaville, R.J., Dye, D.G., Kimball, J.S., McDonald, K.C., Melillo, J.M., Romanovsky, V.E. & Smith, N.V. 2006. Importance of recent shifts in soil thermal dynamics on growing season length, productivity, and carbon sequestration in terrestrial high-latitude ecosystems. *Global Change Biology* 12: 731–750. DOI: 10.1111/j.1365-2486.2006.01113.x

Environment Canada (Website). URL http://www.ec.gc.ca/?lang=En (accessed 3.6.2015).

van Everdingen, R.O. 2005. *Multi-Language Glossary of Permafrost and Related Ground-Ice Terms, International Permafrost Association, University of Calgary, Calgary, Canada*,

French, H.M. 2013. *The periglacial environment*, John Wiley & Sons.

Frey, K.E., McClelland, J.W., Holmes, R.M. & Smith, L.C. 2007. Impacts of climate warming and permafrost thaw on the riverine transport of nitrogen and phosphorus to the Kara Sea. *Journal of Geophysical Research: Biogeosciences* 112: G04S58. DOI: 10.1029/2006JG000369

Fritz, M., Wetterich, S., Meyer, H., Schirrmeister, L., Lantuit, H. & Pollard, W.H. 2011. Origin and characteristics of massive ground ice on Herschel Island (western Canadian Arctic) as revealed by stable water isotope and hydrochemical signatures. *Permafrost and Periglacial Processes* 22: 26–38.

Fritz, M., Wetterich, S., Schirrmeister, L., Meyer, H., Lantuit, H., Preusser, F. & Pollard, W.H. 2012. Eastern Beringia and beyond: late Wisconsinan and Holocene landscape dynamics along the Yukon Coastal Plain, Canada. *Palaeogeography, Palaeoclimatology, Palaeoecology* 319: 28–45.

Grosse, G., Harden, J., Turetsky, M., McGuire, A.D., Camill, P., Tarnocai, C., Frolking, S., Schuur, E.A.G., Jorgenson, T., Marchenko, S., Romanovsky, V., Wickland, K.P., French, N., Waldrop, M., Bourgeau-Chavez, L. & Striegl, R.G. 2011. Vulnerability of high-latitude soil organic carbon in North America to disturbance. *Journal of Geophysical Research: Biogeosciences* 116: G00K06. DOI: 10.1029/2010JG001507

Guide, E.U. 2008. ENVI on-line software user's manual. *ITT Visual Information Solutions*.

Günther, F., Overduin, P.P., Sandakov, A., Grosse, G. & Grigoriev, M.N. 2012. Thermo-erosion along the Yedoma Coast of the Buor Khaya Peninsula, Laptev Sea, East Siberia. In *Proceedings of the Tenth International Conference on Permafrost, Volume 1: International Contributions*. The Northern Publisher, Salekhard, Russia, pp. 137–142.

Günther, F., Overduin, P.P., Sandakov, A.V., Grosse, G. & Grigoriev, M.N. 2013. Short-and long-term thermo-erosion of ice-rich permafrost coasts in the Laptev Sea region. *Biogeosciences* 10: 4297–4318.

Günther, F., Overduin, P.P., Yakshina, I.A., Opel, T., Baranskaya, A.V. & Grigoriev, M.N. 2015. Observing Muostakh disappear: permafrost thaw subsidence and erosion of a ground-ice-rich island in response to arctic summer warming and sea ice reduction. *The Cryosphere* 9: 151–178.

Harden, J.W., Koven, C.D., Ping, C.-L., Hugelius, G., David McGuire, A., Camill, P., Jorgenson, T., Kuhry, P., Michaelson, G.J., O'Donnell, J.A., Schuur, E.A.G., Tarnocai, C., Johnson, K. & Grosse, G. 2012. Field information links permafrost carbon to physical vulnerabilities of thawing. *Geophysical Research Letters* 39: L15704. DOI: 10.1029/2012GL051958

Harden, J.W., Trumbore, S.E., Stocks, B.J., Hirsch, A., Gower, S.T., O'neill, K.P. & Kasischke, E.S. 2000. The role of fire in the boreal carbon budget. *Global Change Biology* 6: 174–184. DOI: 10.1046/j.1365-2486.2000.06019.x

Harris, C., Kern-Luetschg, M., Murton, J., Font, M., Davies, M. & Smith, F. 2008. Solifluction processes on permafrost and non-permafrost slopes: results of a large-scale laboratory simulation. *Permafrost and Periglacial Processes* 19: 359–378.

Hequette, A. & Barnes, P.W. 1990. Coastal retreat and shoreface profile variations in the Canadian Beaufort Sea. *Marine Geology* 91: 113–132. DOI: 10.1016/0025-3227(90)90136-8

Hobbie, S.E., Schimel, J.P., Trumbore, S.E. & Randerson, J.R. 2000. Controls over carbon storage and turnover in high-latitude soils. *Global Change Biology* 6: 196–210. DOI: 10.1046/j.1365-2486.2000.06021.x

Horwath Burnham, J. & Sletten, R.S. 2010. Spatial distribution of soil organic carbon in northwest Greenland and underestimates of high Arctic carbon stores. *Global Biogeochemical*

Cycles 24: GB3012. DOI: 10.1029/2009GB003660

Hudak, D.R. & Young, J.M.C. 2002. Storm climatology of the southern Beaufort Sea. *Atmosphere-Ocean* 40: 145–158.

Hugelius, G. 2012. Spatial upscaling using thematic maps: An analysis of uncertainties in permafrost soil carbon estimates. *Global Biogeochemical Cycles* 26: GB2026. DOI: 10.1029/2011GB004154

Hugelius, G., Bockheim, J.G., Camill, P., Eberling, B., Grosse, G., Harden, J.W., Johnson, K., Jorgenson, T., Koven, C. & Kuhry, P. 2013a. A new data set for estimating organic carbon storage to 3 m depth in soils of the northern circumpolar permafrost region. *Earth System Science Data* 5: 393–402.

Hugelius, G. & Kuhry, P. 2009. Landscape partitioning and environmental gradient analyses of soil organic carbon in a permafrost environment. *Global Biogeochemical Cycles* 23: GB3006. DOI: 10.1029/2008GB003419

Hugelius, G., Kuhry, P., Tarnocai, C. & Virtanen, T. 2010. Soil organic carbon pools in a periglacial landscape: a case study from the central Canadian Arctic. *Permafrost and Periglacial Processes* 21: 16–29.

Hugelius, G., Routh, J., Kuhry, P. & Crill, P. 2012. Mapping the degree of decomposition and thaw remobilization potential of soil organic matter in discontinuous permafrost terrain. *Journal of Geophysical Research: Biogeosciences* 117: G02030. DOI: 10.1029/2011JG001873

Hugelius, G., Strauss, J., Zubrzycki, S., Harden, J.W., Schuur, E., Ping, C.-L., Schirrmeister, L., Grosse, G., Michaelson, G.J. & Koven, C.D. 2014. Estimated stocks of circumpolar permafrost carbon with quantified uncertainty ranges and identified data gaps. *Biogeosciences* 11: 6573–6593.

Hugelius, G., Tarnocai, C., Broll, G., Canadell, J.G., Kuhry, P. & Swanson, D.K. 2013b. The Northern Circumpolar Soil Carbon Database: spatially distributed datasets of soil coverage and soil carbon storage in the northern permafrost regions. *Earth System Science Data* 5: 3–13.

Hugelius, G., Virtanen, T., Kaverin, D., Pastukhov, A., Rivkin, F., Marchenko, S., Romanovsky, V. & Kuhry, P. 2011. High-resolution mapping of ecosystem carbon storage and potential effects of permafrost thaw in periglacial terrain, European Russian Arctic. *Journal of Geophysical Research: Biogeosciences* 116: G03024. DOI: 10.1029/2010JG001606

Hughes, O.L. 1972. *Surficial geology of northern Yukon Territory and northwestern district of Mackenzie, Northwest Territories*, Department of Energy, Mines and Resources.

Hynes, S., Solomon, S.M., Forbes, D.L., Whalen, D. & Manson, G.L. 2014. GIS compilation of coastline variability spanning 60 years, western Beaufort Sea, Yukon and Northwest Territories. *Geological Survey of Canada*. DOI: doi:10.4095/293926

Johnson, K., Solomon, S., Berry, D. & Graham, P. 2003. Erosion progression and adaptation strategy in a northern coastal community. In *8th international conference on Permafrost*. pp. 21–25.

Jones, B.M., Arp, C.D., Jorgenson, M.T., Hinkel, K.M., Schmutz, J.A. & Flint, P.L. 2009. Increase in the rate and uniformity of coastline erosion in Arctic Alaska. *Geophysical Research Letters* 36: L03503. DOI: 10.1029/2008GL036205

Jones, B.M., Hinkel, K.M., Arp, C.D. & Eisner, W.R. 2008. Modern Erosion Rates and Loss of Coastal Features and Sites, Beaufort Sea Coastline, Alaska. *Arctic* 61: 361–372.

Jones, B.M., Stoker, J.M., Gibbs, A.E., Grosse, G., Romanovsky, V.E., Douglas, T.A., Kinsman, N.E.M. & Richmond, B.M. 2013. Quantifying landscape change in an arctic coastal lowland using repeat airborne LiDAR. *Environmental Research Letters* 8: 045025. DOI: 10.1088/1748-9326/8/4/045025

Jones, J.B., Petrone, K.C., Finlay, J.C., Hinzman, L.D. & Bolton, W.R. 2005. Nitrogen loss from watersheds of interior Alaska underlain with discontinuous permafrost. *Geophysical Research Letters* 32: L02401. DOI: 10.1029/2004GL021734

Jorgenson, M.T. & Brown, J. 2005. Classification of the Alaskan Beaufort Sea Coast and estimation of carbon and sediment inputs from coastal erosion. *Geo-Marine Letters* 25: 69–80.

Kizyakov, A.I., Zimin, M.V., Leibman, M.O. & Pravikova, N.V. 2013. Thermal denudation, thermal abrasion of sea shores, thermocirques. *Kriosfera Zemli (Earth Cryosphere),* 17: 36–47.

Kohnert, K., Serafimovich, A., Hartmann, J. & Sachs, T. 2014. Airborne measurements of methane fluxes in Alaskan and Canadian tundra with the research aircraft Polar 5. *Berichte zur Polar-und Meeresforschung (Reports on polar and marine research)* 673.

Kokelj, S.V. & Lewkowicz, A.G. 1998. Long-term influence of active-layer detachment sliding on permafrost slope hydrology, Hot Weather Creek, Ellesmere Island, Canada. In *Seventh International Conference on Permafrost. Collection Nordiciana*. pp. 583–589.

Kokelj, S.V. & Lewkowicz, A.G. 1999. Salinization of Permafrost Terrain Due to Natural Geomorphic Disturbance, Fosheim Peninsula, Ellesmere Island. *Arctic* 52: 372–385.

Koven, C.D., Riley, W.J. & Stern, A. 2013. Analysis of permafrost thermal dynamics and response to climate change in the CMIP5 Earth System Models. *Journal of Climate* 26: 1877–1900.

Koven, C.D., Ringeval, B., Friedlingstein, P., Ciais, P., Cadule, P., Khvorostyanov, D., Krinner, G. & Tarnocai, C. 2011. Permafrost carbon-climate feedbacks accelerate global warming. *Proceedings of the National Academy of Sciences* 108: 14769–14774.

Kuhry, P., Dorrepaal, E., Hugelius, G., Schuur, E.A.G. & Tarnocai, C. 2010. Potential remobilization of belowground permafrost carbon under future global warming. *Permafrost and Periglacial Processes* 21: 208–214.

Kuhry, P. & Vitt, D.H. 1996. Fossil carbon/nitrogen ratios as a measure of peat decomposition. *Ecology* 77: 271–275.

Lacelle, D., Bjornson, J. & Lauriol, B. 2010. Climatic and geomorphic factors affecting contemporary (1950–2004) activity of retrogressive thaw slumps on the Aklavik Plateau, Richardson Mountains, NWT, Canada. *Permafrost and Periglacial Processes* 21: 1–15.

Lamoureux, S.F. & Lafrenière, M.J. 2009. Fluvial impact of extensive active layer detachments, Cape Bounty, Melville Island, Canada. *Arctic, Antarctic, and Alpine Research* 41: 59–68.

Lamoureux, S.F. & Lafrenière, M.J. 2014. Seasonal fluxes and age of particulate organic carbon exported from Arctic catchments impacted by localized permafrost slope disturbances. *Environmental Research Letters* 9: 045002. DOI: 10.1088/1748-9326/9/4/045002

Lantuit, H., Atkinson, D., Paul Overduin, P., Grigoriev, M., Rachold, V., Grosse, G. & Hubberten, H.-W. 2011. Coastal erosion dynamics on the permafrost-dominated Bykovsky Peninsula, north Siberia, 1951–2006. *Polar Research* 30.: DOI: 10.3402/polar.v30i0.7341

Lantuit, H., Overduin, P.P., Couture, N., Wetterich, S., Aré, F., Atkinson, D., Brown, J., Cherkashov, G., Drozdov, D. & Forbes, D.L. 2012a. The Arctic coastal dynamics database: A new classification scheme and statistics on Arctic permafrost coastlines. *Estuaries and Coasts* 35: 383–400.

Lantuit, H., Pollard, W.H., Couture, N., Fritz, M., Schirrmeister, L., Meyer, H. & Hubberten, H.-W. 2012b. Modern and late Holocene retrogressive thaw slump activity on the Yukon coastal plain and Herschel Island, Yukon Territory, Canada. *Permafrost and Periglacial Processes* 23: 39–51.

Lantuit, H. & Pollard, W.H. 2008. Fifty years of coastal erosion and retrogressive thaw slump activity on Herschel Island, southern Beaufort Sea, Yukon Territory, Canada. *Geomorphology* 95: 84–102.

Lantuit, H. & Pollard, W.H. 2005. Temporal stereophotogrammetric analysis of retrogressive thaw slumps on Herschel Island, Yukon Territory. *Natural Hazards and Earth System Science* 5: 413–423.

Lantuit, H., Rachold, V., Pollard, W.H., Steenhuisen, F., Ødegård, R. & Hubberten, H.-W. 2009. Towards a calculation of organic carbon release from erosion of Arctic coasts using non-fractal coastline datasets. *Marine Geology* 257: 1–10. DOI: 10.1016/j.margeo.2008.10.004

Lantz, T.C. & Kokelj, S.V. 2008. Increasing rates of retrogressive thaw slump activity in the Mackenzie Delta region, N.W.T., Canada. *Geophysical Research Letters* 35: L06502. DOI: 10.1029/2007GL032433

Leibman, M., Gubarkov, A., Khomutov, A., Kizyaakov, A. & Vanshtein, B. 2008. Coastal processes at the tabular-ground-ice-bearing area, Yugorsky Peninsula, Russia. In *Proceedings of the 9th International Conference on Permafrost, Fairbanks, Alaska*. pp. 1037–1042.

Lewkowicz, A.G. 2007. Dynamics of active-layer detachment failures, Fosheim Peninsula, Ellesmere Island, Nunavut, Canada. *Permafrost and Periglacial Processes* 18: 89–103.

Lewkowicz, A.G. 1990. Morphology, frequency and magnitude of active-layer detachment slides, Fosheim Peninsula, Ellesmere Island, NWT. In *In: Proceedings of the 5th Canadian Permafrost Conference. Quebec, Canada*. pp. 111–118.

Lewkowicz, A.G. & Clarke, S. 1998. Late-summer solifluction and active layer depths, Fosheim Peninsula, Ellesmere Island, Canada. In *Proceedings of the 6th International Conference on Permafrost. Centre d'études nordiques, Université Laval*. pp. 641–666.

Lewkowicz, A.G. & Harris, C. 2005a. Frequency and magnitude of active-layer detachment failures in discontinuous and continuous permafrost, northern Canada. *Permafrost and Periglacial Processes* 16: 115–130.

Lewkowicz, A.G. & Harris, C. 2005b. Morphology and geotechnique of active-layer detachment failures in discontinuous and continuous permafrost, northern Canada. *Geomorphology* 69: 275–297.

Mackay, J.R. 1959. Glacier ice-thrust features of the Yukon coast. *Geographical Bulletin* 13: 5–21.

Mahoney, A.R., Eicken, H., Gaylord, A.G. & Gens, R. 2014. Landfast sea ice extent in the Chukchi and Beaufort Seas: The annual cycle and decadal variability. *Cold Regions Science and Technology* 103: 41–56.

Mars, J.C. & Houseknecht, D.W. 2007. Quantitative remote sensing study indicates doubling of coastal erosion rate in past 50 yr along a segment of the Arctic coast of Alaska. *Geology* 35: 583–586.

Matsuoka, N. 2001. Solifluction rates, processes and landforms: a global review. *Earth-Science Reviews* 55: 107–134.

McGuire, A.D., Anderson, L.G., Christensen, T.R., Dallimore, S., Guo, L., Hayes, D.J., Heimann, M., Lorenson, T.D., Macdonald, R.W. & Roulet, N. 2009. Sensitivity of the carbon cycle in the Arctic to climate change. *Ecological Monographs* 79: 523–555.

Meyers, P.A. 1994. Preservation of elemental and isotopic source identification of sedimentary organic matter. *Chemical Geology* 114: 289–302.

Michaelson, G.J., Ping, C.L. & Kimble, J.M. 1996. Carbon storage and distribution in tundra soils of Arctic Alaska, USA. *Arctic and Alpine Research* 28: 414–424.

Myers-Smith, I.H., Hik, D.S., Kennedy, C., Cooley, D., Johnstone, J.F., Kenney, A.J. & Krebs, C.J. 2011. Expansion of canopy-forming willows over the twentieth century on Herschel Island, Yukon Territory, Canada. *Ambio* 40: 610–623.

Myers-Smith, I.H., McGuire, A.D., Harden, J.W. & Chapin, F.S. 2007. Influence of disturbance on carbon exchange in a permafrost collapse and adjacent burned forest. *Journal of Geophysical Research: Biogeosciences* 112: G04017. DOI: 10.1029/2007JG000423

Obu, J., Lantuit, H., Myers-Smith, I., Heim, B., Wolter, J. & Fritz, M. in press. Effect of terrain characteristics on soil organic carbon and total nitrogen stocks in soils of Herschel Island, western Canadian Arctic. *Permafrost and Periglacial Processes*.

O'Donnell, J.A., Harden, J.W., McGuire, A.D. & Romanovsky, V.E. 2011. Exploring the sensitivity of soil carbon dynamics to climate change, fire disturbance and permafrost thaw in a black spruce ecosystem. *Biogeosciences* 8: 1367–1382.

Overduin, P.P., Strzelecki, M.C., Grigoriev, M.N., Couture, N., Lantuit, H., St-Hilaire-Gravel, D., Günther, F. & Wetterich, S. 2014. Coastal changes in the Arctic. *Geological Society, London, Special Publications* 388: 103–129. DOI: 10.1144/SP388.13

Overeem, I., Anderson, R.S., Wobus, C.W., Clow, G.D., Urban, F.E. & Matell, N. 2011. Sea ice loss enhances wave action at the Arctic coast. *Geophysical Research Letters* 38: L17503. DOI: 10.1029/2011GL048681

Pachauri, R.K., Allen, M.R., Barros, V.R., Broome, J., Cramer, W., Christ, R., Church, J.A., Clarke, L., Dahe, Q., Dasgupta, P., Dubash, N.K., Edenhofer, O., Elgizouli, I., Field, C.B., Forster, P., Friedlingstein, P., Fuglestvedt, J., Gomez-Echeverri, L., Hallegatte, S., Hegerl, G., Howden, M., Jiang, K., Jimenez Cisneroz, B., Kattsov, V., Lee, H., Mach, K.J., Marotzke, J., Mastrandrea, M.D., Meyer, L., Minx, J., Mulugetta, Y., O'Brien, K., Oppenheimer, M., Pereira, J.J., Pichs-Madruga, R., Plattner, G.-K., Pörtner, H.-O., Power, S.B., Preston, B., Ravindranath, N.H., Reisinger, A., Riahi, K., Rusticucci, M., Scholes, R., Seyboth, K., Sokona, Y., Stavins, R., Stocker, T.F., Tschakert, P., van Vuuren, D. & van Ypserle, J.-P. 2014. *Climate Change 2014: Synthesis Report. Contribution of Working Groups I, II and III to the Fifth Assessment Report of the Intergovernmental Panel on Climate Change* R. K. Pachauri & L. Meyer, eds., Geneva, Switzerland: IPCC.

Pautler, B.G., Simpson, A.J., Mcnally, D.J., Lamoureux, S.F. & Simpson, M.J. 2010. Arctic permafrost active layer detachments stimulate microbial activity and degradation of soil organic matter. *Environmental Science & Technology* 44: 4076–4082.

Pavlis, N.K., Holmes, S.A., Kenyon, S.C. & Factor, J.K. 2008. An earth gravitational model to degree 2160: EGM2008. *EGU General Assembly.* 13–18.

Pei, T., Qin, C.-Z., Zhu, A.-X., Yang, L., Luo, M., Li, B. & Zhou, C. 2010. Mapping soil organic matter using the topographic wetness index: a comparative study based on different flow-direction algorithms and kriging methods. *Ecological Indicators* 10: 610–619.

Pinchin, B.M., Nairn, R.B. & Philpott, K.L. 1985. Beaufort Sea Coastal Sediment Study: Numerical estimation of sediment transport and nearshore profile adjustment at coastal sites in the Canadian Beaufort Sea. *Geol. Surv. Can. Open-File Rep* 1259: 712.

Ping, C.-L., Michaelson, G.J., Guo, L., Jorgenson, M.T., Kanevskiy, M., Shur, Y., Dou, F. & Liang, J. 2011. Soil carbon and material fluxes across the eroding Alaska Beaufort Sea coastline. *Journal of Geophysical Research: Biogeosciences* 116: G02004. DOI: 10.1029/2010JG001588

Pizano, C., Barón, A.F., Schuur, E.A.G., Crummer, K.G. & Mack, M.C. 2014. Effects of thermo-erosional disturbance on surface soil carbon and nitrogen dynamics in upland arctic

tundra. *Environmental Research Letters* 9: 075006. DOI: 10.1088/1748-9326/9/7/075006

Pollard, W.H. 1990. The nature and origin of ground ice in the Herschel Island area, Yukon Territory. In *Proceedings, Fifth Canadian Permafrost Conference, Québec*. pp. 23–30.

Pries, C.E.H., Schuur, E.A. & Crummer, K.G. 2012. Holocene carbon stocks and carbon accumulation rates altered in soils undergoing permafrost thaw. *Ecosystems* 15: 162–173.

Rachold, V., Eicken, H., Gordeev, V.V., Grigoriev, M.N., Hubberten, H.-W., Lisitzin, A.P., Shevchenko, V.P. & Schirrmeister, L. 2004. Modern terrigenous organic carbon input to the Arctic Ocean. In *The organic carbon cycle in the Arctic Ocean*. Springer, pp. 33–55.

Rachold, V., Grigoriev, M.N., Are, F.E., Solomon, S., Reimnitz, E., Kassens, H. & Antonow, M. 2000. Coastal erosion vs riverine sediment discharge in the Arctic Shelf seas. *International Journal of Earth Sciences* 89: 450–460.

Rampton, V.N. 1982. *Quaternary geology of the Yukon coastal plain*, Geological survey of Canada.

Richter, R. 1996. Atmospheric correction of satellite data with haze removal including a haze/clear transition region. *Computers & Geosciences* 22: 675–681.

Romanovsky, V.E., Smith, S.L. & Christiansen, H.H. 2010. Permafrost thermal state in the polar Northern Hemisphere during the international polar year 2007–2009: A synthesis. *Permafrost and Periglacial processes* 21: 106–116.

Schaefer, K., Lantuit, H., Romanovsky, V.E., Schuur, E.A.G. & Witt, R. 2014. The impact of the permafrost carbon feedback on global climate. *Environmental Research Letters* 9: 085003. DOI: 10.1088/1748-9326/9/8/085003

Schuur, E.A., Bockheim, J., Canadell, J.G., Euskirchen, E., Field, C.B., Goryachkin, S.V., Hagemann, S., Kuhry, P., Lafleur, P.M. & Lee, H. 2008. Vulnerability of permafrost carbon to climate change: Implications for the global carbon cycle. *BioScience* 58: 701–714.

Schuur, E.A.G., McGuire, A.D., Schädel, C., Grosse, G., Harden, J.W., Hayes, D.J., Hugelius, G., Koven, C.D., Kuhry, P. & Lawrence, D.M. 2015. Climate change and the permafrost carbon feedback. *Nature* 520: 171–179.

Schuur, E.A., Vogel, J.G., Crummer, K.G., Lee, H., Sickman, J.O. & Osterkamp, T.E. 2009. The effect of permafrost thaw on old carbon release and net carbon exchange from tundra. *Nature* 459: 556–559.

Shaver, G.R. & Chapin III, F.S. 1980. Response to fertilization by various plant growth forms in an Alaskan tundra: nutrient accumulation and growth. *Ecology* 61: 662–675.

Short, N., Brisco, B., Couture, N., Pollard, W., Murnaghan, K. & Budkewitsch, P. 2011. A comparison of TerraSAR-X, RADARSAT-2 and ALOS-PALSAR interferometry for monitoring permafrost environments, case study from Herschel Island, Canada. *Remote Sensing of Environment* 115: 3491–3506.

Smith, C.A.., Kennedy, C.., Hargrave, A.E. & McKenna, K.M. 1989. *Soil and vegetation of Herschel Island*, Research Branch, Agriculture Canada.

Smith, M.W. & Riseborough, D.W. 2002. Climate and the limits of permafrost: a zonal analysis. *Permafrost and Periglacial Processes* 13: 1–15.

Solomon, S.M. 2005. Spatial and temporal variability of shoreline change in the Beaufort-Mackenzie region, Northwest Territories, Canada. *Geo-Marine Letters* 25: 127–137.

Solomon, S.M., Forbes, D.L. & Kierstead, B. 1994. *Coastal impacts of climate change: Beaufort Sea erosion study*, Geological Survey of Canada.

Sörensen, R., Zinko, U. & Seibert, J. 2006. On the calculation of the topographic wetness index: evaluation of different methods based on field observations. *Hydrology and Earth System Sciences Discussions* 10: 101–112.

Stocker, T., Qin, D., Plattner, G.-K., Tignor, M., Allen, S.K., Boschung, J., Nauels, A., Xia, Y., Bex, V. & Midgley, P.M. 2014. *Climate change 2013: The physical science basis*, Cambridge University Press Cambridge, UK, and New York.

Tarnocai, C., Canadell, J.G., Schuur, E. a. G., Kuhry, P., Mazhitova, G. & Zimov, S. 2009. Soil organic carbon pools in the northern circumpolar permafrost region. *Global Biogeochemical Cycles* 23: GB2023. DOI: 10.1029/2008GB003327

Team, R.C. 2015. R: A language and environment for statistical computing. Vienna, Austria; 2014. *URL http://www. R-project.*

Toutin, T. 2011. State-of-the-art of geometric correction of remote sensing data: a data fusion perspective. *International Journal of Image and Data Fusion* 2: 3–35.

Turetsky, M., Wieder, K., Halsey, L. & Vitt, D. 2002. Current disturbance and the diminishing peatland carbon sink. *Geophysical Research Letters* 29: 21–1. DOI: 10.1029/2001GL014000

Vonk, J.E., Sánchez-García, L., van Dongen, B.E., Alling, V., Kosmach, D., Charkin, A., Semiletov, I.P., Dudarev, O.V., Shakhova, N. & Roos, P. 2012. Activation of old carbon by erosion of coastal and subsea permafrost in Arctic Siberia. *Nature* 489: 137–140.

Wahl, H.E., Fraser, D.B., Harvey, R.C. & Maxwell, J.B. 1987. Climate of Yukon. Climatological Studies Number 40. *Atmospheric Environment Service, Environment Canada* 233.

Wegner, C., Bennett, K.E., de Vernal, A., Forwick, M., Fritz, M., Heikkilä, M., Lacka, M., Lantuit, H., Laska, M. & Moskalik, M. in press. Variability in transport of terrigenous material on the shelves and the deep Arctic Ocean during the Holocene. *Polar Research*.

White, S.A. & Wang, Y. 2003. Utilizing DEMs derived from LIDAR data to analyze morphologic change in the North Carolina coastline. *Remote sensing of environment* 85: 39–47.

Williams, P.J. & Smith, M.W. 1989. *The frozen earth*, New York: Cambridge University Press.

Woods, G.C., Simpson, M.J., Pautler, B.G., Lamoureux, S.F., Lafrenière, M.J. & Simpson, A.J. 2011. Evidence for the enhanced lability of dissolved organic matter following permafrost slope disturbance in the Canadian High Arctic. *Geochimica et Cosmochimica Acta* 75: 7226–7241.

Young, A.P. & Ashford, S.A. 2006. Application of Airborne LIDAR for Seacliff Volumetric Change and Beach-Sediment Budget Contributions. *Journal of Coastal Research* 307–318. DOI: 10.2112/05-0548.1

Zhang, T., Barry, R.G., Knowles, K., Heginbottom, J.A. & Brown, J. 2008. Statistics and characteristics of permafrost and ground-ice distribution in the Northern Hemisphere. *Polar Geography* 31: 47–68.

Zimov, S.A., Schuur, E.A. & Chapin III, F.S. 2006. Permafrost and the global carbon budget. *Science(Washington)* 312: 1612–1613.

Zubrzycki, S., Kutzbach, L., Grosse, G., Desyatkin, A. & Pfeiffer, E.M. 2013. Organic carbon and total nitrogen stocks in soils of the Lena River Delta. *Biogeosciences* 10: 3507–3524.

Acknowledgements

At first, I would like to thank Hugues Lantuit for willing to take the responsibility of supervising my PhD project and providing scientific and financial support. I especially appreciated his quick responses to my questions, proof reading of manuscripts, and giving the opportunity for frequent meetings. Great thanks go also to my co-supervisors Michael Fritz, Frank Günther and Isla Myers-Smith for their priceless advices and guidance through my PhD. Thanks also to Torsten Sachs and Veit Helm for providing LIDAR scanning and processing the datasets. I would also like to thank all other paper co-authors for their help with paper writing, useful comments and suggestions.

My PhD would not be possible without financial support of the Slovene Human Resources Development and Scholarship Fund, which supported me with a scholarship. My field work, conferences and material costs were financially supported by COPER Young Researchers Group and Alfred Wegener Institute. Many thanks also to POLMAR and PoGS graduate schools, which funded my research stay at UNIS, many courses, workshops and conferences.

I would like to sincerely thank all my colleagues at AWI for their support, discussions and useful advices during my work at AWI. I am very grateful for the help with translations and proofreading to Juliane Wolter and Justine Ramage. Thanks also to Potsdam DokTeam Liv Heinecke, Daniel Kreyling, Markus Kayser and Bastian Niemeyer for helping me with many bureaucratic issues and persisting in their efforts to improve the situations of AWI PhDs. I would also like to thank Ute Kuschel, Dyke Scheidemann and Daniel Gorzawski for the guidance and help with sample processing at AWI laboratories.

Eidesstattliche Erklärung

Hiermit versichere ich, dass ich die vorliegende Arbeit selbstständig verfasst und keine anderen als die angegebenen Quellen und Hilfsmittel verwendet habe.

Ich habe diese kumulative Dissertation am Alfred-Wegener-Institut Helmholtz Zentrum für Polar und Meeresforschung in Potsdam erarbeitet und in englischer Sprache angefertigt. Diese Dissertation wird erstmalig und ausschließlich an der Universität Potsdam eingereicht.

Die dem Promotionsverfahren zugrundeliegende Promotionsordnung vom 18.09.2013 ist mir bekannt.

Potsdam, den 17.11.2015 Jaroslav Obu